Orbit and Altimetric Corrections for the ERS Satellites Through Analysis of Single and Dual Satellite Crossovers

Stuart Carnochan

Doctor of Philosophy

The University of Aston in Birmingham

October 1996

The University of Aston in Birmingham

Orbit and Altimetric Corrections for the ERS Satellites Through Analysis of Single and Dual Satellite Crossovers

Stuart Carnochan

Doctor of Philosophy

October 1996

Thesis Summary

Due to the failure of PRARE the orbital accuracy of ERS-1 is typically 10-15 cm radially as compared to 3-4cm for TOPEX/Poseidon. To gain the most from these simultaneous datasets it is necessary to improve the orbital accuracy of ERS-1 so that it is commensurate with that of TOPEX/Poseidon. For the integration of these two datasets it is also necessary to determine the altimeter and sea state biases for each of the satellites.

Several models for the sea state bias of ERS-1 are considered by analysis of the ERS-1 single satellite crossovers. The model adopted consists of the sea state bias as a percentage of the significant wave height, namely 5.95 %.

The removal of ERS-1 orbit error and recovery of an ERS-1 - TOPEX/Poseidon relative bias are both achieved by analysis of dual crossover residuals. The gravitational field based radial orbit error is modelled by a finite Fourier expansion series with the dominant frequencies determined by analysis of the JGM-2 co-variance matrix. Periodic and secular terms to model the errors due to atmospheric density, solar radiation pressure and initial state vector mis-modelling are also solved for. Validation of the dataset unification consists of comparing the mean sea surface topographies and annual variabilities derived from both the corrected and uncorrected ERS-1 orbits with those derived from TOPEX/Poseidon. The global and regional geographically fixed/variable orbit errors are also analysed pre and post correction, and a significant reduction is noted.

Finally the use of dual/single satellite crossovers and repeat pass data, for the calibration of ERS-2 with respect to ERS-1 and TOPEX/Poseidon is shown by calculating the ERS-1/2 sea state and relative biases.

Keywords: altimeter range bias, radial orbit error, sea state bias, TOPEX/Poseidon

for Nicki

Acknowledgements

Several people are due thanks for their invaluable contributions to the work contained in this thesis. Firstly thanks are due to Dr Philip Moore and Dr Philip Woodworth for their supervision, advice and support. Also, Dr Moore's contribution to section 8.4.2 'Annual Sea Surface Variability Comparisons' is acknowledged.

Many thanks are also due to my colleagues (past and present) Henno Boomkamp, Rob Cullen, Simon Ehlers, Gordon Jolly, Chris Lam, Chris Murphy, Ruaraidh MacKenzie, Matt Reynolds and Russ Walmsley for their advice and contributions over many months, particularly Chris Murphy for his help in producing several of the plots contained within this work.

Thanks are also given to my parents and my wife, Nicki, whose love and support have been instrumental in the successful completion of this thesis.

Finally, I would like to thank the Particle Physics and Astronomy research Council (previously SERC) and Proudman Oceanographic Laboratory for their financial assistance.

Contents

List of Figures

List of Tables

Chapter 1

Introduction

Chapter 1

Introduction

With the launch of ERS-1 in 1991, TOPEX/Poseidon in 1992 and ERS-2 in 1995 there exists an unprecedented amount of altimetry data that is available to the scientific community. If the most is to be obtained from these datasets, as well as from past and future missions, it is vital that the data from different satellites be as homogenous as possible. This means that the orbit and altimetric errors present in each dataset must be carefully understood and controlled such that they are at a minimum.

TOPEX/Poseidon, being in a relatively high orbit of altitude 1350km, is not heavily perturbed by the atmosphere and gravity field. This and the comprehensive tracking of TOPEX/Poseidon with laser range, DORIS range rate and GPS psuedo range and carrier phase measurements has resulted in the orbital accuracy being at the level of 3-4cm rms in the radial direction [Marshal et al, 1995]. ERS-1 orbits, however, have not been so accurate because of the failure of PRARE, resulting in laser range and crossover differences being the only tracking data available. TOPEX/Poseidon altimetry has therefore become the first choice dataset for the majority of oceanographic applications which, in turn, has resulted in satellite dependent altimetric corrections, such as sea state bias, being well modelled for this satellite. The ERS missions, however, provide data at higher latitudes and, with a much denser resolution than TOPEX/Poseidon, provide a complimentary dataset over the oceans and a unique set over the ice sheets.

The aim of this thesis is therefore to reduce some of the errors in the ERS altimeter datasets, by analysis of single and dual satellite altimeter observations, so that they are commensurate with those of TOPEX/Poseidon. At the time this study was undertaken (1992), two of the dominant error sources present within the ERS-1 altimeter dataset were radial orbit error and the sea state bias model used. In the intervening years more accurate dynamic ERS-1 orbits, the accuracy inreasing from 10-15cm rms (1992) to 5-7cm rms (1996) radially, have become available through the use of improved gravity field models and the recovery of empirical parameters in the dynamic solution. This, however, does not lessen the significance of the work presented in this thesis as the present orbits for ERS-1 are still not of the same accuracy as TOPEX/Poseidon. Until better atmospheric models are available for orbits of satellites at the ERS heights, the use of empirical corrections either non-dynamically or in the form of empirical parameters in the dynamic solution will be required to provide orbital accuracies approaching TOPEX/Poseidon.

As an introduction to the work contained in this thesis, chapter 2 discusses the principles of satellite altimetry whilst chapter 3 briefly describes the satellite instrumentation and missions for ERS-1, ERS-2 and TOPEX/Poseidon. Finally chapter 4 describes the precise orbit determination software used at Aston to determine the ERS-1 orbits that underpin the work contained in this thesis.

In chapter 5 the sea state bias for ERS-1 is determined from analysis of single satellite crossover residuals. Several models that consist of terms relating to wind speed and significant wave height are considered. It is found that the correction provided on the OPR dataset is a significant underestimation to the extent that the model recommended for ERS-1 throughout this thesis is the simple linear relationship with significant wave height.

The largest part of this thesis consists of reducing the radial error in the orbits of ERS-1. This is done in chapter 6 by modelling the error due to the gravitational field by a finite Fourier expansion series with additional secular and periodic terms to model the errors caused by atmospheric density, solar radiation pressure and initial state vector mis-modelling. In chapter 7 several error recovery strategies utilising ERS-1 single satellite and TOPEX/Poseidon - ERS-1 dual satellite crossovers are attempted for cycle 9 of ERS-1's multi-disciplinary phase. The dominant gravitational terms are identified from the JGM-2 co-variance matrix . An optimal strategy for the recovery of ERS-1 radial orbit error is identified and then applied to 13 cycles (cycles 6-18, there being no TOPEX/Poseidon altimetry before cycle 6) of altimetry data in chapter 8. This large (in excess of 440 days) altimeter dataset is used to determine the relative range biases between TOPEX/Poseidon and ERS-1 and to compare the mean sea surfaces and annual variability observed by ERS-1 with those observed by TOPEX. The accuracy of the corrected ERS-1 orbits is also estimated by analysis of the geographically correlated (mean and variable) radial error and by comparison to ERS-1 orbits corrected by cubic splines.

Chapter 9 describes part of the exercise carried out at Aston University as its contribution to ESA's ERS-2 Radar Altimeter and Microwave Radiometer Commissioning Working Group. This involves determining the relative altimeter range bias between ERS-1 and ERS-2 and, to a lesser extent, the relative altimeter range biases between the ERS satellites and TOPEX.

Finally, in chapter 10 the conclusions that can be drawn are discussed. Further, the acheivements in relation to the aims of reducing errors present in the ERS altimeter datasets are outlined. Some suggestions for future work are also presented.

Chapter 2

An Introduction To Satellite Altimetry

2.1 Introduction

The principle of satellite altimetry was first demonstrated as early as 1973 by astronauts on SKYLAB operating a hand held device. Whilst this manned mission only lasted ten months (May 73 - Feb 74) and the altimeter only operated occasionally with a precision poor by today's standards, the experiment showed the possibilities and laid the foundations for altimetric global monitoring of the world's oceans.

The next mission to carry an altimeter, GEOS-3, was launched in April 1975. This mission continued until December 1978 with a range precision of approximately 50cm [Stanley, 1979]. This precision is inadequate for most oceanographic purposes but GEOS-3 altimetry has been used in the development of the most recent gravity field models such as the GEM [Lerch et al, 1994] and JGM [Nerem et al, 1994] model series.

1978 then saw the launch of the first satellite dedicated to ocean monitoring in the form of SEASAT. This satellite had a much improved altimeter precision of approximately 10cm [Tapley et al, 1982], however, the mission only lasted three months due to a power supply fault resulting in the mission's termination.

A gap of seven years was then experienced until the launch of GEOSAT, a US

Navy satellite, in 1985. This satellite, with an altimeter range precision of 3.5cm [Wakker et al, 1990], had the mission objectives of determining a better geoid and ocean mesoscale. The GEOSAT mission consisted of two stages. The first of these was initially classified, lasted 18 months and was called the geodetic mission. The second phase called the exact repeat mission had a repeat period of 17 days (similar to SEASAT).

As this satellite used gravity gradient stabilization as part of it's attitude control the satellite design resulted in a degradation in orbit accuracy for periods of increased solar activity. Also the lack of an instrument to measure the atmosphere's water content for the determination of the wet tropospheric correction limited the accuracy of the altimeter data.

Table 2.1. Altimetric Satellite Height and Inclinations.

Satellite	Height (km)	Inclination (deg)
GEOS-3	848	114.9
SEASAT	793	108.0
GEOSAT	791	108.0
ERS-1	785	98.0
TOPEX/Poseidon	1350	66.0
ERS-2	785	98.0

The range accuracy of each of these missions has increased to the extent that the altimeter precision is no longer a significant error source for most altimetric missions, and is now dominated by radial orbit and media correction errors. Initially the radial orbit error for these missions was quite poor (being in excess of 1m for SEASAT [Schrama, 1989]) and the limiting factor in the use of the altimeter data. However, with improvements in the gravity field models through analysis of satellite tracking data, the radial errors for these

satellites (in the latest recomputed orbits) and for current missions are much lower, being sub 20cm rms [Schum et al, 1990].

With the launch of ERS-1, TOPEX/Poseidon and ERS-2 (see chapter 3 for descriptions of these satellites and their missions) two altimetric satellite missions have been operating simultaneously from 1992. The ERS satellites are of similar design, with the exception of the GOME experiment, and orbit at the same orbital height and in the same orbital plane. Orbits of the ERS satellites have radial orbital accuracies of 10-15cm [Scharroo et al, 1993] whilst the altimeter precision is 3cm [Schum et al, 1994]. TOPEX/Poseidon, with it's much better defined orbit (due to its higher altitude and comprehensive tracking with DORIS, SLR and GPS data) and state of the art dual frequency altimeter, has a radial orbit accuracy of 3-4cm [Marshal et al, 1995] and an altimeter range precision of 2cm [Tapley et al, 1994].

If the data sets of these overlapping (and finally non overlapping) missions are to be merged for long term ocean studies it is necessary to reduce the errors in the satellite orbits and altimeter measurements to the extent that they are minimal and as near homogeneous as possible.

This thesis is therefore primarily concerned with the integration of ERS-1 and TOPEX/Poseidon altimeter data through the reduction of ERS-1 orbit error; the estimation of the TOPEX/Poseidon - ERS-1 relative range biases and analysis of the sea state bias for ERS-1.

First, however, the principles of satellite altimetry, the measurements and the corrections that need to be applied are discussed.

2.2 The Principles of a Satellite Altimeter.

Essentially an altimeter is a device that measures the two way propagation

delay and characteristics of a microwave radar pulse return signal that has been reflected from the Earth. Whilst this thesis is only concerned with altimetry over the oceans, altimeter data also has many applications over land and ice as altimeter data can be used for the determination of the shape of the Earth, it's elevation and surface roughness, measuring the wavelength and direction of ocean waves, observing the direction and strength of winds over the ocean surface and monitoring the size and thickness of ice floes in the polar regions.

The altimeter transmits a series of microwave radar pulses towards the Earth (as shown in figure 2.1) and the return echo's shape , power and propagation delay are then measured.

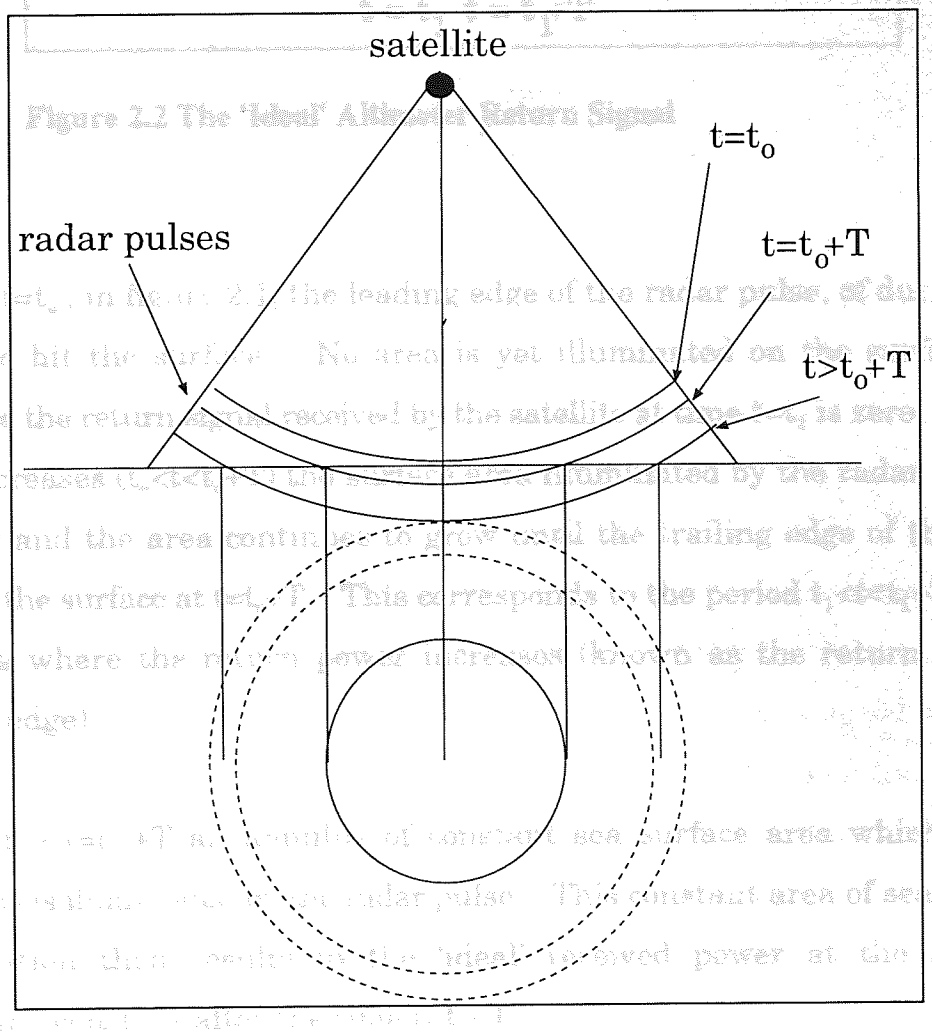

Figure 2.1 The Satellite Altimeter Radar Pulse

Assuming the reflective surface is flat (a reasonable approximation for the oceans) the reflection will be purely specular. This would result in the return signal received by the satellite as shown in figure 2.2.

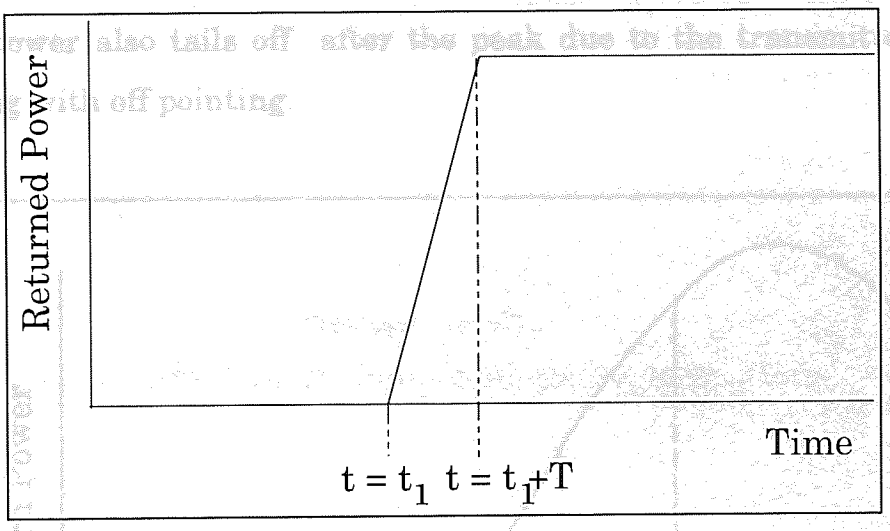

Figure 2.2 The 'Ideal' Altimeter Return Signal

At time $t=t_o$, in figure 2.1, the leading edge of the radar pulse, of duration T, starts to hit the surface. No area is yet illuminated on the surface and therefore the return signal received by the satellite at time $t=t_1$ is zero. As the time increases ($t_o<t<t_o+T$) the surface area illuminated by the radar pulse is circular and the area continues to grow until the trailing edge of the pulse reaches the surface at $t=t_o+T$. This corresponds to the period $t_1<t<t_1+T$ at the satellite where the return power increases (known as the return signal's leading edge).

After time $t=t_o+T$ an annulus of constant sea surface area which moves outwards is illuminated by the radar pulse. This constant area of sea surface illumination then results in the 'ideal' received power at the satellite remaining constant after the time $t=t_1+T$.

In reality, however, the oceans are not smooth (due to wind driven waves) so that some signal before $t=t_o$ is returned as the leading edge strikes the peaks of the rough surface. Similarly at time $t=t_o+T$ not all of the trailing edge has been reflected because of the wave troughs on the surface. This results in the actual return signal being stretched (as shown in figure 2.3). The return signal's power also tails off after the peak due to the transmitted power decreasing with off pointing.

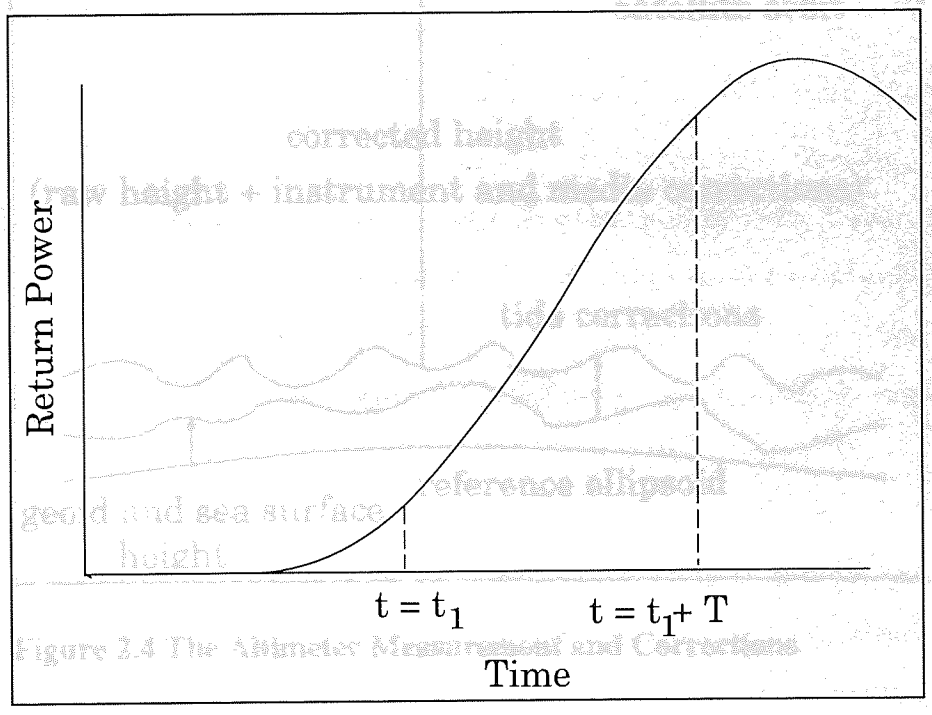

Figure 2.3 The 'True' Altimeter Return Signal

Analysis of the return signals allows several distinct measurements to be made. The mid point of the leading edge is used to determine the propagation delay (hence the range to the instantaneous sea surface can be calculated), the slope of the stretched leading edge is dependent upon the surface roughness (thus allowing the significant wave height to be determined) and the power of the return signal will give details regarding the reflective properties of the illuminated surface (ie backscatter coefficient which is related to wind speed).

2.3 The Altimeter Range Measurement

For practical use the raw altimeter range measurement must be corrected for several instrumental and atmospheric factors. Figure 2.4 illustrates how a typical raw range measurement is corrected to give the satellite height above the reference ellipsoid.

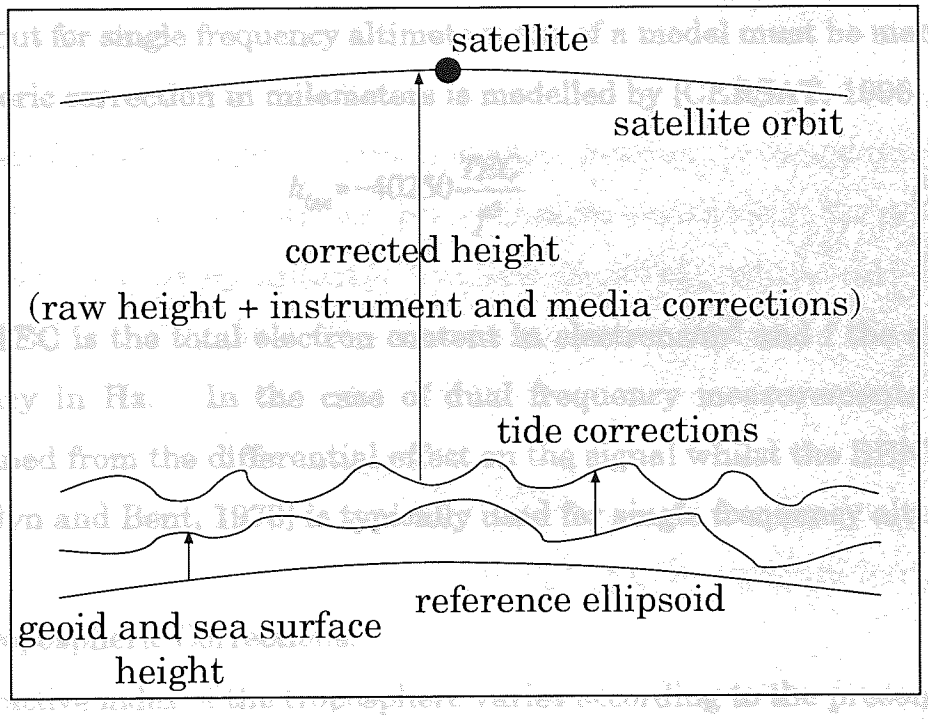

Figure 2.4 The Altimeter Measurement and Corrections

The corrected altimeter range measurement, h_{corr}, which is a measure of the satellite's height above the instantaneous sea height, can be expressed by equation (2.1),

$$h_{corr}=h_{raw}+h_{ion}+h_{wet}+h_{dry}+h_{inv}-h_{ssb}-h_{bias} \qquad (2.1)$$

where h_{raw} , h_{ion} , h_{wet} , h_{dry} , h_{inv} , h_{ssb} and h_{bias} are the raw altimeter range measurement, ionospheric correction, wet tropospheric correction, dry tropospheric correction, inverse barometer correction, sea state bias and altimeter bias respectively. The final two corrections are subtracted as convention states that biases should be removed.

2.3.1 The Ionospheric Correction.

As the radar pulse travels through the ionosphere the path's refractive index varies due to the presence of free electrons. This variation is not only dependent upon height but also local solar time, time of the year, solar activity and signal frequency. The most precise determination of it's effect on the altimeter range measurement can be made from analysis of dual frequency signals but for single frequency altimeters use of a model must be made. The ionospheric correction in milemeters is modelled by [CERSAT, 1996],

$$h_{ion} = -40250\frac{TEC}{f^2} \qquad (2.2)$$

where TEC is the total electron content in electrons/m^2 and f the altimeter frequency in Hz. In the case of dual frequency measurements TEC is determined from the differential effect on the signal whilst the BENT Model [Llewellyn and Bent, 1973] is typically used for single frequency altimeters.

2.3.2 Tropospheric Corrections.

The refractive index of the troposphere varies according to the presence of air and water vapour which also require correcting. Corrections for the troposphere thus consist of two components.

(i)Dry Tropospheric Correction. This correction whilst large, being of the order of two meters, remains relatively constant and compensates for the change in refractive index due to the presence of air. The dry tropospheric correction in milimeters is defined by equation (2.3) [CERSAT, 1996],

$$h_{dry} = -2.277P_{surf}(1+0.0026cos2\Phi) \qquad (2.3)$$

where Φ is the satellite latitude and P_{surf} is the surface pressure of the atmosphere at the sub satellite point as defined by meteorological models and measured in milibars .

(ii)Wet Tropospheric Correction. Unlike the dry tropospheric correction this is highly variable, is of the order of decimeters and compensates for the change in refractive index due to the presence of water vapour. The correction is obtained from measurements of total integrated water vapour from a microwave radiometer on board the satellite or by use of meteorological models.

2.3.3 The Inverse Barometric Correction

This correction is an empirical correction which attempts to compensate for the fact that variations in atmospheric pressure cause variations in the sea surface and is approximately equivalent to 1cm for each mb of pressure variance from 1 atmosphere (1013.3mb). The inverse barometric correction in milimeters is modelled by equation (2.4) [AVISO, 1992],

$$h_{inv} = -9.948(P_{surf} - 1013.3) \qquad (2.4)$$

where the surface atmospheric pressure, P_{surf} , can be obtained from the dry tropospheric correction (equation (2.3)).

Whilst this empirical correction is known to be quite accurate for most latitudes, errors in excess of 100% have been observed close to the equator [Woodworth, 1996]

2.3.4 The Sea State Bias.

Due to the distribution of sea surface reflective facets and the altimeter tracker's properties, altimeter measurements are biased towards the troughs of waves (range measurement is too long). The correction applied to account for this is called the sea state bias. A more detailed discussion of the sea state bias, and how it is modelled, can be found in chapter 5.

2.3.5 The Altimeter Range Bias.

All altimeters have a unique offset called an altimeter bias. This is caused by electronic delays within the altimeter itself and is usually determined from the altimeter data during the commissioning phase of the satellite. It is of great importance to determine this offset accurately as different satellites will possess different altimeter biases (as is also the case for sea state biases) and the integration of altimeter datasets requires the removal of these offsets.

Once all geophysical and instrumental corrections have been applied a measure of the instantaneous sea height averaged over the altimeter's footprint is obtained. In order to measure the mean sea height it is also necessary to correct for tidal effects (such as ocean, loading, pole and solid earth tides). The corrected altimeter range to the mean sea surface is then added to the geoid and mean sea surface heights (as defined in figure (2.4)) at the sub satellite point to give the height above the reference ellipsoid.

As altimeter data is typically available in one second averaged values (the satellite will move approximately 6-7km along track in one second) it is apparent that satellite altimetry is an extremely valuable global tool for the long term monitoring of the world's oceans.

2.4 The Crossover

Often, such as in satellite tracking, the errors (usually geoid and sea surface) present in the altimeter range measurements are too large. This has resulted in satellite crossovers being used for tracking purposes and for oceanographic studies of variability.

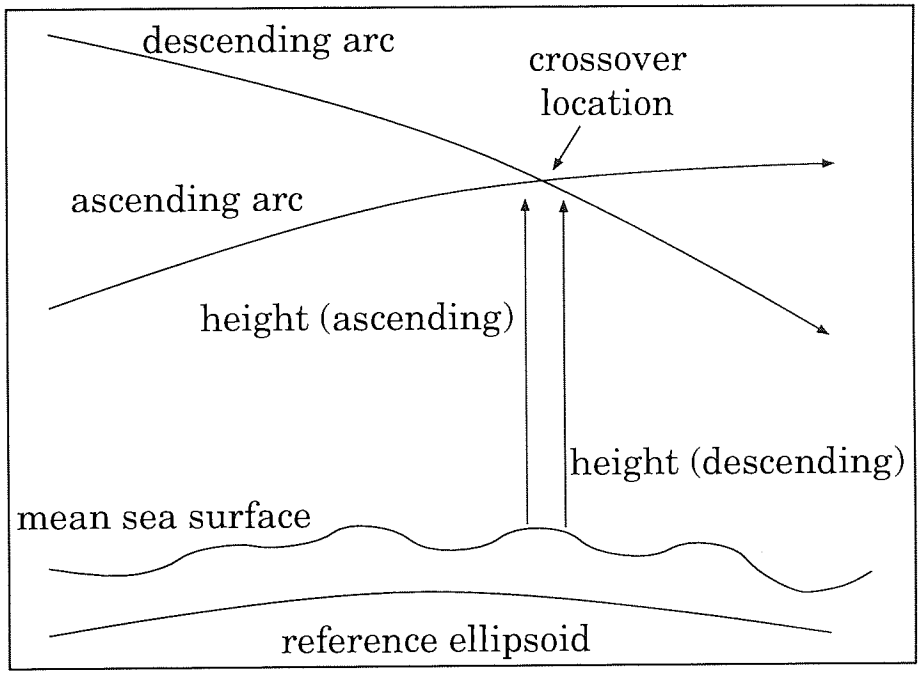

Figure 2.5 The Crossover

Figure 2.5 shows the single satellite crossover as the intersection of two groundtrack passes, one ascending and the other descending. At a crossover the geoid and sea surface topography (providing the time difference between observations is not too large) will be the same for both epochs and therefore cancel in the formation of the dataset. This allows time varying parameters such as sea surface variability and ocean tides to be monitored more accurately. Alternatively the time varying signal can be treated as noise and the crossover difference used in orbit determination as a measure of the normal height differences between the two epochs.

With the launch of TOPEX/Poseidon the availability of two simultaneous altimeter datasets has allowed dual satellite as well as single satellite crossovers to be used. Dual satellite crossovers use the intersection of groundtracks from different satellites and may be composed of two descending, two ascending or one ascending and one descending arc depending upon the orbital charecteristics of the satellites in question. Thus whilst the time independent errors (such as geoid and mean sea surface) still cancel,

information that cannot be obtained from single satellite crossovers (such as the geographically correlated orbit error) is now recoverable.

The bulk of this thesis uses single and dual satellite crossovers as a means of unifying and calibrating different altimeter datasets.

Chapter 3

Altimetric Satellite Mission Overviews for 1991 - 1996

3.1 Introduction

With the launch of ERS-1 (European Remote Sensing satellite 1), ERS-2 (European Remote Sensing satellite 2) and TOPEX/Poseidon there exists for the first time three altimetric satellites which for part of their missions are operating simultaneously. Whilst ERS-1 is the primary satellite as far as this thesis is concerned, and altimetry the data set utilised, some basic information regarding ERS-2, TOPEX/Poseidon and the other instruments carried by these three satellites is provided.

3.2 ERS-1

ERS-1 is an ESA (European Space Agency) multipurpose earth observation satellite. It was launched on 17th July 1991 by an Ariane 4 rocket, from Kourou in French Guiana, into an orbit of inclination 98.5 degrees and nominal altitude 785km. The orbit is almost circular and is sun synchronous, in which the orbital plane rotates at the same rate as the Earth about the Sun thus ensuring near uniform shadowing for the SAR (Synthetic Aperture Radar) along any repeat tracks. The orbital elements have also been chosen so that the orbit is 'frozen' [Cook, 1966] therefore ensuring that the perigee location remains fixed at 90 degrees. Figure 3.1 shows the ERS-1 satellite and its scientific payload.

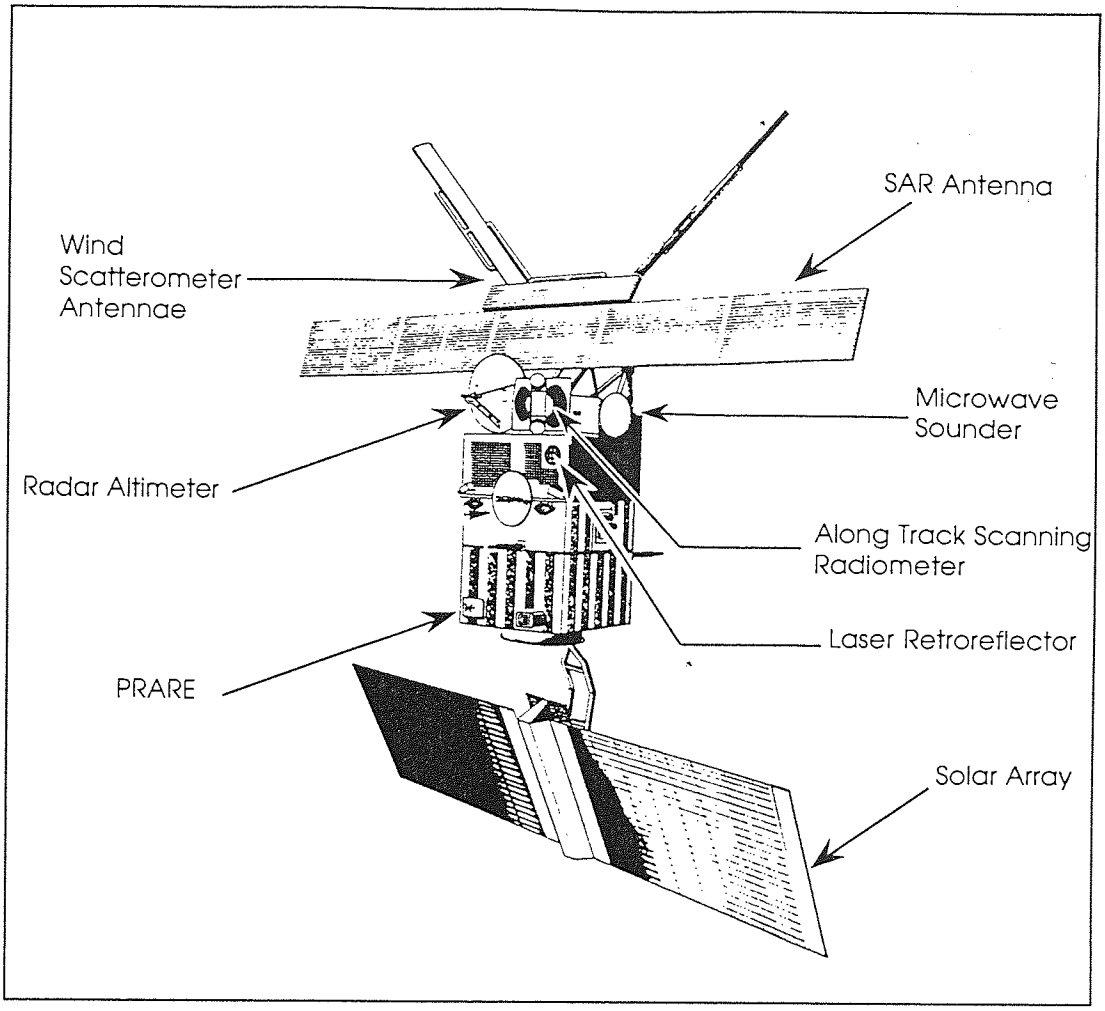

Figure 3.1 The ERS-1 Satellite, BNSC [1990].

3.3 ERS-1 Instrumentation

Due to ERS-1 being a multipurpose satellite the instruments carried are many and include an earth pointing radar altimeter, an along track scanning radiometer, an active microwave instrument, precise range and range rate equipment and a laser retro reflector. A brief description of each now follows.

3.3.1 Earth Pointing Radar Altimeter.

The altimeter onboard ERS-1 is a single frequency (13.8GHz) radar altimeter which operates in two measurement modes. These modes are optimised for measurements over ice and ocean. In the ocean mode the altimeter measures

the instantaneous sea height, wave height and surface wind speed over a footprint of diameter 7km. Whilst in ice mode the altimeter can make measurements (although of a much coarser resolution than ocean mode) of ice/land topography.

3.3.2 ATSR (Along Track Scanning Radiometer).

The ATSR consists of two components known as the Infrared Radiometer and the Microwave Sounder.

The Infrared Radiometer measures the sea surface and cloud top temperatures, which are accurate to near 0.5K, over an area of 50km by 50km [CERSAT, 1996].

The Microwave Sounder is a nadir viewing passive radiometer which measures the total water content of the atmosphere within a 20km diameter footprint. This information is used to correct the Infrared Radiometer's sea surface temperature as well as determine the wet tropospheric correction for the altimeter.

3.3.3 Active Microwave Instrument.

This instrument also consists of two components, these being the SAR (Synthetic Aperture Radar) and the Wind Scatterometer.

Synthetic Aperture Radar - This produces images of the sea/land surface in 100km wide strips. Due to power/thermal constraints imposed by the satellite design it is only able to operate for a maximum of twelve minutes each orbit. The high data rate (105 Mbit/s) is too high for on board recording and constrains the operation of the instrument to when the satellite is in contact with a receiving ground station.

Wind Scatterometer - This instrument consists of three sideways looking antennae which illuminate a 500km wide swath and measure the radar backscatter enabling the surface wind vectors to be deduced.

3.3.4 PRARE (Precise Range and Range Rate Equipment).

An all weather microwave tracking system, this instrument, in conjunction with a network of ground based transponders takes two way range and range rate measurements. The system was intended to enhance the global coverage of satellite tracking available by providing data in the southern hemisphere where there is a shortage of laser range data. However, shortly after launch the system suffered permanent radiation damage resulting in it being switched off. This initially caused the ERS-1 orbits to be much poorer than expected, particularly for the early part of the ERS-1 mission when solar activity was high resulting in large changes in atmospheric density. With the reduction in solar activity, improvement in gravity field models and orbit determination procedures to absorb along track mis-modelling, the accuracy of ERS-1 orbits has, however, been greatly improved.

3.3.5 Laser Retro Reflector

This is a passive device, consisting of an array of corner cubes, which is used as a target for ground based laser stations. These laser range measurements are then used for satellite tracking. With the failure of PRARE laser range data has been the primary tracking data set for ERS-1.

3.4 ERS-1 Mission Details

Due to the multipurpose nature of ERS-1's mission the satellite has undergone several mission phases. Each of these phases are now described.

3.4.1 Commissioning Phase (31 Jul 91 - 20 Dec 91)

Starting soon after launch this phase had a 3 day repeat period, consisting of

43 orbital revolutions, which results in an equatorial ground track spacing of approximately 930km as shown in figure 3.2.

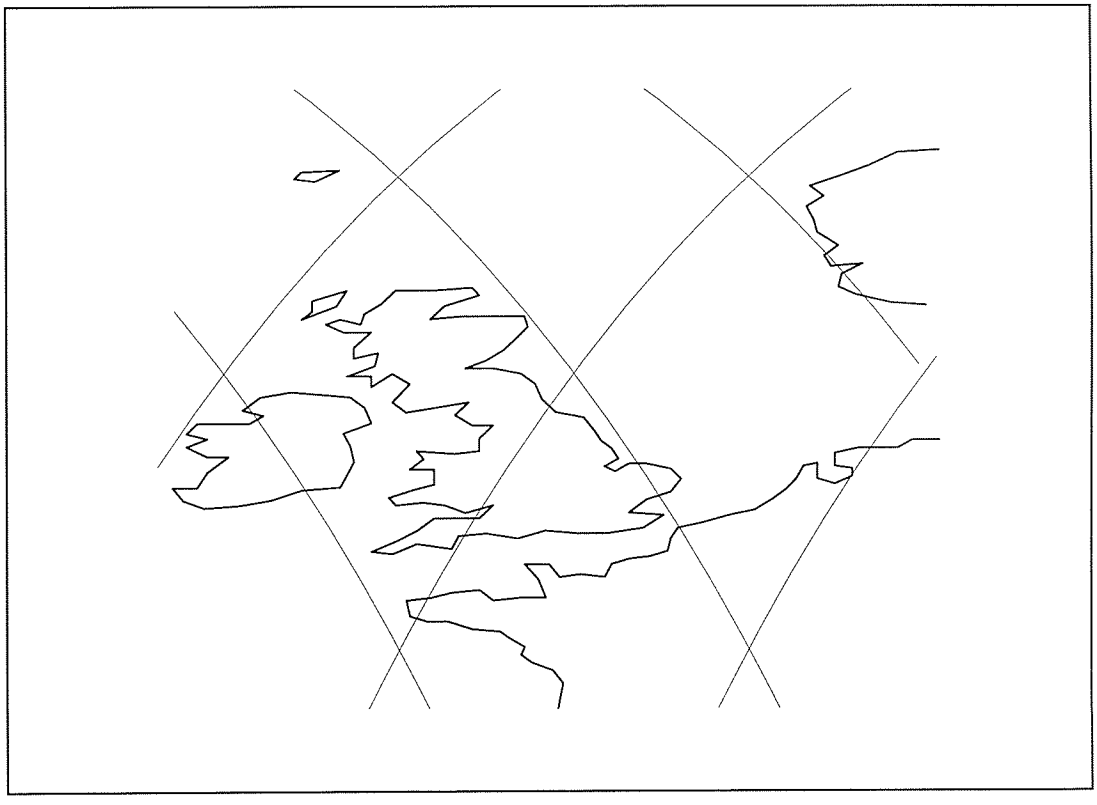

Figure 3.2 ERS-1's Commissioning Phase Groundtrack.

The commissioning phase was primarily concerned with the calibration of the instruments (such as the Venice tower calibration exercise [Francis, 1993]) which required frequent observations at the various calibration sites.

3.4.2 First Ice Phase (28 Dec 91 - 30 Mar 92)

Following the Commissioning Phase the satellite ground track was shifted some 2° westwards (still retaining the 3 day repeat period) so that specific ice zones in the arctic and antarctic were overflown frequently. This 2° westwards shift resulted in the ground track passing very close to the Herstmonceux laser range station and this close overpass has been used to

determine the absolute ERS-1 altimeter range bias from short arc analysis [Lam et al, 1993].

3.4.3 First Multi-disciplinary Phase (14 Apr 92 - 20 Dec 93)

Using a 35 day repeat period with 501 orbital revolutions, giving an equatorial ground track spacing of 80km, as described in figure 3.3 this phase was primarily designed for land/ice mapping using the Synthetic Aperture Radar.

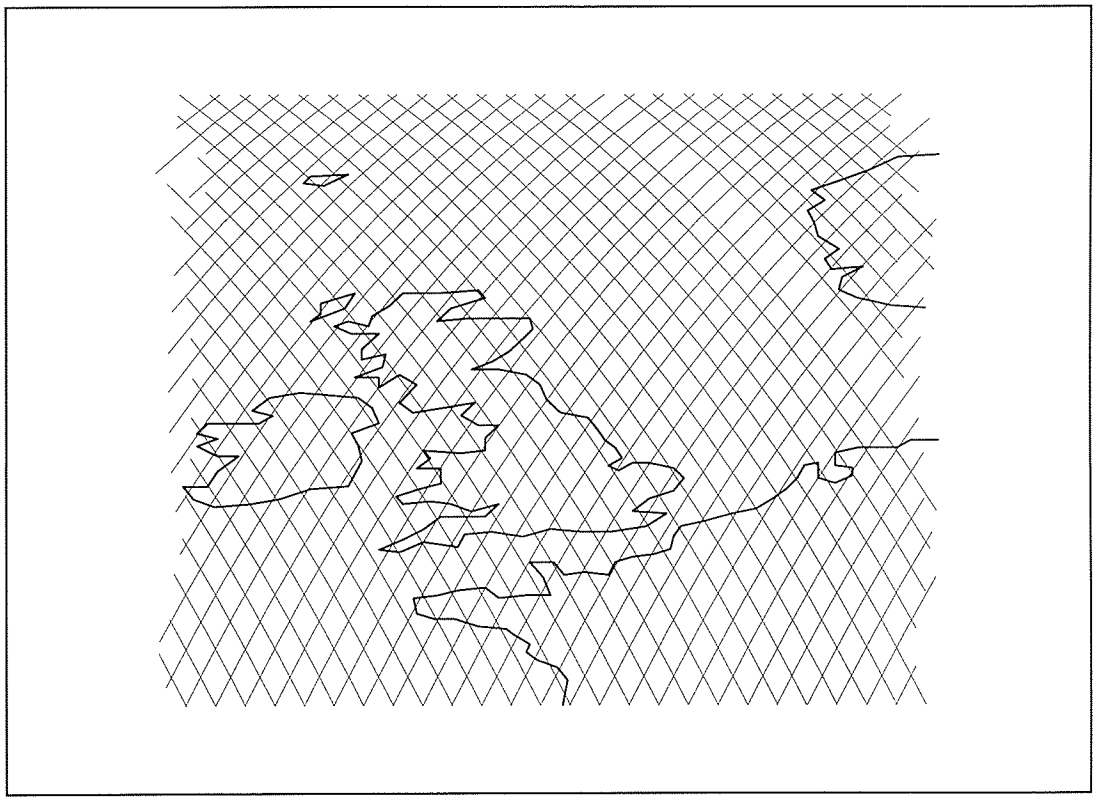

Figure 3.3 ERS-1's Multi-disciplinary Phase Groundtrack.

The much denser spatial coverage of the worlds oceans and the relatively frequent repeat period, however, provides a very valuable oceanographic altimeter data set.

3.4.4 Second Ice Phase (23 Dec 93 - 10 Apr 94)

Essentially this phase, although carried out two years later, was the same as

the first ice phase.

3.4.5 First Geodetic Phase (10 Apr 94 - 27 Sep 94)

Using a 168 day repeat track of 2411 orbital revolutions, with an equatorial ground track spacing of 16km, as shown in figure 3.4, this phase gives a dense spatial coverage of the worlds oceans and was primarily dedicated to accurate mapping of the marine geoid.

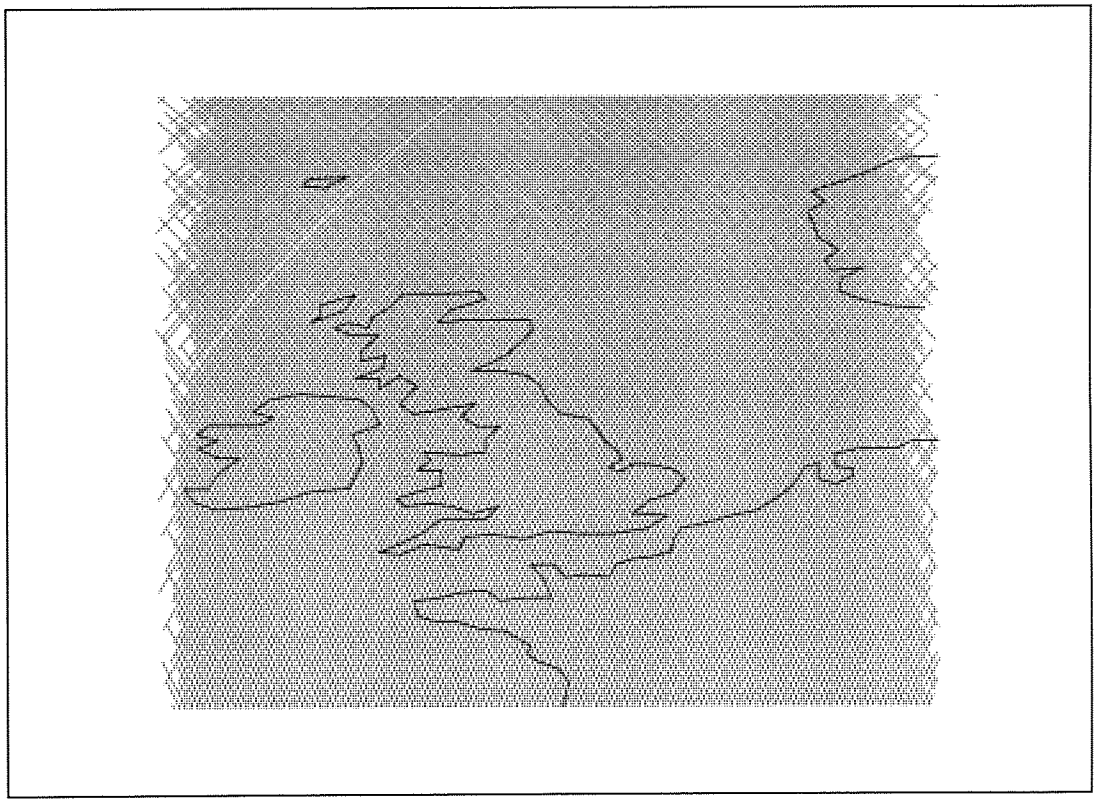

Figure 3.4 ERS-1's Geodetic Phase Groundtrack.

3.4.6 Second Geodetic Phase (27 Sep 94 - 21 Mar 95)

This phase was very similar to the first geodetic phase except that the ground track had been shifted 8km longitudinally to double the resolution of the recoverable marine geoid.

3.4.7 Second Multi-disciplinary Phase (21 Mar 95 - Jun 96)

Using the same repeat period (35 days), this phase was primarily a continuation of the first multi-disciplinary phase. With the launch of ERS-2 (see section 3.5) a tandem satellite period lasting between May 95 and June 96 provided a unique ERS-1/2 dual satellite altimeter data set. During this period ERS-1 was designated the primary ESA satellite with ERS-2 fulfilling a secondary role.

3.4.8 Dormant (Jun 96 until ERS-2 Failure)

After operating in the tandem phase ERS-1 was 'switched off', in the sense that data is no longer continually transmitted by the satellite to the ground stations, in June 1996. The plan is to keep ERS-1 in a dormant mode to extend it's lifetime until the failure of ERS-2 when it is 'expected' to be returned to 'life' thus ensuring that any possible gap between the failure of ERS-2 and launch of ENVISAT will be covered. This overlap of data will allow ENVISAT to be calibrated with respect to ERS missions allowing a consistent merging of the data sets to be carried out.

3.5 ERS-2

Launched from Kourou, French Guiana, by an Ariane 4 rocket on 21st April 1995 ERS-2 is the second ESA remote sensing satellite. Based on ERS-1, the design of ERS-2 is essentially the same as ERS-1. ERS-2, however, also carries the new GOME experiment and the PRARE equipment has been enhanced with redundant capability. The orbital characteristics of ERS-2 are identical to those of ERS-1 with the exception that ERS-2 orbits some 20 minutes behind ERS-1, with the result that the two ground tracks are the same but with ERS-2 altimeter epochs 24 hours after those of ERS-1.

The repeat period for ERS-2 is 35 days with 501 orbital revolutions (as in ERS-1's multi-disciplinary phases) but there are no plans to change this throughout

the mission life. The first four cycles of ERS-2's mission were dedicated to the calibration of ERS-2 and chapter 9 describes part of Aston University's contribution to this exercise. Initially, ERS-2 fulfilled the role of secondary satellite to ERS-1, however, after June 1996, just prior to ERS-1 entering it's dormant status, ERS-2 became ESA's primary altimeter satellite.

3.6 ERS-2 Instrumentation

With the following exceptions the instrumentation on board ERS-2 is identical to that carried onboard ERS-1.

3.6.1 Radar Altimeter.

The design of the ERS-2 altimeter is the same as for ERS-1. However, the onboard tracking software has been slightly modified which has resulted in small differences between the ERS-1 and ERS-2 altimeter data sets (refer to chapter 9 for more details).

3.6.2 PRARE.

Unlike the PRARE system on board ERS-1 (see section 3.3) this system is fully operational and is being used as a tracking device for ERS-2. After the failure of PRARE onboard ERS-1 ESA took a larger responsibility (the system was only an announcement of opportunity on ERS-1) of the PRARE onboard hardware ensuring that it was radiation hardened and that the system had inbuilt redundancies. The system was then tested onboard the Russian satellite Meteor 3. Whilst some problems have been experienced with the network of ground beacons it is expected that PRARE will improve the accuracy of ERS-2's orbits such that crossovers will not be required for the orbit determination process.

3.6.3 Global Ozone Monitoring Experiment (GOME)

Carried for the first time on ERS-2 this instrument is a nadir viewing

spectrometer which observes the transmission and/or scattering of solar radiation by the Earth's atmosphere. From these observations quantities of various trace constituents of the troposphere and stratosphere, such as ozone, nitrogen dioxide and water vapour, can be measured.

3.7 TOPEX/Poseidon

The joint NASA/CNES (US/French) satellite TOPEX/Poseidon was launched on August 10th 1992. It was inserted into a near circular orbit of 66 degrees inclination and baseline altitude of 1350 km and is a dedicated altimeter mission for the monitoring of the world's oceans.

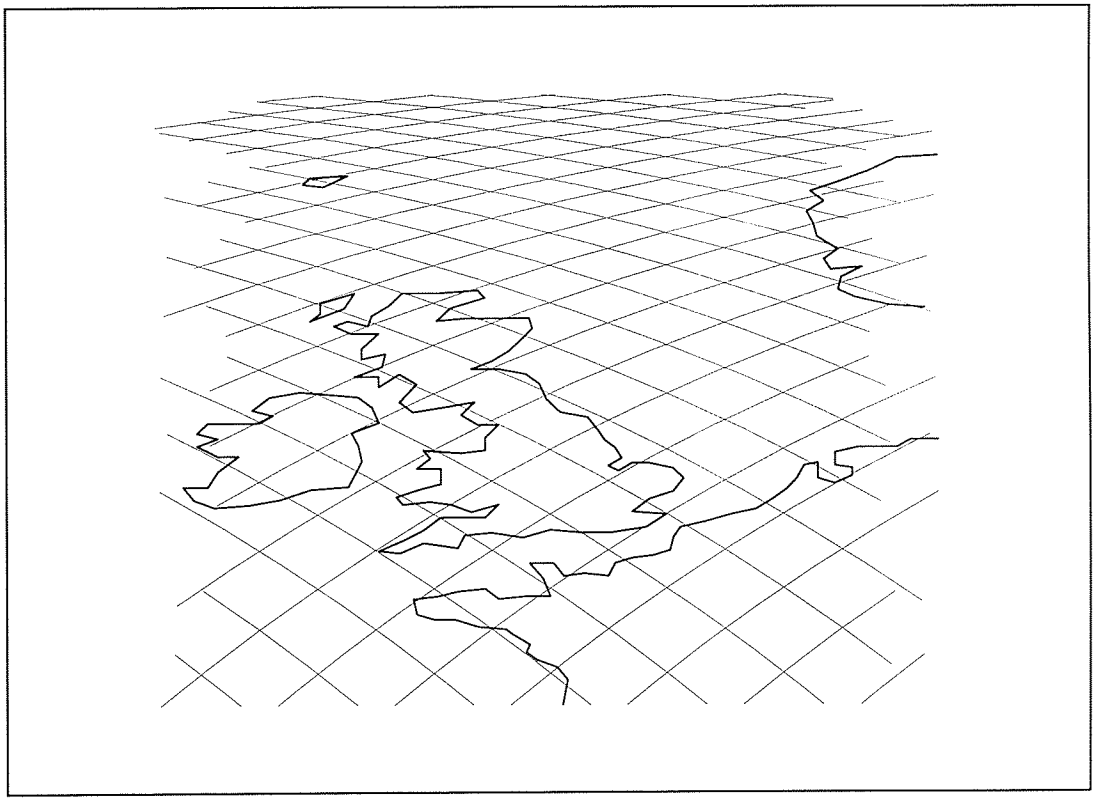

Figure 3.5 TOPEX/Poseidon's Groundtrack

Figure 3.6 shows the design of TOPEX/Poseidon and the instruments carried on board whilst figure 3.5 shows a portion of the 9.92 day repeat ground track of TOPEX/Poseidon consisting of 127 orbits with an equatorial ground track

spacing of 315 km.

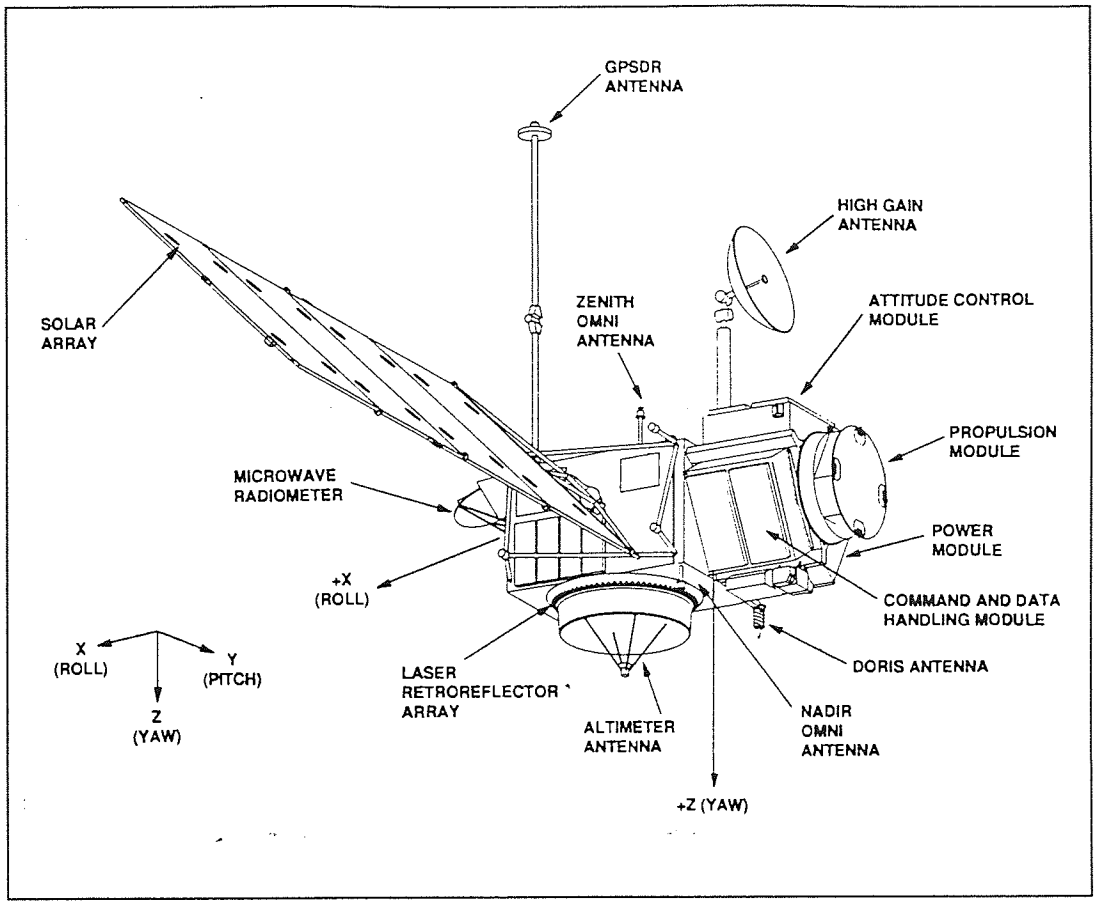

Figure 3.6 The TOPEX/Poseidon Satellite, Fu et al, [1994]

3.8 TOPEX/Poseidon Instrumentation

As Topex/Poseidon is purely an altimetric satellite it's instrumentation consists of the two altimeters (TOPEX and Poseidon) and supporting hardware. Other devices such as DORIS and GPS receivers are carried for satellite tracking purposes.

3.8.1 The TOPEX Altimeter.

An acronym for Topography Experiment this NASA dual frequency (5.3 Ghz C band and 13.6 Ghz Ku band) altimeter is the primary instrument on board

the satellite. It is operational some 90% of the time with ionospheric corrections derived from the dual frequency signal. The wet tropospheric correction is gained from the three frequency (18, 21 and 37 GHz) TOPEX Microwave Radiometer (TMR). After application of the corrections the altimeter range accuracy is approximately 5cm.

3.8.2 The Poseidon Altimeter.

Limited to operating for 10% of the mission time due to sharing the antennae dish with TOPEX, the CNES single frequency (13.65GHz) altimeter is a state-of-the-art solid state altimeter. Poseidon is smaller, lighter and more energy efficient that it's TOPEX counterpart, however, it's experimental status has resulted in it being designated the secondary altimeter. As the altimeter only operates at a single frequency it is necessary to use alternative instrumentation to determine the ionospheric correction.

3.8.3 DORIS (Doppler Orbitography in Space) Receiver.

This instrument is an all weather tracking system that measures the satellite range rate by observing the Doppler shift of two frequencies transmitted by a network of globally distributed omni-directional beacons. The secondary function of this instrument uses the dual frequency signal as a means of determining the ionospheric correction for the single frequency Poseidon altimeter.

3.8.4 GPS (Global Positioning System) Receiver.

This instrument is a NASA experimental tracking device which provides near continual coverage by utilising the network of GPS satellites. The Orbits generated using this data are very accurate, however, as these orbits are determined with a 'reduced dynamic solution' they are only used as an independent check of the primary, DORIS and SLR, orbits.

3.8.5 Laser Retro Reflector.

In addition to the DORIS and GPS receivers the satellite has a ring of laser reflecting corner arrays. This allows ground based laser ranging stations to track the satellite.

3.9 Conclusions

The mission phases and objectives as well as the instrumentation for the satellites ERS-1, ERS-2 and TOPEX/Poseidon have been discussed in this chapter. The ERS satellites being multipurpose missions have orbits that are a compromise between the requirements of the SAR and altimeter. This has resulted in a degradation in the achievable orbital accuracies for ERS-1. TOPEX/Poseidon providing the more accurate orbits, due to it's higher altitude and more comprehensive tracking data, is undoubtably of more immediate use to oceanographers. However, the denser and higher latitude global coverage of the ERS satellites means that the altimeter data obtained by these satellites is still of vital scientific importance, particularly for the monitoring of ice sheets in the Arctic and Antarctic. Furthermore the continuation of the ERS satellites and expected overlap with ENVISAT implies that the ERS altimeter data sets will be useful for long term ocean studies.

Chapter 4

Precise Orbit Determination.

4.1 Introduction

With the continual improvement in altimeter accuracies (as described in chapter 2) the need for precise orbits for altimetric satellites has increased dramatically since the SKYLAB experiment of 1973. This chapter describes the precise orbit determination procedure/software (the package being called SATAN-A) currently employed at Aston University that underpins the work in the following chapters.

Precise orbit determination is an iterative process in which the estimated orbital position is refined in a least squares sense to best fit the tracking data. Each iterative step consists of two stages namely orbit prediction and orbit correction.

4.2 Orbit Prediction

To predict a satellite's position an 8^{th} order Gauss-Jackson numerical integrator is used to integrate the equations of motion and the variational equations in the J2000 co-ordinate system.

4.2.1 Co-ordinate Systems

The pseudo inertial reference frame used in the orbit determination is a cartesian co-ordinate system known as J2000. This system is defined by the Earth's axis of rotation and the first point of Aries (as shown in figure 4.1).

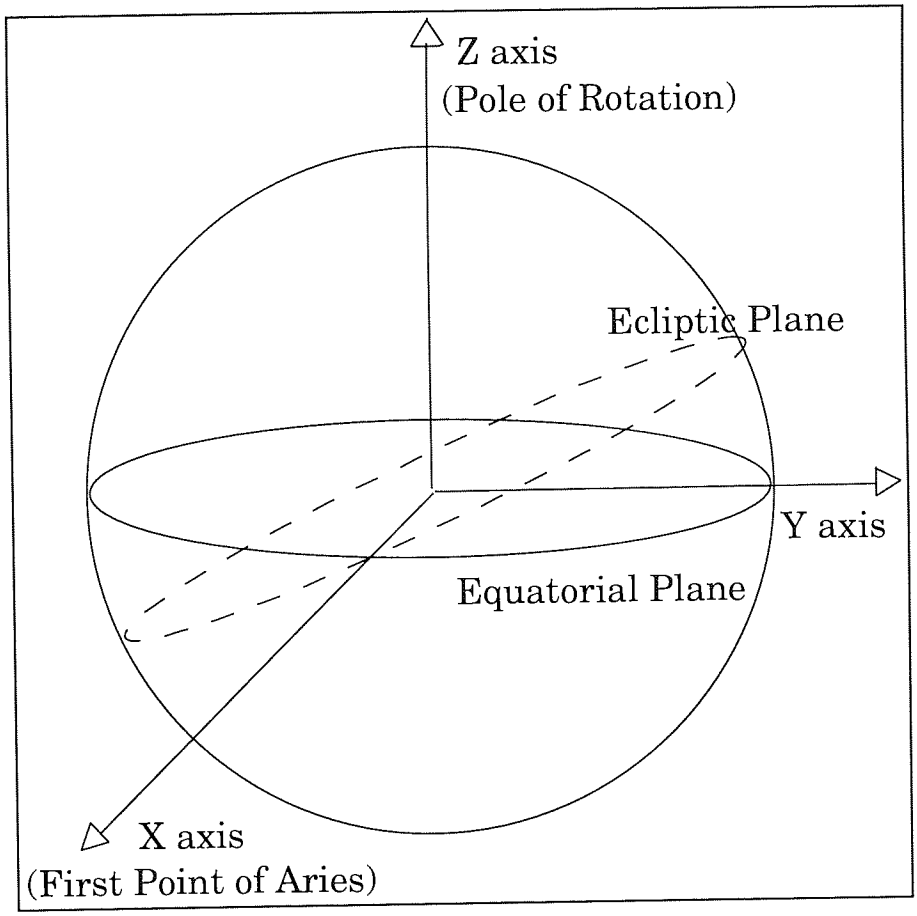

Figure 4.1 The J2000 Co-ordinate System

As the equatorial plane is not constant due to movement of the Earth's rotational axis, caused by nutation and precession, and the ecliptic plane slowly changes with time, a specific reference date (1st January 2000) is used. Sometimes it is desirable to work in a co-ordinate system based upon the current axis of rotation and first point of Aries. This is called the true of date axis system and is obtained by simple axis rotations to account for the precession and nutation of the pole and change in the plane of the ecliptic.

Finally an Earth fixed system is used when the satellite's position relative to the Earth is important (such as determining the Earth's gravity). This co-ordinate system is defined by rotating the true of date axes to account for the Earth's rotation and polar motion (that caused by the Earth's crust moving

with respect to the core) so that the x axis intersects the Greenwich meridian. This then allows terrestrial measurements such as latitude and longitude to be defined and translated to the J2000 system. In essence to express a vector $\underline{x}_{J2000}$ which is defined in the J2000 co-ordinate system as a vector $\underline{x}_{EF}$ in the earth fixed system requires three rotation matrices N, P and S for nutation, precession and 'rotation', where

$$\underline{x}_{EF}=SNP\underline{x}_{J2000} \tag{4.1}$$

4.2.2 Equations of Motion

The equations of motion for a satellite orbiting the Earth can be expressed by equation (4.2),

$$m\ddot{\underline{x}}=F_{grav}+F_{surf}+F_{body}+F_{emp} \tag{4.2}$$

where m is the satellite mass, $\ddot{\underline{x}}$ is the satellite acceleration vector and F_{grav} , F_{surf} , F_{body} and F_{emp} are the force vector due to the Earth's gravitational attraction, atmospheric drag and radiation pressure (surface forces), third body gravitation and empirical forces respectively.

4.2.3 The Earth's Gravitational Attraction

Typically the gravitational potential (U) of the Earth is described in terms of latitude (Φ), longitude (λ) and distance from the Earth's centre (r) by the spherical harmonic expansion given in equation (4.3),

$$U=\sum_{l=2}^{l=\infty}\sum_{m=0}^{m=l}\frac{\mu a_e^{\,l}}{r^{l+1}}\overline{P_{lm}}(\sin\Phi)(\overline{C_{lm}}\cos m\lambda+\overline{S_{lm}}\sin m\lambda)) \tag{4.3}$$

where $\overline{P_{lm}}$ are the normalised associated Legendre polynomials, $\overline{C_{lm}}$ and $\overline{S_{lm}}$ the normalised zonal and tesseral harmonics of degree l and order m (the zonal harmonics having order zero), a_e the Earth's mean equatorial radius and μ the product of the universal gravitational constant

and the Earth's mass.

The gravitational force vector, F_{grav} , can then be described for a satellite of mass m as,

$$F_{grav}=m\nabla U \tag{4.4}$$

Most global gravity field models (such as the JGM series [Nerem et al, 1994]) used in orbit determination are complete to degree and order 70, although some models (ie the OSU series [Rapp et al, 1991]) are complete to degree and order 360

4.2.4 Atmospheric and Solar Radiation Forces

Remote sensing satellites are typically in sufficiently low orbits (altitudes of approximately 1000km) that the Earth's atmosphere, whilst thin, is still dense enough to significantly perturb the satellite motion. For a spherical satellite atmospheric drag is modelled by equation (4.5) [King-Hele, 1987],

$$F_{drag}=-\frac{1}{2}\rho v^2 S C_D \underline{\hat{v}} \tag{4.5}$$

where ρ is the atmospheric density, v the satellite velocity with respect to the atmosphere (the direction being denoted by the unit vector $\underline{\hat{v}}$), S the area per unit mass perpendicular to the air flow and C_D the drag coefficient.

Similarly the force exerted on a satellite by direct solar radiation perturbs the satellite's motion. Whilst for lower orbits (such as for the ERS satellites) this force is small compared to drag, it is still a major source of orbit error if not modelled accurately. The direct solar radiation force for a spherical satellite, with reflectivity coefficient C_R, is given by equation (4.6) [Ries et al, 1992],

$$F_{rad} = -\frac{\Phi}{c} C_R A \hat{\underline{s}} \qquad (4.6)$$

where Φ is the solar flux at the satellite, c the speed of light and A the area per unit mass perpendicular to the satellite sun vector (denoted by the unit vector $\hat{\underline{s}}$)

Both atmospheric drag and solar radiation pressure, are perhaps the most difficult to model accurately due to uncertainties in the atmospheric density (thermospheric models such as MSIS83 [Hedin, 1983] can be wrong by as much as 50-100%) as well as the complexity of modelling gas molecule/ radiation interaction with non-spherical satellite surfaces.

For non spherical satellites a simple approximation to the shape is utilised. Thus for TOPEX/Poseidon a simple box and wing model is adopted whilst for ERS-1 the Aston model [Ehlers, 1993] uses a structure incorporating triangular and quadrilateral panels to represent the satellite body, solar array, SAR antenna and wind scatterometer antennae. For both ERS-1 and TOPEX/Poseidon the orientation of the solar panels relative to the sun is modelled for aerodynamic and solar radiation pressure forces. For drag modelling of the satellite TOPEX/Poseidon the estimated area perpendicular to the satellite vector is derived whilst for solar radiation pressure the surface parameters defined by the TOPEX/Poseidon macro model [Marshal et al, 1992 and Antreasian and Rosborough, 1992] are used.

Extensive studies of ERS-1 have been undertaken at Aston to improve the atmospheric and solar radiation pressure force models. This has resulted in the generation of surface tables for appropriate viewing angles that allow the interpolation of a significant component of each force.

The atmospheric drag model defines the drag force vector, F_{drag} , as ,

$$F_{drag}=A_s\cos\Theta(-P\underline{n}+\tau\underline{t}) \qquad (4.9)$$

where $A_s\cos\Theta$ is the surface perpendicular to the air flow (as shown in figure 4.2) and is derived by the interpolation of the atmospheric force tables described earlier. $\underline{n}$ and $\underline{t}$ are the surface normal and tangent vectors whilst P and τ are the momentum changes for the air flow in the normal and tangential directions.

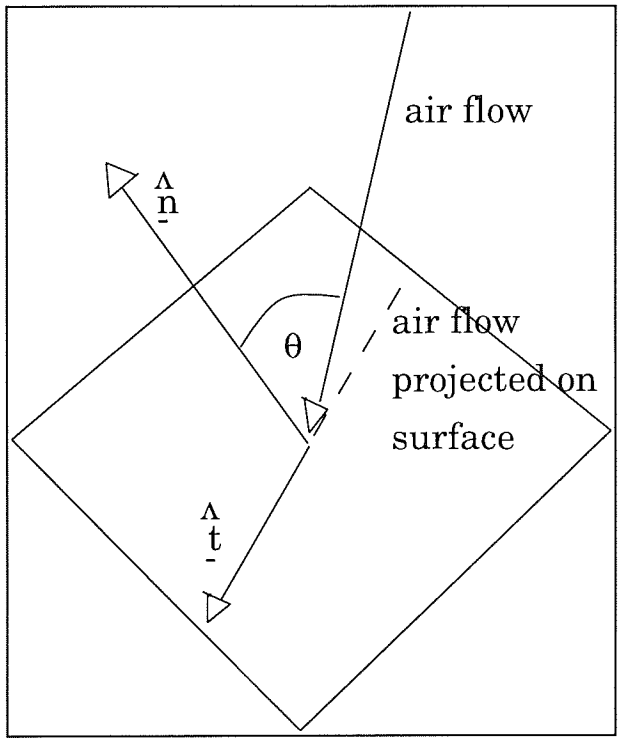

Figure 4.2 Projected Surface Area to Air Flow

The expressions for P and τ [Ehlers, 1993] are complex and dependent upon atmospheric conditions (atmospheric density, temperature and mean molecular mass - as given by the thermospheric model) and properties of the satellite surfaces (such as reflectivity and absorbivity coefficients).

The solar radiation pressure force vector for an i^{th} surface of ERS-1 is defined by the model expressed in equation (4.8),

$$F_{sol}^{i}=\nu\frac{E_o d_{se}^2}{d_{ss}^2}[A_s\cos\Theta_s((1-t_s-r_s)\underline{d}-2(r_s\cos\Theta_s+\frac{r_d-t_d}{3}\underline{n})] \qquad (4.8)$$

where $\underline{d}$ is the incident radiation vector, d_{se} is the sun to Earth distance and d_{ss} is the sun-satellite distance. Further, E_0 is the solar flux per unit area at the Earth and ν a factor ranging from 0-1 depending upon whether the satellite is in the Earth's shadow, penumbra or sunlight. $A_s,\theta_s, t_s,r_s,r_d,t_d$ are the area of the surface, angle of the surface normal with respect to $\underline{d}$, coefficient of transmisivity for specular reflection, coefficient of reflectivity for specular reflectivity, coefficient of reflectivity for diffuse reflection and coefficient of transmisivity for diffuse reflection.

The expression in the square parenthesis of equation (4.8) is similarly interpolated from the solar radiation area tables whilst the multiplier is calculated using planetary data at each integration step.

4.2.5 Earth and Albedo Radiation Forces

The Earth acts as a source of two additional kinds of radiation that influence satellite motion. Of the radiation from the Sun that hits the Earth some is reflected (the percentage known as the albedo) back out to space and therefore affects the satellite motion. This obviously only occurs when the satellite is above a sunlight portion of the Earth.

Given the heat balance of the Earth the remainder of the Sun's radiation incident on the Earth is re-emitted in the form of infra-red radiation. This infra-red radiation will then be reflected by the satellite thus causing an additional continuous acceleration irrespective of whether the satellite is over the sunlit portion of the Earth or not.

To model these additional radiation sources the visible portion of the Earth, with respect to the satellite, is split into 13 regions of equal area when projected onto a plane perpendicular with the geocentric satellite position vector. If the Earth surface element i has area A_i then the force vector, F_{earth}, experienced by the satellite is,

$$F_{earth} = -\sum_{i=1}^{i=13} (\lambda_i \nu C_R P \cos\Theta + P_{IR})(\frac{A_R A_i \cos\alpha}{\pi c d^2})\hat{\underline{e}} \qquad (4.9)$$

where λ_i is the albedo of the Earth element i and ν the shadow factor discussed in section 4.2.4. P and P_{IR} are the solar and earth radiation fluxes per unit area at the Earth (as derived from tables [Vonder Haar and Suomi, 1971]) and the angles Θ and α are defined by the normal vector of the Earth's surface element i (figure 4.3). Finally C_R is the reflectivity coefficient, d the distance between the Earth's surface element and the satellite, A_R the satellite area perpendicular to the satellite's geocentric position vector $\underline{e}_d$ and c the speed of light.

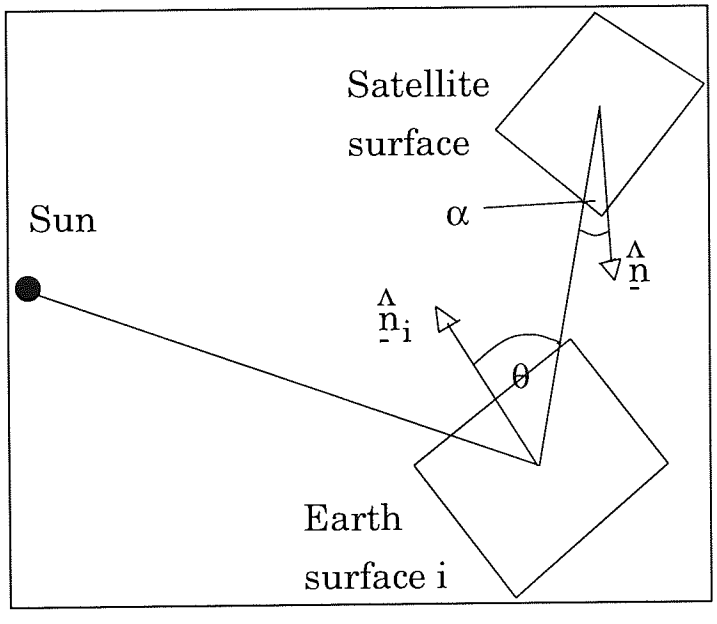

Figure 4.3 Definition of Angles for Earth and Albedo Radiation

The surface force vector, F_{surf}, is therefore defined by equation (4.10),

$$F_{surf}=F_{atmos}+F_{sol}+F_{earth} \tag{4.10}$$

as the sum of the atmospheric, solar radiation and earth radiation forces. No thermal forces for ERS-1 are currently modelled.

4.2.6 Third Body Gravitational Forces

Several celestial bodies are sufficiently massive that their gravitational attractions have a significant effect on satellite motion. These bodies have direct and indirect gravitational attractions.

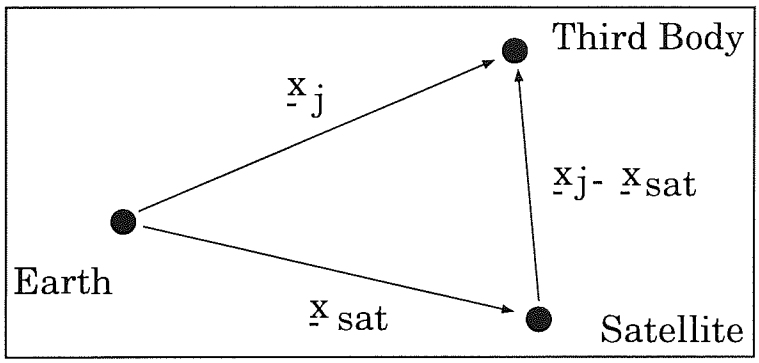

Figure 4.4 The Three Body Problem

The direct gravitational force can be modelled by considering the three body problem described in figure 4.4, where the gravitational acceleration vector, $\ddot{\underline{x}}$, experienced by the satellite (from the Earth and the third body j) is expressed by equation (4.11),

$$\ddot{\underline{x}}=-G\left(\frac{M_E \underline{x}_{sat}}{|\underline{x}_{sat}|^3}-\frac{M_J(\underline{x}_J-\underline{x}_{sat})}{|\underline{x}_j-\underline{x}_{sat}|^3}\right) \tag{4.11}$$

if the mass of the Earth, M_E, j^{th} disturbing body, M_J and satellite M_{sat} , are considered to be point masses.

Now the acceleration vector of the Earth ($\ddot{\underline{x}}_E$) due to the third body (the satellite mass being considered negligible) is given by,

$$\ddot{\underline{x}}_E = G\left(\frac{M_J \underline{x}_J}{|\underline{x}_J|^3}\right) \tag{4.12}$$

so that the acceleration vector for the satellite with respect to the Earth , $\ddot{\underline{x}}_{dir}$, caused by all the third bodies (the moon, sun and planets, Venus, Mars, Jupiter and Saturn) is,

$$\ddot{\underline{x}}_{dir} = G\sum_{J=1}^{J=6} M_J\left(\frac{\underline{x}_J - \underline{x}_{sat}}{|\underline{x}_J - \underline{x}_{sat}|^3} - \frac{\underline{x}_J}{|\underline{x}_J|^3}\right) \tag{4.13}$$

The indirect gravitational attractions of the Sun and moon are also important. As the Earth is not a rigid body the Sun and Moon's gravitational attraction cause a deformation in the shape of the Earth (known as solid Earth and ocean tides). This deformation causes a change in the Earth's gravitational potential which in turn results in the gravitational attraction, as experienced by the satellite, being altered. The change in gravity field caused by the ocean tides is modelled by the JGM-2 ocean tide model [Nerem et al, 1994] and the frequency dependent variation in the Earth's potential is modelled by variations in the coefficients C_{lm} and S_{lm} of equation (4.3). The frequency independent variation, ΔU_{indir}, caused by body J is modelled by equation (4.14),

$$\Delta U_{indir} = \frac{GM_J}{|\underline{x}_J|^3}\sum_{l=2}^{l=\infty} k_l\left(\frac{r}{|\underline{x}_J|}\right)^l\left(\frac{r}{|\underline{x}_{sat}|}\right)^{l+1} P_{l0}(\cos S) \tag{4.14}$$

where the terms S and r are defined in figure 4.5, whilst k_l are the potential love numbers of order l and P_{l0} are the Legendre polynomials.

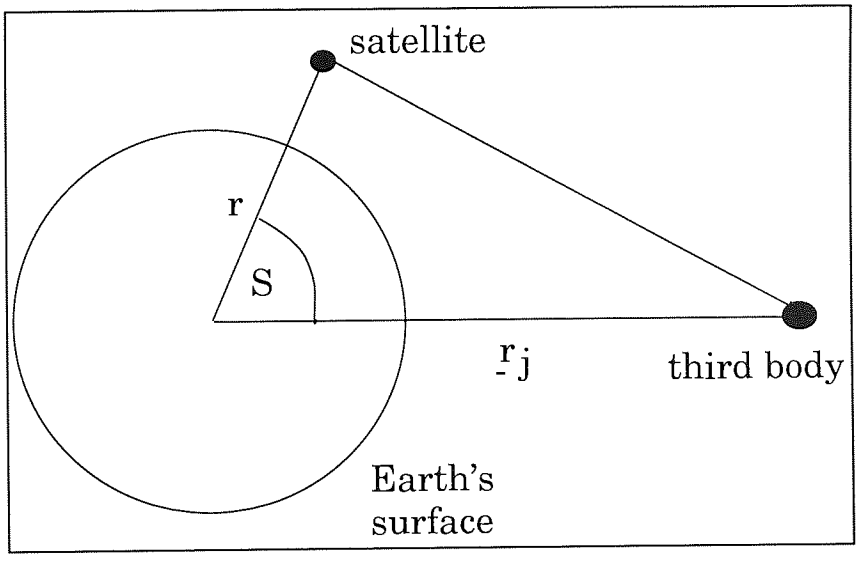

Figure 4.5 Indirect Tidal Forces

As all terms , except for order 2, are considered negligible the indirect gravitational force vector, F_{indir}, experienced by the satellite can be expressed by,

$$F_{indir}=m\nabla(\Delta U_{indir}) \tag{4.15}$$

where

$$\Delta U_{indir}=G\sum_{J=1}^{J=2}\frac{M_J}{|\underline{x}_J|^3}\frac{r^5}{|\underline{x}_{sat}|^3}k_2(\frac{3}{2}\cos^2 S-\frac{1}{2})$$

The resultant force vector due to third body gravitational effects, F_{body}, is therefore expressed by equation (4.16),

$$F_{body}=F_{indir}+m\ddot{\underline{x}}_{dir} \tag{4.16}$$

4.2.7 Empirical Accelerations

Due to imperfections in the modelling of certain forces that act on the satellite it has become customary to include some empirical accelerations in the force

model [Ries et al, 1992]. These empirical acceleration vectors result in the force vector being described by equation (4.17),

$$F_{emp}=m(A\sin U+B\cos U)\underline{a}+(C\sin U+D\cos U)\underline{c} \qquad (4.17)$$

where A,B,C and D are the amplitudes of the once per revolution accelerations in the along track, $\underline{a}$, and cross track, $\underline{c}$, directions. m is the satellite mass and U is the argument of latitude (angle measured in the orbital plane from the ascending node).

In the case of ERS-1 the empirical cross track forces are normally set to zero because the errors are predominantly along track, being caused by drag and gravity field mis-modelling. With TOPEX/Poseidon the empirical forces compensate for mis-modelling in the solar radiation pressure forces so both cross track and along track accelerations are used.

4.3 Orbit Correction

Due to inaccuracies in the satellite's initial position/velocity and force model (and hence equations of motion) significant errors occur at subsequent epochs, and the predicted ephemeris requires correction. This correction is performed by solving for certain force model and orbital parameters using the method of least squares to best fit the tracking data.

4.3.1 Solved for Parameters

The parameters solved for in the orbits determined for this thesis are initial state vector, drag scale factors, a reflectivity scale factor and empirical once per revolution along track accelerations.

The initial state vector is solved for so that the initial position and velocity of the satellite is accurately defined (important for the numerical integration as initial errors will have a knock on effect), whilst the multiple drag scale factors

compensate for mismodelling of the atmosphere and/or satellite geometry (and to a lesser extent gravitational field) by multiplying the atmospheric forces by a continuous saw tooth function (the parameters defining node values at certain intervals). The empirical parameters recovered are the constants A,B,C and D defined in equation (4.17) and the reflectivity scale factor is a multiplier for the solar radiation force.

Current orbit determination procedures involve the recovery of a significantly larger number of parameters. Typically daily values of along and cross track once per revolution accelerations (adding 18 new parameters for an arc of 5 days length) and range biases for the laser range stations are recovered. This has resulted in the rms fits to the laser range and crossover datasets of current ERS-1 orbits being much lower than those outlined in chapters 7 and 8 for the orbits before correction by the non-dynamic procedure.

4.3.2 Dynamic Correction Procedure

The dynamic correction procedure utilised is the least squares differential correction process. This involves using tracking data (such as laser range, altimeter, crossover, DORIS and PRARE data) to refine the orbit parameters, outlined in section 4.3.1, by minimising the function I, defined in equation (4.18),

$$I=\sum_{i=1}^{i=No.Obs} W_i(O_i-C_i)^2 \qquad (4.18)$$

where W_i is the weight attached to each observation O_i (observed measurement of the satellite position) and C_i is the calculated measurement as derived from the satellite's position given by the orbit prediction process.

If the satellite orbit is defined by the model parameters $\underline{P}$ (described in section 4.3.1) where $\underline{P}^+$ are the current estimates, $\underline{P}^*$ the true values and $\underline{\Delta P}$ the corrections to the model parameters, equation (4.18) must be minimised with

respect to all j parameters such that,

$$\frac{\partial I}{\partial P_j} = -2\sum_{i=1}^{i=No.Obs} W_i(O_i - C_i^*)\frac{\partial C_i^*}{\partial P_j} = 0 \qquad (4.19)$$

where C_i^* is the calculated position using the true model parameters $\underline{P}^*$.

Expansion of C_i^* by Taylor's theorem gives,

$$C_i^* = C_i^+ + \sum_{k=1}^{k=No.Param} \frac{\partial C_i^+}{\partial P_k}\Delta P_k + O(\Delta P^2) \qquad (4.20)$$

which on substitution into equation (4.19) yields,

$$\sum_{i=1}^{i=No.Obs} W_i[(O_i - C_i^+) - \sum_{k=1}^{k=No.Param} \frac{\partial C_i^+}{\partial P_k}\Delta P_k]\frac{\partial C_i^+}{\partial P_j} = 0 \qquad (4.21)$$

for each parameter.

The partial derivatives $\frac{\partial C_i^+}{\partial p_j}$ are computed from,

$$\frac{\partial C_i^+}{\partial p_j} = \frac{\partial C_i^+}{\partial \underline{x}}\frac{\partial \underline{x}}{\partial p_j} + \frac{\partial C_i^+}{\partial \dot{\underline{x}}}\frac{\partial \dot{\underline{x}}}{\partial p_j} \qquad (4.22)$$

where the variation equations $\frac{\partial \underline{x}}{\partial p_j}$ are derived within the orbit prediction program as follows. On using equation (4.2) and differentiating with respect to p_j,

$$\frac{\partial \ddot{\underline{x}}}{\partial p_j} = \frac{\partial \underline{F}}{\partial p_j} \qquad (4.23)$$

or,

$$\frac{d}{dt^2}\left(\frac{\partial \underline{x}}{\partial p_j}\right) = \frac{\partial \underline{F}}{\partial \underline{x}}\frac{\partial \underline{x}}{\partial p_j}$$

where $\underline{F}$ is the sum of force vectors acting on the satellite, such that the partials of $\underline{x}$ with respect to p_j (and $\dot{\underline{x}}$ with respect to p_j if required) are estimated by integrating the three second order differential equations along side the equations of motion.

Solving for all parameters, equation (4.21) can therefore be rearranged and written in matrix form (known as the normal equations) as shown in equation (4.24),

$$D\Delta\underline{P}=\underline{b} \tag{4.24}$$

where D is the positive definite matrix with dimensions equal to the number of parameters sought and each element, D_{kj}, defined by,

$$D_{kj}=\sum_{i=1}^{i=No.Obs} W_i \frac{\partial C_i^+}{\partial P_j}\frac{\partial C_i^+}{\partial P_k}$$

and b_j is the j^{th} term of $\underline{b}$ the column vector as expressed by,

$$b_j=\sum_{i=1}^{i=No.Obs} W_i(O_i-C_i^+)\frac{\partial C_i^+}{\partial P_j}$$

The parameter corrections, $\Delta\underline{P}$, can therefore be calculated by pre multiplying equation (4.24) by the inverse of matrix D such that,

$$\Delta\underline{P}=D^{-1}\underline{b} \tag{4.25}$$

Once these parameter corrections have been determined the corrected parameters are then used in the prediction procedure and the prediction-correction procedure continued iteratively until $\Delta\underline{P}\approx 0$.

Utilization of laser range and crossover data in the dynamic solution of typically 5 or 6 days duration for ERS-1 and 10 days for TOPEX/Poseidon provides a radial accuracy of the order 10 - 15 cm for ERS-1 (when using the

JGM-2 gravity field) as opposed to the 3-4 cm typically quoted for TOPEX/Poseidon. It is, however, sometimes possible to improve these long arc dynamic solutions by calculating an additional non-dynamic correction from analysis of altimeter and crossover, single and/or dual satellite, observations.

4.3.3 Non-Dynamic Corrections

Two types of non dynamic correction exist. The simplest of these is the empirical correction such as that employed by [Le Traon et al, 1995] based upon a cubic spline fit where no orbit theory is used. These processes will result in signals other than the orbit error, such as ocean tides and geophysical correction errors, also being removed. Whilst this can be advantageous, caution must be taken that the desired oceanographic signals are not also removed. The alternative is to utilise some orbit theory to minimise the removal of non orbit based signals. Such procedures have been used by many authors [Sandwell et al 1986, Engelis, 1988, Wagner and Melchioni, 1989 and Gray, 1993], and chapters 6,7 and 8 describe the use of such a method for the improvement of ERS-1 orbits.

4.4 Conclusions

Throughout this chapter the force model used in Aston University's orbit prediction software has been described. The process of refining orbits using the method of least squares in a dynamic sense has been discussed and the concept of non-dynamic orbit correction introduced.

Chapter 5

Sea State Bias Determination for ERS-1

5.1 Introduction

In chapter 3 the basic principle of radar altimetry was discussed in that it was shown that the radar altimeter measures the satellite altitude above the instantaneous sea surface by measuring the two way propagation delay of a radar return pulse signal. The mid point of the return signal's leading edge is used by the altimeter tracker to provide a measure of the height of the sea surface's horizontal reflective surface.

As early as 1971 [Yaplee et al, 1971] it had been established that altimeters overestimate the range to the sea level (in this case observations were made from a tower based altimeter) due to the reflective facets being predominantly in the troughs of the wind disturbed sea surface. This phenomenon is commonly known as the electromagnetic bias. In addition to the electromagnetic bias, the onboard tracker and skewness biases form what is generally known as the sea state bias.

5.2 The Sea State Bias

As stated previously this bias has three components. The electromagnetic bias occurs because the altimeter measures the heights of the sea surface's reflective facets which are biased towards the troughs. This results in a difference between the sea surface height as measured by the altimeter (ie the height of the reflective facets) and the true sea surface height. Theoretical

[Barrick and Lippa, 1985 , Srokosz, 1986] and empirical [Douglas and Agreen,1983 , Walsh et al, 1991] studies have shown that this component has dependencies upon significant wave height (if the surface was perfectly flat there would be no distribution of reflective facets), degree of wave development (as older waves have a different distribution of reflective surfaces) and altimeter frequency. As most satellite altimeters operate at similar frequencies (13.5GHz) the electromagnetic bias is usually altimeter independent.

A skewness bias is caused by the on-board altimeter tracker tracking the median height of the specular facets rather than the mean. A consequence of this is that an additional bias towards the surface troughs is introduced. Typically this value is significantly lower than that for the electromagnetic bias

As the tracker assumes a gaussian distribution of sea surface reflective facets, and this is generally not the case, the tracker's determination of the median height is in error and this contribution to the sea state bias is known as the altimeter's tracker bias. As this bias is dependant upon the altimeter tracker it can be significantly different from satellite to satellite.

5.3 The Sea State Bias Model

Whilst theoretical models for the electromagnetic bias exist these are usually deficient in modelling the sea state bias as the other components, skewness and tracker biases, can be significant and vary from satellite to satellite. This has resulted in the sea state bias typically being determined from satellite crossovers [Gaspar et al, 1994] and /or repeat pass tracks [Born et al, 1982, Douglas and Agreen, 1983, Fu and Glazman, 1991 and Glazman et al, 1994]

The simplest electromagnetic bias models usually considered consist of the

electromagnetic bias (h_{emb}) being directly proportional to the significant wave height ($h_{1/3}$) as shown in equation (5.1).

$$h_{emb}=ah_{\frac{1}{3}} \qquad (5.1)$$

Empirical studies utilising airborne altimeters [Walsh et al, 1991] to determine the electromagnetic bias using this model have yielded results varying from 2% (a=0.02) to 4% (a=0.04) of the significant wave height depending upon the altimeter frequency.

The ERS-1 OPR (Ocean Product) version 2 altimeter data uses a model based upon a statistical theory for free gravity waves [Barrick and Lipa,1985], namely,

$$h_{emb}=h_{\frac{1}{3}}*\frac{\lambda}{8} \qquad (5.2)$$

where the skewness co-efficient is defined by equation (5.3),

$$\lambda=0.25(h_{\frac{1}{3}})^{-0.28} \qquad (5.3)$$

Other models [Fu and Glazman, 1991], such as the CNES model used to define the electromagnetic bias on the early TOPEX/Poseidon GDRs, have attempted to account for the degree of wave development,

$$h_{emb}=kh_{\frac{1}{3}}m^{-l} \qquad (5.4)$$

by parameterising the pseudo wave age as,

$$m=\frac{gh_{\frac{1}{3}}}{U^2} \qquad (5.5)$$

where g is the gravitational acceleration, U the wind speed and the terms k and l are altimeter dependent.

Post launch analysis of TOPEX/Poseidon crossover data, however, has resulted in an improved empirical four parameter model [Gaspar et al, 1994] being adopted for the TOPEX and Poseidon altimeters. This model takes the form,

$$h_{ssb} = -h_{\frac{1}{3}}(a + bU + cU^2 + dh_{\frac{1}{3}}) \qquad (5.6)$$

where h_{ssb} is the sea state bias rather than the electromagnetic bias. The parameters a,b,c and d are altimeter dependent and have been recovered for both the TOPEX and Poseidon altimeters.

It was therefore decided that this four parameter model, and simpler versions of it, would be used in the analysis of ERS-1 data to determine the sea state bias.

5.4 Recovery of the Sea State Bias for ERS-1

In total some 84,000 crossovers from 4 cycles (cycles 2,3,4 and 9) of ERS-1's first multi-disciplinary (35 day repeat) phase are used to determine the sea state bias coefficients for equation (5.6) and its simpler forms. Crossover data rather than individual altimeter points are used in order to remove geographically correlated errors, such as radial orbit, geoid and mean sea surface errors, from the data.

The crossover data utilises the corrections provided on the OPR dataset with the following exceptions. The ocean tide model used is the Cartwright and Ray [Cartwright and Ray, 1990] tide model as derived from GEOSAT data. Corrections for the inverse barometer effect have been calculated by deriving the atmospheric pressure from the dry tropospheric correction and analysis of

the data records/flags has allowed the altimeter dataset to be 'cleaned up'. This involves rejecting those points over shallow water (where the tide model is deficient) as well as those where the standard deviation of the 20Hz data used to create the 1 second normal points is greater than 20cm (to try and remove unreliable data such as that over ice).

The precise orbits were recovered using Aston University's SATAN-A orbit determination suite with both laser ranges and crossover differences used as tracking data. The orbits determined, were typically 5 days in length except in near proximity to satellite manoeuvres and utilised the JGM-2 gravity field [Nerem et al, 1994], MSIS83 thermospheric model [Hedin, 1983] and Aston University's surface area model [Ehlers, 1993] for aerodynamic and radiation pressure modelling. The parameters recovered were initial state vector, 6 hour drag scale factors, a single scale factor for solar radiation pressure and an empirical once per revolution along track acceleration.

It was considered necessary to use crossovers as tracking data because of the poor coverage provided by laser range measurements, particularly in the southern oceans where the majority of altimetry is present. This should not corrupt the sea state bias recovery as orbit error is predominantly long wavelength whilst the changes in significant wave height and wind speed are pseudo random. However, to check the sensitivity of the solutions to the orbits used a comparison of sea state bias solutions derived with the less accurate laser range tracked orbits provided on the OPR dataset was made.

The global fits to the crossover data, for each cycle when the OPR sea state bias and a 60cm rejection level are used, are given in table 5.1.

Table 5.1 The ERS-1 Crossover Datasets

Cycle No.	MJD	No. Crossovers	RMS
2	48761 - 48796	20,223	15.8 cm
3	48796 - 48831	13,662	16.2 cm
4	48831 - 48866	20,517	17.0 cm
9	49006 - 49041	29,695	17.1 cm

The low number of crossovers in cycle 3 is caused by several days worth of altimetry data being unavailable around satellite manoeuvres, whilst the high number of crossovers for cycle 9 can be attributed to the fact that cycle 9 occurs during the southern hemisphere summer, so that fewer points are rejected due to contamination by ice.

The complete dataset of crossovers (no restrictions on the time difference between crossover epochs) has been employed in the recovery of the sea state bias parameters using a least squares approach. The ERS-1 sea state bias solutions obtained using the Aston 'precise orbits', as well as the formal errors derived from the normal matrix, multiplied by a factor of 100 are presented in table 5.2 where the 4 models reflect the successive suppression of parameters recovered.

Table 5.2 Recovered ERS-1 Sea State Bias Parameters Using Aston Orbits.

	Param a	Param b	Param c	Param d
Model 1	5.72 ± 0.23	0.165 ± 0.022	-0.016 ± 0.001	0.183± 0.039
Model 2	6.49 ± 0.13	0.151 ± 0.022	-0.015 ± 0.001	-
Model 3	7.75 ± 0.10	-0.129 ± 0.006	-	-
Model 4	5.95 ± 0.06	-	-	-

The values of the TOPEX/Poseidon satellite altimeters' parameters (multiplied by a factor of 100) as determined by Gaspar et al [1994] are given in table 5.3 along with the ERS-1 parameters recovered using the OPR version 2 orbit heights so that inter altimeter/orbit comparisons and observations can be made. The values given for TOPEX are those for the Ku band.

Table 5.3 TOPEX/Poseidon and ERS-1 OPR Orbit Sea State Bias Parameters.

Altimeter	Param a	Param b	Param c	Param d
TOPEX	1.93	0.368	- 0.014	-0.268
Poseidon	5.12	0.233	-0.011	-0.176
ERS-1	4.91 ± 0.26	0.186 ± 0.025	-0.016 ± 0.001	0.232 ± 0.045
ERS-1	5.65 ± 0.06	-	-	-

The global rms values, in centimetres, for the crossover data as corrected by each of the sea state bias solutions given in tables 5.2 and 5.3, are presented in table 5.4.

Table 5.4 ERS-1 Crossover Rms Fits for Different Sea State Bias Models.

No. SXO	Zero SSB	OPR SSB	Mod. 1	Mod. 2	Mod. 3	Mod. 4
84,097	17.13	16.62	16.06	16.07	16.08	16.13

5.5 Observations Regarding the Recovered Sea State Biases

Table 5.4 suggests that the model used on the OPR version 2 dataset significantly under estimates the ERS-1 sea state bias, as the rms fit to the crossover dataset using this model is significantly higher than those for the recovered models. Each of the recovered models significantly reduces the rms fit to the crossover data, however, the more complex models only provide a

small improvement in comparison to the improvement obtained by the single parameter solution (model 4). This has repercussions for the estimation of the ERS-1 altimeter bias as the OPR electromagnetic bias is equivalent to approximately 2.0% (a=0.02 in equation (5.1)) of the significant wave height. This underestimation by almost 4% of the significant wave height will result in an 8cm bias being present in the altimetry if a global mean significant wave height of 2m is assumed.

Analysis of the four parameter model values in tables 5.2 and 5.3 reveals that the significant wave height term for ERS-1 (a=0.0572) is much higher than that for TOPEX-Ku Band (a=0.0193) and marginally higher than that for Poseidon (a=0.0512). As all three altimeters operate at similar frequencies the electromagnetic bias component of the sea state bias should be similar for each satellite. This then leaves the skewness and/or tracker biases or significant wave height measurements as the only possible sources for these large discrepancies.

It has been shown [Queffeulou, 1994] that ERS-1 underestimates the significant wave height by as much as 20%. This alone does not account for the TOPEX - ERS-1 discrepancy although it suggests that the ERS-1 and Poseidon values are similar. As the ERS-1 and Poseidon trackers are closely related (both being based upon Dumont [1985]) this suggests that the tracker bias is responsible for the large difference between TOPEX - ERS-1 and TOPEX - Poseidon.

It is also apparent that the solutions obtained using the OPR version 2 orbit heights produce significant wave height terms which are lower than those derived with the Aston orbits in both the four and single parameter models. This lower value of sea state bias is also observed by Gaspar and Ogor [1994] who derived the ERS-1 sea state bias as 5.5% (a=0.055) of the significant wave

height when using the OPR orbit heights and analysing all 18 cycles of the first multi-disciplinary phase. Analysis of the results obtained by Gaspar and Ogor [1994] for cycles 2,3,4 and 9 gives the percentages of significant wave height as 5.75%, 5.25%, 5.15% and 5.35% (a=0.0575, 0.0525, 0.0515 and 0.0535 respectively) which on averaging (if each value is given equal weight) provides a value close to 5.4% (a=0.054). Clearly the use of the smaller dataset has not hampered the recovery of the sea state bias as a simple linear relationship with significant wave height.

The differences in values caused by using different orbits could be due to the distribution of crossovers, which are predominantly in the southern oceans (where significant wave height can be quite high), and the poor coverage of laser range data causing some of the orbit error of the OPR orbits to be aliased into the recovery of the sea state bias. Alternatively the use of crossovers (with a poor sea state bias) in the orbit determination could have caused some of the sea state bias to be absorbed. The author is inclined to believe that the first explanation is probably more likely as in chapter 9 it can be seen that the variance in sea state bias for the orbit determination process does not result in a significant change in the recovered sea state bias.

Finally, Gaspar and Ogor [1994] observed that if the four parameter model solutions for ERS-1, TOPEX and Poseidon are compared it is possible to see that for ERS-1 the significant wave height squared term (parameter d) has the opposite sign to the other two altimeters. This has the effect of increasing the relative sea state bias (sea state bias as a percentage of significant wave height) for higher values of significant wave height when the opposite is observed for both the TOPEX and Poseidon altimeters (figures 5.1 and 5.2).

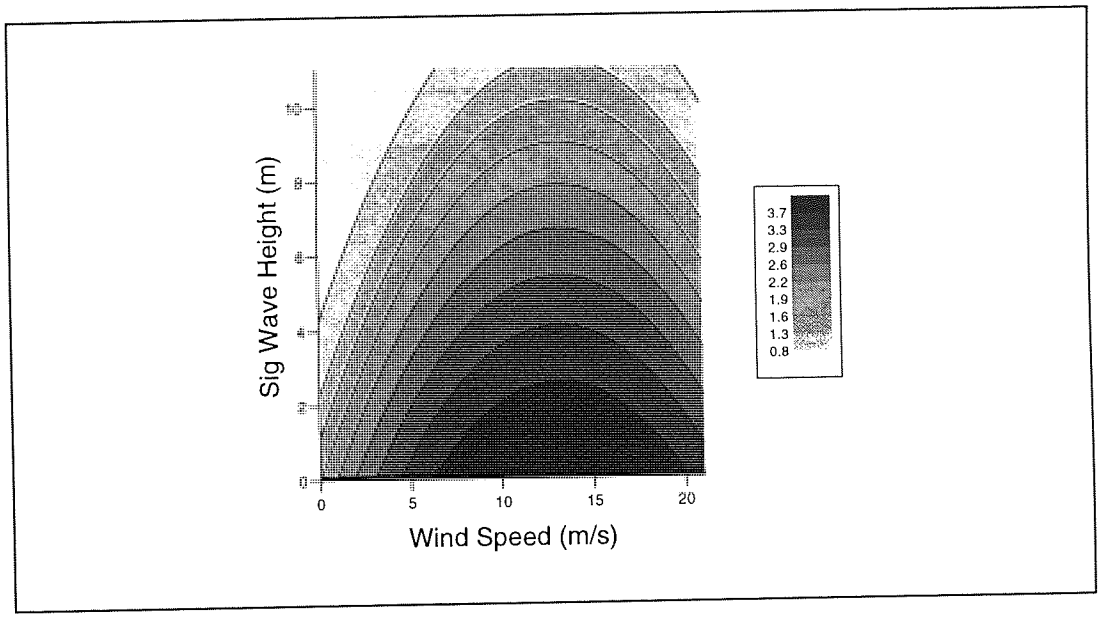

Figure 5.1 Relative Sea State Bias for TOPEX

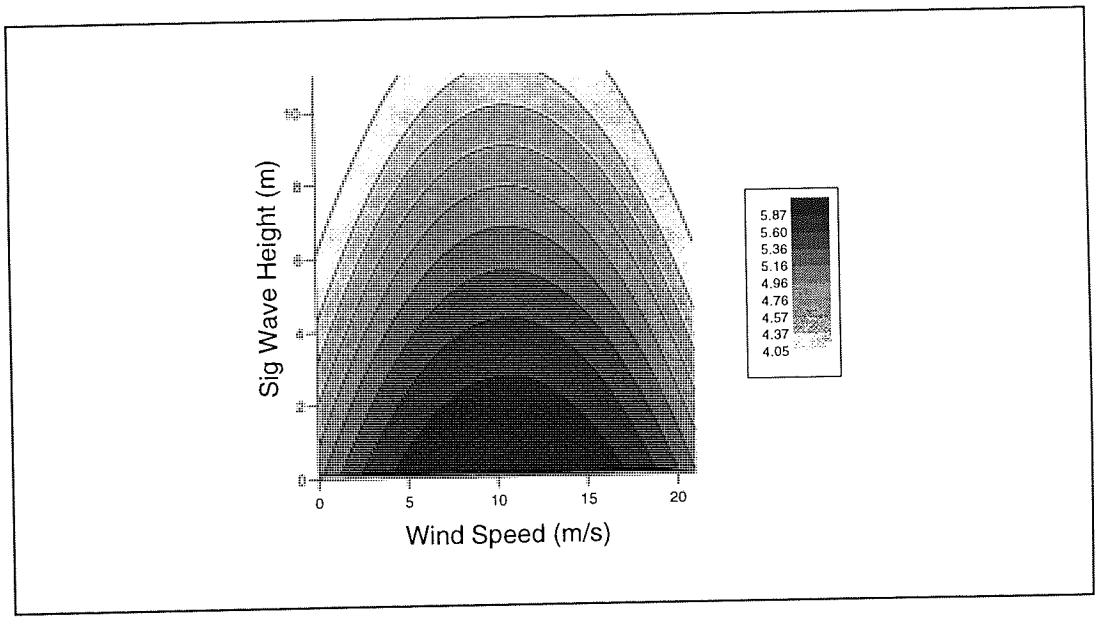

Figure 5.2 Relative Sea State Bias for Poseidon

The four parameter model recovered using the Aston 'precise' orbits also exhibits this peculiar trend (figure 5.3). This phenomenon can only be attributed to the tracker onboard ERS-1 and it will be interesting to see if the same occurs for ERS-2 (although this is beyond the scope of this thesis).

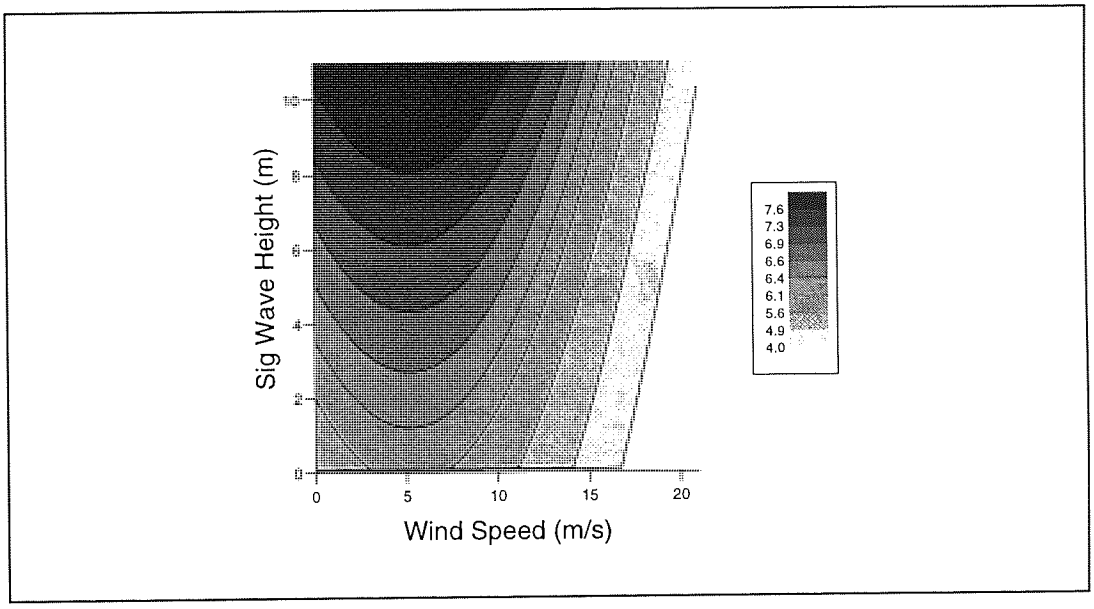

Figure 5.3 Relative Sea State Bias for ERS-1

5.6 Conclusions.

Using several models the sea state bias for ERS-1 has been recovered through the analysis of 4 cycles of crossover data. It has been found that the model used on the OPR data underestimates the sea state bias by a considerable amount and this has implications for determining the altimeter bias of ERS-1. All the models recovered provide an improvement over the OPR model with the 4 parameter model giving the best fit to the crossover dataset. This model, however, reveals some strange behaviour by the ERS-1 altimeter and as the improvement is small compared to that obtained using the simpler linear relationship with significant wave height it has not been chosen to define the ERS-1 sea state bias. The model chosen is therefore the single parameter model (model4) where the constant, a, is defined by 0.0595 (or 5.95%).

Comparisons of the results obtained using the OPR and Aston 'precise' orbits also reveals a worrying trend in that the OPR orbits provide lower sea state biases than the Aston orbits. This cannot be fully explained although it is believed to be due to poorer orbits provided on the OPR altimeter dataset.

Chapter 6
The Radial Orbit Error Model

6.1 Introduction

In chapter 4 reference was made to the use of non dynamic correction procedures to improve the 'precise' orbits generated by the prediction-correction software. This chapter derives the model used for a non dynamic correction of ERS-1 radial orbit error for application in chapter 7.

Initially the Keplerian elements are introduced and then an analytical expression for the radial orbit error in terms of these elements is derived. The contributing factors to the radial orbit error considered are: mis-modelling of the gravitational field, atmospheric density, solar radiation pressure reflectivity coefficient and initial state vector.

6.2 The Keplerian Elements

In chapter 4 the various Cartesian co-ordinate systems (J2000, true of date and earth fixed) typically used in orbit determination were described. Often it is desirable to define the satellite's position with respect to the orbital plane and a reference point within that plane.

The Keplerian elements i, Ω, ω (defined in figure 6.1), a, e and f (shown in figure 6.2) known as inclination, right ascension of the ascending node, argument of perigee, semi-major axis, eccentricity and true anomaly are used to define the orbital plane relative to the given x,y,z co-ordinate system as well

as to describe the position relative to the perigee (point P) such that r, the

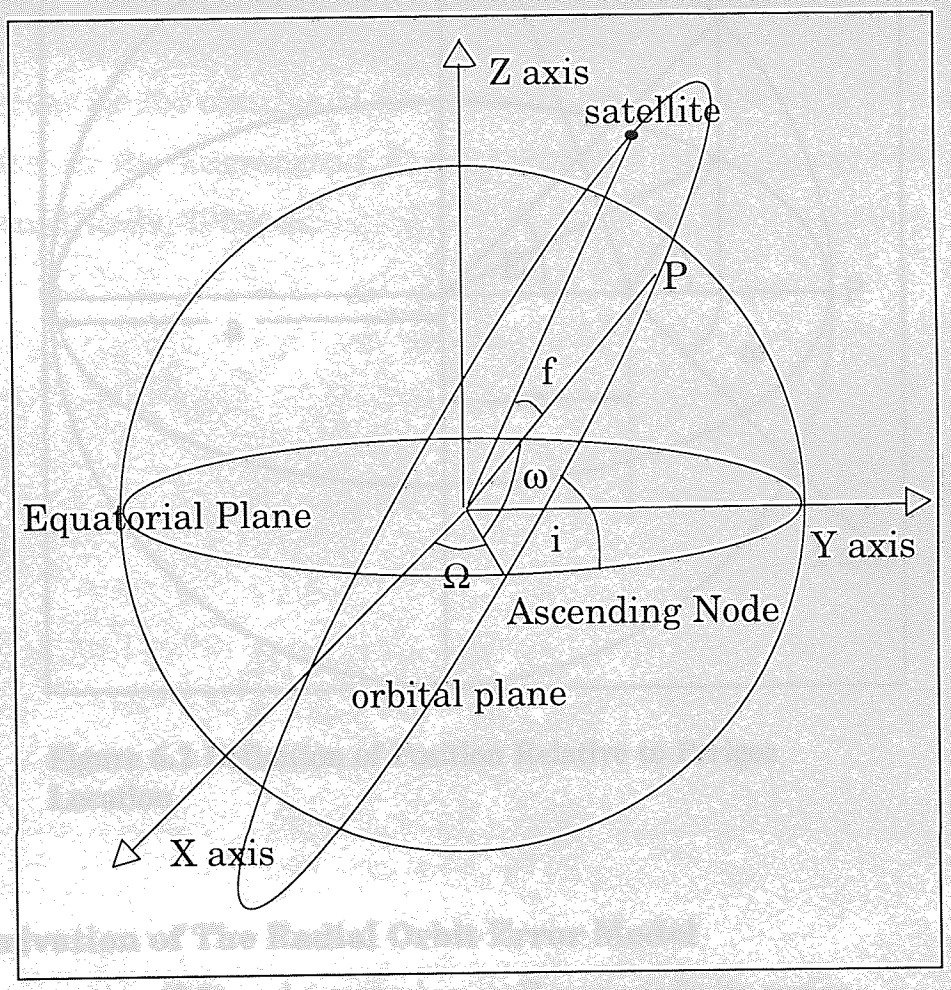

Figure 6.1 Definition of the Orbital Plane

radial distance to any point on the orbit, can be defined by equation (6.1) [Roy, 1988],

$$r=\frac{a(1-e^2)}{1+ecosf} \tag{6.1}$$

or equation (6.2) [Rosborough and Tapley, 1987],

$$r=a(1-ecosE) \tag{6.2}$$

where E is the eccentric anomaly (also defined in figure 6.2).

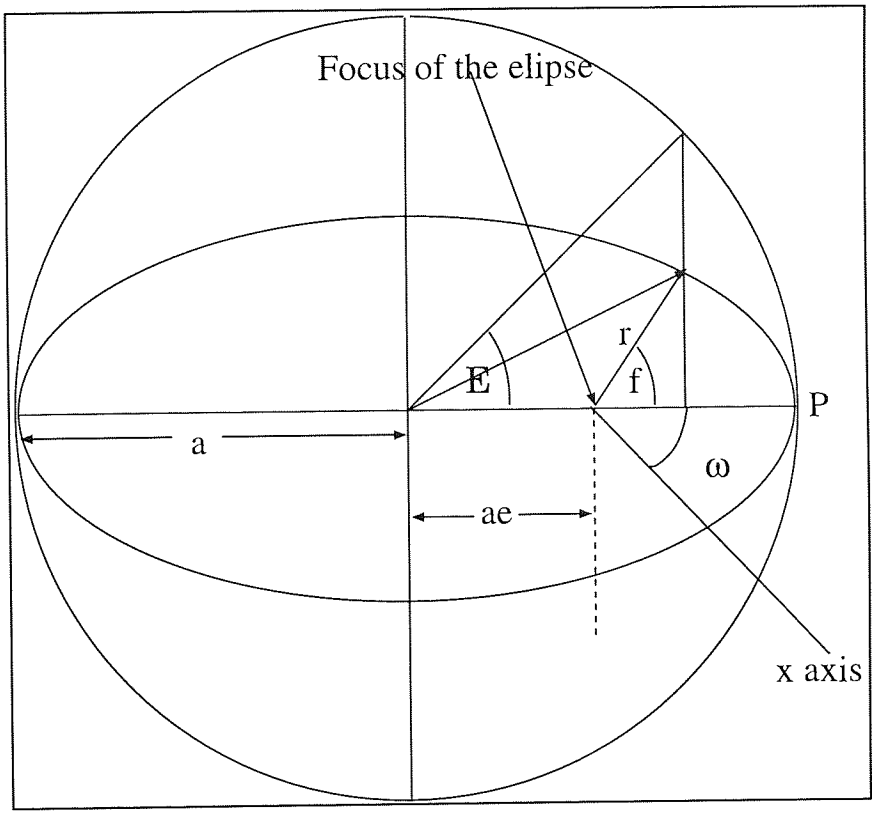

Figure 6.2 Definition of Position Relative to Perigee Location

6.3 Derivation of The Radial Orbit Error Model

Taking equation (6.2) and expressing cosE as an infinite series,

$$cosE = -\frac{e}{2} + \sum_{n=1}^{\infty} \frac{2}{n^2} J_n'(ne)\cos(nM) \qquad (6.3)$$

where J'_n is the Bessel function of the first kind which has been differentiated with respect to e [Smart, 1953], it is possible to express r by equation (6.4),

$$r = a(1 - ecosM + \frac{e^2}{2} - \frac{e^2}{2}\cos 2M) + O(e^3) \qquad (6.4)$$

where M is the mean anomaly and terms of order e^3 and above are ignored (e being small). Making small changes in a, e and M (due to mis-modelling) results in a change in r, Δr, such that the radial error can be defined by

equation (6.5) [Moore and Rothwell, 1990].

$$\Delta r=\Delta a(1-ecosM)-a\Delta e(cosM-e+ecos2M)+ae\Delta M(sinM+esin2M)+O(e^2) \quad (6.5)$$

Expressions for the changes in the elements a,e,i,Ω,ω and M, with respect to time due to the Lagrangean F are expressed by Lagrange's Planetary Equations [Kaula, 1966] as,

$$\frac{da}{dt}=\frac{2}{na}\frac{\partial F}{\partial M} \quad (6.6a)$$

$$\frac{di}{dt}=\frac{1-e^2}{na^2e}\frac{\partial F}{\partial M}-\frac{\sqrt{(1-e^2)}}{na^2e}\frac{\partial F}{\partial \omega} \quad (6.6b)$$

$$\frac{de}{dt}=\frac{1-e^2}{na^2e}\frac{\partial F}{\partial M}-\frac{\sqrt{(1-e^2)}}{na^2e}\frac{\partial F}{\partial \omega} \quad (6.6c)$$

$$\frac{dM}{dt}=-\frac{1-e^2}{na^2e}\frac{\partial F}{\partial e}-\frac{2}{na}\frac{\partial F}{\partial a} \quad (6.6d)$$

$$\frac{d\omega}{dt}=-\frac{\cos i}{na^2\sin i\sqrt{(1-e^2)}}\frac{\partial F}{\partial i}+\frac{\sqrt{(1-e^2)}}{na^2e}\frac{\partial F}{\partial e} \quad (6.6e)$$

$$\frac{d\Omega}{dt}=\frac{1}{na^2\sin i\sqrt{(1-e^2)}}\frac{\partial F}{\partial i} \quad (6.6f)$$

where n is the mean motion of the satellite described by equation (6.7)

$$n=\sqrt{(\frac{\mu}{a^3})} \quad (6.7)$$

and F=U-T where U is the potential energy and T the kinetic energy.

Using these expressions it is possible to determine an analytical model for the radial orbit error by considering each of the error sources individually.

6.3.1 Radial Orbit Error due to the Gravitational Field

Section 4.2.3 described the gravitational potential, U, in the form of a spherical harmonic expansion where the potential is dependent upon latitude, longitude and distance from the Earth's centre. U can be split into two components: a central potential, μ/r, due to the Earth's sphericity and a perturbing potential (or disturbing function), R, due to the Earth's non sphericity.

$$U=\frac{\mu}{r}+R \tag{6.8}$$

On converting the co-ordinate system from geocentric latitude and longitude to Keplerian elements [Kaula, 1966] and using lumped harmonics [Moore and Rothwell, 1990], the disturbing function can be written as,

$$R=\frac{\mu}{a}\sum_{k=-L}^{k=L}\sum_{m=0}^{m=L}\sum_{q=-Q}^{q=Q}U_{kmq} \tag{6.9}$$

where L is the maximum degree of the gravity field considered and U_{kmq} is defined by equation (6.10),

$$U_{kmq}=\nu_{km}(C_m^{-kq}\cos\dot{\Psi}_{kmq}t+S_m^{-kq}\sin\dot{\Psi}_{kmq}t) \tag{6.10}$$

where the lumped harmonics C_m^{-kq} and S_m^{-kq} are functions of the inclination and eccentricity functions ($F_{lmp}(i)$ and $G_{lpq}(e)$) [Kaula, 1966] and gravitational coefficients C_{lm} and S_{lm}. ν_{lm} is defined by equation (6.11) where the power in the square brackets is the integer part,

$$\nu_{km}=(-1)^{[\frac{k-m+1}{2}]} \tag{6.11}$$

and the frequency $\dot{\Psi}_{kmq}$ by,

$$\dot{\Psi}_{kmq}=k\dot{\omega}+(k+q)\dot{M}+m(\dot{\Omega}-\dot{\Theta}) \tag{6.12}$$

where $\dot{\Theta}$ is the rate of change in the Greenwich sidereal angle.

Equation (6.6) expresses the variation in each of the elements a,e and M with respect to time for the Lagrangean F. Now as F=U-T, by substitution of U gives,

$$F=\frac{\mu}{2a}+R \tag{6.13}$$

thus the rate of change of a and e with respect to time can be written as,

$$\frac{da}{dt}=\frac{2}{na}\frac{\partial R}{\partial M} \tag{6.14a}$$

$$\frac{de}{dt}=\frac{(1-e^2)}{na^2e}\frac{\partial R}{\partial M}-\frac{\sqrt{(1-e^2)}}{na^2e}\frac{\partial R}{\partial \omega} \tag{6.14b}$$

Now,

$$-\frac{2}{na}\frac{\partial}{\partial a}\left(\frac{\mu}{2a}\right)=\frac{\mu}{na^3}=n$$

so that the rate of change in M is,

$$\frac{dM}{dt}=n-\frac{(1-e^2)}{na^2e}\frac{\partial R}{\partial e}-\frac{2}{na}\frac{\partial R}{\partial a} \tag{6.14c}$$

Using the method of linear perturbations it is possible to express the change in any element ζ by equation (6.15),

$$\Delta\zeta=\frac{d\Delta\dot{\zeta}}{\dot{\Psi}_{kmq}}d\Psi_{kmq} \tag{6.15}$$

such that substitution of equations (6.14) into equation (6.15) allows the error in each of the elements a,e and M to be written in terms of the error in the potential (ΔR) and mean motion (Δn) as,

$$\Delta a=\frac{2}{na}\int_{\Psi_{kmq}(t_o)}^{\Psi_{kmq}(t)}\frac{(\frac{\partial \Delta R}{\partial M})}{\dot{\Psi}_{kmq}}d\Psi_{kmq} \tag{6.16a}$$

$$\Delta e=\frac{\sqrt{(1-e^2)}}{na^2e}\int_{\Psi_{kmq}(t_o)}^{\Psi_{kmq}(t)}\frac{(\sqrt{(1-e^2)}\frac{\partial \Delta R}{\partial M}-\frac{\partial \Delta R}{\partial \omega})}{\dot{\Psi}_{kmq}}d\Psi_{kmq} \tag{6.16b}$$

$$\Delta M=\Delta n-\frac{1}{na}\int_{\Psi_{kmq}(t_o)}^{\Psi_{kmq}(t)}\frac{(\frac{1-e^2}{ae}\frac{\partial \Delta R}{\partial e}+2\frac{\partial \Delta R}{\partial a})}{\dot{\Psi}_{kmq}}d\Psi_{kmq} \tag{6.16c}$$

where ΔR is obtained from R by replacing the gravitational coefficients C_{lm} and S_{lm} by their errors ΔC_{lm} and ΔS_{lm}.

Finally after integration of equation (6.16) with respect to Ψ_{kmq} the errors in a,e and M due to errors in the gravitational coefficients ΔC_{lm} and ΔS_{lm} can be expressed by,

$$\Delta a=(\frac{2\mu v_{km}(k+q)}{na^2\dot{\Psi}_{kmq}})(H_1(t)-H_1(t_o)) \tag{6.17a}$$

$$\Delta e=(\frac{\mu v_{km}(2q(1-e^2)-ke^2)}{2na^3e\dot{\Psi}_{kmq}})(H_1(t)-H_1(t_o)) \tag{6.17b}$$

$$\Delta M=(\frac{3\mu\nu_{km}(k+q)t}{a^3\dot{\Psi}_{kmq}}H_1(t_o)+(\frac{\mu\nu_{km}}{a^2\dot{\Psi}_{kmq}})((\frac{3(k+q)}{\dot{\Psi}_{kmq}a}-\frac{2}{na})+$$

$$+(\frac{1}{nae}\frac{\partial}{\partial e}+\frac{2}{n}\frac{\partial}{\partial a}))(H_2(t)-H_2(t_o)) \qquad (6.17c)$$

where,

$$H_1(t)=(C_m^{-kq}\cos\dot{\Psi}_{kmq}t+S_m^{-kq}\sin\dot{\Psi}_{kmq}t)$$

and

$$H_2(t)=(S_m^{-kq}\cos\dot{\Psi}_{kmq}t-C_m^{-kq}\sin\dot{\Psi}_{kmq}t)$$

On substitution of these equations into equation (6.5),and ignoring terms of order e^2 or greater (ie taking q=0 ± 1) it is possible to express the radial error as,

$$\Delta r_{grav}=\sum_{k=-L}^{k=L}\sum_{m=0}^{m=L}\sum_{q=-1}^{q=1}(A_{kmq}\cos\dot{\Psi}_{kmq}t+B_{kmq}\sin\dot{\Psi}_{kmq}t)+$$

$$+C_1^{grav}+C_2^{grav}(t-t_o)\sin M \qquad (6.18)$$

where A_{kmq}, B_{kmq} , C_1^{grav} and C_2^{grav} are constant for a given satellite orbit.

Now as the perigee position remains constant for altimetric satellites ($\dot{\omega}$=0) the frequency term $\dot{\Psi}_{kmq}$,expressed by equation (6.12), can be simplified. Also as only values of q=0 ± 1 need consideration for a near circular satellite orbit it is possible to collect together terms of the same frequency and eliminate the summation over q, to the extent that the radial error due to mis-modelling of the gravity field is given by,

$$\Delta r_{grav}=\frac{\mu}{na^2}\sum_{k=-L-1}^{k=L+1}\sum_{m=0}^{m=L}(A_{km}\cos\dot{\Psi}_{km}t+B_{km}\sin\dot{\Psi}_{km}t)+$$

$$+C_1^{grav}+C_2^{grav}(t-t_o)\sin M \qquad (6.19)$$

where equation (6.20) defines the frequency $\dot{\Psi}_{km}$.

$$\dot{\Psi}_{km}=k\dot{M}+m(\dot{\Omega}-\dot{\Theta}) \qquad (6.20)$$

6.3.2 Radial Orbit Error due to Atmospheric Density

In chapter 4 the atmospheric force experienced by a satellite in a low earth orbit was discussed. If the density of the atmosphere is mis-modelled the drag force (and hence equations of motion) are miscalculated which for some satellites, such as ERS-1, can cause large orbit errors.

To model the radial orbit error due to mis-modelling of the atmospheric density it is assumed that the density ,ρ , decreases exponentially with height such that [Moore and Rothwell, 1990],

$$\rho=\rho_p\exp^{(\frac{r_p-r}{H})} \qquad (6.21)$$

where the subscript p refers to the perigee location and H is a constant representing density scale height. The error in atmospheric density can then be related to the error in density at the perigee location by,

$$\Delta\rho=\Delta\rho_p\exp^{(\frac{r_p-r}{H})} \qquad (6.22)$$

where equation (6.23),

$$r - r_p = ae(1 - cosE) \tag{6.23}$$

describes the difference in height between the point in question and perigee.

Substitution of equation (6.23) into (6.22) and expansion of the exponential in equation (6.22) as a power series in z=ae(1-cosE)/H gives the density error as equation (6.24),

$$\Delta\rho = \Delta\rho_p(1 - \frac{ae}{H} + \frac{aecosE}{H}) + O(z^2) \tag{6.24}$$

which is accurate to the order z^2.

The mis-modelling, or error component, of the atmospheric drag force for a spherical satellite in the along track direction (ΔF_{drag}) can then be defined by (cf equation (4.5)[King-Hele, 1987]),

$$\Delta F_{drag} = -\frac{1}{2} C_D S v^2 \Delta\rho_p(1 - \frac{ae}{H} + \frac{aecosE}{H}) \tag{6.25}$$

Modified versions of the Lagrangian planetary equations (Equations(6.6)) given by King-Hele [1987] express the variations in a,e and M with respect to time and forces in the radial, along track and cross track directions thus allowing Δa, Δe and ΔM to be determined if the satellite's surface area relative to the atmosphere is assumed to be constant (ie a spherical satellite).

On substitution of the expression ΔF_{drag} into the modified Lagrangian equations and converting the independent variable to E, yields the error in r for a satellite with low eccentricity as [Moore and Rothwell, 1990],

$$\Delta r = -a^2 C_D S \Delta\rho_p(E(t) - E(t_o))(1 - \frac{ae}{H} - \frac{ae}{2H}\cos E(t)) \tag{6.26}$$

plus periodic terms of frequency one and two cycles per revolution, which on further simplification can be written as,

$$\Delta r_{drag} = C_1^{drag}(t-t_o) + C_2^{drag}(t-t_o)cosM + \sum_{i=1}^{i=2}(A_i^{drag} siniM + B_i^{drag} cosiM) \qquad (6.27)$$

where,

$$E(t) - E(t_o) = n(t-t_o)$$

Due to the density error at the perigee changing continually with atmospheric conditions the drag error terms should ideally be solved for each recovered drag scale factor. However, for the purpose of this thesis only one set of terms are used to model the radial orbit error for each ephemeris.

6.3.3 Radial Orbit Error due to Solar Radiation Pressure

Due to the complex geometry and surface optical properties of altimetric satellites it is necessary to make some assumptions in the investigation of likely errors due to the mis-modelling of solar radiation pressure. These assumptions include; a constant sunlight cross sectional area (ie a spherical satellite); the solar radiation force acts along (or parallel) to the sun-earth line and the penumbra is defined by the two eccentric anomalies E_1 and E_2. It is also assumed that there are no error contributions from Earth or albedo reflected radiation.

On using equation (4.6) the mis-modelled solar radiation force, ΔF_{sol}, due to an error in the reflectivity coefficient ΔC_R is given by,

$$\Delta F_{sol} = -\Delta C_R \frac{\Phi}{c} A \underline{\hat{s}} \qquad (6.28)$$

Using the variations in a, e and M with respect to time given by Asknes [1976] it is possible to determine Δa, Δe and ΔM as a function of the transverse, normal and radial components of radiation force experienced at the satellites

perigee position.

Allowing for the absorption of along track error terms by the recovery of multiple drag scale factors and initial state vector , the radial error for k satellite revolutions after the reference epoch t_o can be expressed as [Moore and Rothwell, 1990],

$$\Delta r_{srp} = \Delta a^{(k)} - a\Delta e^{(k)} \cos E - ae(\Delta\omega^{(k)} + \Delta\Omega^{(k)} cosi) sinE \qquad (6.29)$$

where,

$$\Delta a^{(k)} = kC_a$$

$$\Delta e^{(k)} = k(C_{1e} + C_{2e}\delta E)$$

$$\Delta\omega + \Delta\Omega = \frac{k}{e}(C_{1\omega} + C_{2\omega}\delta E)$$

and C_a, C_{1e}, C_{2e},$C_{1\omega}$ and $C_{2\omega}$ are constants on assuming the direction cosines of the force vary slowly with time, and δE is the portion of the arc in sunlight (E_2-E_1).

Equation (6.29) can therefore be simplified such that the radial orbit error is predominantly a sinusoidal variation in M of increasing amplitude superimposed upon a secular trend.

$$\Delta r_{sol} = C_1^{sol}(t - t_o) + C_2^{sol}(t - t_o) sinM + C_3^{sol}(t - t_o) \cos M \qquad (6.30)$$

As only one reflectivity coefficient factor is recovered for each arc in the orbit generation equation (6.30) should be perfectly adequate.

By taking t_o as the mid point of the ephemeris (defined as t_*) the error

recovered assumes the 'bow tie' pattern observed by Colombo [1984].

6.3.4 Radial Orbit Error due to the Initial State Vector.

Equation (6.5) defines the error in r when errors in the elements a,e and M are introduced. If the estimates of a,e and M at time t_o (as derived from the initial state vector) are erroneous then the error in r at time t due to these initial errors can be described by,

$$\Delta r_{is}(t)=\Delta a_0(1-ecosM)-a\Delta e_0(cosM-e+ecos2M)+$$

$$+ae\Delta M_{is}(sinM+esin2M) \qquad (6.31)$$

where ΔM_{is} is the summation of ΔM_o , the initial error in M, and ΔM_{init} , the subsequent error in M due to Δa_o.

This therefore gives

$$\Delta M_{is}=\Delta M_0-\frac{3n}{2a}\Delta a_0(t-t_0) \qquad (6.32)$$

which on substitution into equation (6.31) gives,

$$\Delta r_{is}=\Delta a_0(1-ecosM)-a\Delta e_0(cosM-e+ecos2M)+$$

$$+ae(\Delta M_o-\frac{3n}{2a}\Delta a_o(t-t_o))(sinM+esin2M) \qquad (6.33)$$

This can then be simplified further to give,

$$\Delta r_{is}(t)=C_1^{init}+C_2^{init}(t-t_0)sinM+C_3^{init}(t-t_0)sin2M+\sum_{i=1}^{i=2}(A_i^{init}\cos iM+B_i^{init}\sin iM) \qquad (6.34)$$

6.4 Conclusions

By considering the mis-modelling of the gravitational field, atmospheric density, solar radiation reflectivity coefficient and initial state vector it has been possible to derive analytical expressions for the radial orbit error in terms of the Keplerian elements for each of these sources. These expressions are used in chapter 7 to derive the radial orbit error of ERS-1 through analysis of dual crossovers with TOPEX/Poseidon.

Chapter 7

Recovery of the ERS-1 Radial Orbit Error

7.1 Introduction

In chapter 6 , analytical expressions for components of the radial orbit error were shown to be,

$$\Delta r_{grav} = \sum_{k=-L-1}^{k=L+1} \sum_{m=0}^{m=L} (A_{km}^{grav} \cos\Psi_{km}(t-t_o) + B_{km}^{grav} \sin\Psi_{km}(t-t_o)) +$$

$$+ C_1^{grav} + C_2^{grav}(t-t_o)\sin M \qquad (6.19)$$

$$\Delta r_{drag} = C_1^{drag}(t-t_o) + C_2^{drag}(t-t_o)cosM + \sum_{i=1}^{i=2} (A_i^{drag} \sin iM + B_i^{drag} \cos iM) \qquad (6.27)$$

$$\Delta r_{sol} = C_1^{sol}(t-t_o) + C_2^{sol}(t-t_o)sinM + C_3^{sol}(t-t_o)cosM \qquad (6.30)$$

$$\Delta r_{init} = C_1^{init} + C_2^{init}(t-t_o)sinM + C_3^{init}(t-t_o)sin2M + \sum_{i=1}^{i=2} (A_i^{init} \cos iM + B_i^{init} \sin iM) \qquad (6.34)$$

where t_o is the initial epoch.

The complete radial orbit error can therefore be described by,

$$\Delta r=\sum_{k=-L-1}^{k=L+1}\sum_{m=1}^{m=L}(A_{km}\cos\dot{\Psi}_{km}(t-t_o)+B_{km}\sin\dot{\Psi}_{km}(t-t_o))+C_1+C_2(t-t_*)+$$

$$+C_3(t-t_*)sinM+C_4(t-t_*)cosM+C_5(t-t_*)sin2M+C_6sinM+$$

$$+C_7cosM+C_8sin2M+C_9cos2M \qquad (7.1)$$

when the reference epoch for the secular terms (C_2,C_3,C_4,C_5) is redefined as t_*, the mid point of the arc, such that the bow tie effect is observed [Colombo,1984], and the m=0 terms from the k,m summation are lumped with the cosM, sinM, cos2M and sin2M terms.

To analyse a period consisting of more than one ephemeris a slightly different form of equation (7.1) must be considered. As the gravitational field errors can be considered the same for each arc, (ie arc independent) but the errors due to atmosphere, solar radiation pressure and initial state vector mis-modelling are arc dependent, equation (7.2) is used to describe the radial orbit error for multiple arc solutions,

$$\Delta r_i=\sum_{k=-L-1}^{k=L+1}\sum_{m=1}^{m=L}(A_{km}\cos\dot{\Psi}_{km}(t-t_o)+B_{km}\sin\dot{\Psi}_{km}(t-t_o))+\sum_{i=1}^{i=NoArcs}\delta_i(C_1^i+$$

$$+C_2^i(t-t_*^i)+C_3^i(t-t_*^i)sinM+C_4^i(t-t_*^i)cosM+C_5^i(t-t_*^i)sin2M+C_6^isinM+$$

$$+C_7^icosM+C_8^isin2M+c_9^icos2M) \qquad (7.2)$$

where $\delta_i=1$ if the observation lies within the i^{th} arc, but is zero otherwise.

This chapter discusses how these models of the radial error are used to improve the orbits of ERS-1 by analysis of single and dual satellite crossovers with the joint NASA/CNES satellite TOPEX/Poseidon.

7.2 The Crossover Datasets and Unobservable Terms.

In 2.4 the concept of single and dual satellite crossovers was outlined. When using the crossover datasets to recover the radial error terms given in equation (7.1) it is necessary to account for several deficiencies due to certain terms being unobservable and others leading to a singular solution if all terms in certain combinations are sought.

7.2.1 Single Satellite Crossovers.

A single satellite crossover residual, being the difference in altimeter residuals at the intersection of ascending and descending ground tracks, is defined by equation (7.3),

$$\Delta_{SXO}=(Obs_1-Calc_1)-(Obs_2-Calc_2) \qquad (7.3)$$

where Obs_i and $Calc_i$ are the observed and calculated heights above the reference ellipsoid at epoch i. As the geoid and mean sea surface heights cancel the crossover residual is a good measure of the satellite's radial orbit accuracy such that,

$$\Delta_{SXO}=\Delta r_1-\Delta r_2+noise \qquad (7.4)$$

where Δr_i is the radial orbit error at epoch i.

Other signals, such as the variation in the sea surface and altimeter media correction errors, will contribute to the single satellite crossover residual. However, these signals can be assumed to be random in nature (ie do not occur at the same frequencies as orbit error) and consequently are taken to be noise. On ignoring these additional signals, equation (7.5) is used to describe the single satellite crossover residual.

$$\Delta_{SXO}=\sum_{k=-L-1}^{k=l+1}\sum_{m=1}^{m=L}(A_{km}\cos\dot{\Psi}_{km}t_1+B_{km}\sin\dot{\Psi}_{km}t_1-A_{km}\cos\dot{\Psi}_{km}t_2-B_{km}\sin\dot{\Psi}_{km}t_2)+$$

$$+(C_1+C_2(t_1-t_*)+C_3(t_1-t_*)\sin M_1+C_4(t_1-t_*)\cos M_1+C_5(t_1-t_*)\sin 2M_1+C_6\sin M_1+$$

$$+C_7\cos M_1+C_8\sin 2M_1+C_9\cos 2M_1)-(C_1+C_2(t_2-t_*)+C_3(t_2-t_*)\sin M_2+$$

$$+C_4(t_2-t_*)\cos M_2+C_5(t_2-t_*)\sin 2M_2+C_6\sin M_2+C_7\cos M_2+C_8\sin 2M_2+C_9\cos 2M_2) \quad (7.5)$$

Examination of equation (7.5) reveals that several of the error terms are unobservable. Obviously the constant component is unrecoverable as it will cancel in a similar manner to the geoid and mean sea surface errors. Further as ERS-1 and TOPEX/Poseidon are in orbits where the perigee position, ω, is effectively fixed at 90 degrees the cosM and cos2M terms are also unobservable due to $M_1 \approx -M_2$. Also some of the frequencies are linearly dependent and an ill-conditioned solution is obtained if all the terms are recovered simultaneously. Sandwell et al [1986] have shown the sets of linearly dependent frequencies for $k \leq 2$ to be those given in table 7.1.

Table 7.1. Linearly Dependent Frequencies in Single Satellite Crossovers.

Set	Linearly Dependant Frequency Terms
1	$\dot{\Psi}_{1,1}$, $\dot{\Psi}_{-1,1}$
2	$\dot{\Psi}_{2,1}$, $\dot{\Psi}_{0,1}$, $\dot{\Psi}_{-2,1}$
3	$\dot{\Psi}_{2,2}$, $\dot{\Psi}_{0,2}$, $\dot{\Psi}_{-2,-2}$

If all the terms in each of the above sets are to be recovered then additional

radial data in the form of short arc data, accurate altimeter measurements over non oceanographic surfaces (such as from transponders) or dual crossovers are required. Analysis of single satellite crossovers alone therefore cannot allow a complete recovery of the radial orbit error.

7.2.2 Dual Satellite Crossovers.

Dual satellite crossovers formed at the intersection of different satellite ground tracks are similar to single satellite crossovers in that the mean sea surface and geoid heights cancel. However, dual satellite crossovers form a more comprehensive data set and come in the form of ascending/ascending, descending/descending as well as ascending/descending ground track intersections, the combinations being dependent upon the orbital parameters of the two satellites. As the geoid and mean sea surface heights cancel the dual crossover residual provides a measure of the relative orbit error of the two satellites, which for TOPEX/Poseidon - ERS-1 dual crossovers can be described by equation (7.6),

$$\Delta_{DXO}=\Delta r_{T/P}-\Delta r_{E1}+noise \qquad (7.6)$$

where the subscripts T/P and E1 refer to TOPEX/Poseidon and ERS-1 respectively.

Ignoring the altimetric correction error signals (defined as noise in equation (7.6)), although acknowledging that different media corrections (particularly for the ionosphere) may cause orbit error like signals, the dual crossover residual is defined by equation (7.7).

$$\Delta_{DXO}=\sum_{k=-L-1}^{k=L+1}\sum_{m=1}^{m=L}(A_{km}^{T/P}\cos\Psi_{km}^{T/P}(t^{T/P}-t_o^{T/P})+B_{km}^{T/P}\sin\Psi_{km}^{T/P}(t^{T/P}-t_o^{T/P})-$$

$$-(A_{km}^{E1}\cos\Psi_{km}^{E1}(t^{E1}-t_o^{E1})+B_{km}^{E1}\sin\Psi_{km}^{E1}(t^{E1}-t_o^{E1}))+C_1^{T/P}+C_2^{T/P}(t^{T/P}-t_*^{T/P})+$$

$$+C_3^{T/P}(t^{T/P}-t_*^{T/P})\sin M^{T/P}+C_4^{T/P}(t^{T/P}-t_*^{T/P})\cos M^{T/P}+C_5^{T/P}(t^{T/P}-t_*^{T/P})\sin 2M^{T/P}+$$

$$+C_6^{T/P}\cos M^{T/P}+C_7^{T/P}\sin M^{T/P}+C_8^{T/P}\cos 2M^{T/P}+C_9^{T/P}\sin 2M^{T/P}-(C_1^{E1}+$$

$$+C_2^{E1}(t^{E1}-t_*^{E1})+C_3^{E1}(t^{E1}-t_*^{E1})\sin M^{E1}+C_4^{E1}(t^{E1}-t_*^{E1})\cos M^{E1}+C_5^{E1}(t^{E1}-t_*^{E1})sin2M^{E1}+$$

$$+C_6^{E1}\sin M^{E1}+C_7^{E1}cosM^{E1}+C_8^{E1}\sin 2M^{E1}+C_9^{E1}\cos 2M^{E1}) \qquad (7.7)$$

Any attempt to solve for all terms in equation (7.7) yields similar deficiencies to the single satellite crossover residual data set. Only one constant term, as a measure of the relative difference between $C_1^{T/P}$ and C_1^{E1}, can be recovered. The cosines of one and two cycles per revolution are linearly dependent as the latitudes for both observations are the same such that,

$$\sin U^{E1}\sin i^{E1}=\sin U^{T/P}\sin i^{T/P}$$

where U is the argument of latitude and i the orbital inclination. Thus,

$$\cos M^{E1}=\frac{\sin i^{T/P}}{\sin i^{E1}}\cos M^{T/P}$$

if the perigee locations are fixed for both satellites at 90 degrees. On using the above expression for $\cos M^{E1}$, and the standard identity for cos2M it can also be shown that the $\cos 2M^{E1}$ and $\cos 2M^{T/P}$ terms are linearly dependent if the constant offset is also recovered.

[Moore and Ehlers,1993] list the additional sets of linear dependent

frequencies for k less than or equal to 2 as those defined in table 7.2.

Table 7.2 Linear Dependent Frequencies in Dual Satellite Crossovers.

Set No.	Linear Dependent Frequencies
1	$\dot{\Psi}^{T/P}_{1,1}$, $\dot{\Psi}^{T/P}_{1,-1}$, $\dot{\Psi}^{EI}_{1,1}$, $\dot{\Psi}^{EI}_{1,-1}$
2	$\dot{\Psi}^{T/P}_{2,1}$, $\dot{\Psi}^{T/P}_{0,1}$, $\dot{\Psi}^{T/P}_{-2,1}$, $\dot{\Psi}^{EI}_{2,1}$, $\dot{\Psi}^{EI}_{0,1}$, $\dot{\Psi}^{EI}_{-2,1}$
3	$\dot{\Psi}^{T/P}_{2,2}$, $\dot{\Psi}^{T/P}_{0,2}$, $\dot{\Psi}^{T/P}_{-2,2}$, $\dot{\Psi}^{EI}_{2,2}$, $\dot{\Psi}^{EI}_{0,2}$, $\dot{\Psi}^{EI}_{-2,2}$

Suppression of any one of the TOPEX/Poseidon frequencies from each of these sets allows the recovery of all the ERS-1 terms. Therefore the use of dual crossovers allows near complete recovery of the ERS-1 and TOPEX/Poseidon radial orbit error.

7.3 Recovered Terms

Examination of equation (7.1) reveals that if all terms were to be recovered for an orbit defined by a gravitational field of degree and order 70 the estimation of parameters for 9940 frequencies would be required. It is therefore necessary to determine which terms are significant and require recovery.

Several authors , Sandwell et al [1986] in the analysis of SEASAT single satellite crossovers and Moore and Ehlers [1993] in the analysis of simulated TOPEX/Poseidon - ERS-1 dual satellite crossovers, reduced the number of recoverable terms by only considering those frequencies below two cycles per revolution as this is the domain of the most significant error contributing frequencies. This still leaves a very large number of frequencies (1002 for ERS-1 when in the multi-disciplinary phase and 254 for TOPEX/Poseidon) if all combinations of k and m are considered. Moore and Ehlers [1993] reduced

this number further by considering only those frequencies where m is less than 43. This had the effect of removing one frequency from each triplet of correlated frequencies such that only 170 frequencies for ERS-1 required recovery and in the process ensured a stable solution for the simulated data. However, this simple means of reducing the number of parameters recovered also resulted in some of the significant frequencies (ie those with m=43 and m= 57, corresponding to near resonance for ERS-1) being omitted from the solution.

To determine which frequencies are significant contributors to the orbit error the covariance matrix for the JGM-2 gravity field has been used to quantify the radial errors due to the gravity field harmonics (ΔC_{lm} and ΔS_{lm}).

If the radial error for a particular pair of k and m is expressed by equation (7.8),

$$\Delta r_{km} = \underline{c}^T \, \underline{\Delta grav} \qquad (7.8)$$

where $\underline{\Delta grav}$ is the matrix of terms corresponding to ΔC_{lm} and ΔS_{lm} and $\underline{c}$ is the coefficient vector that describes the error in terms of the inclination/ eccentricity functions and satellite orbit parameters then the expected error, or standard error, σ_r, in Δr for the same k and m can be described by equation (7.9),

$$(\sigma_{r_{km}}) = \underline{c}^T C \underline{c} \qquad (7.9)$$

if C is the gravity field covariance matrix.

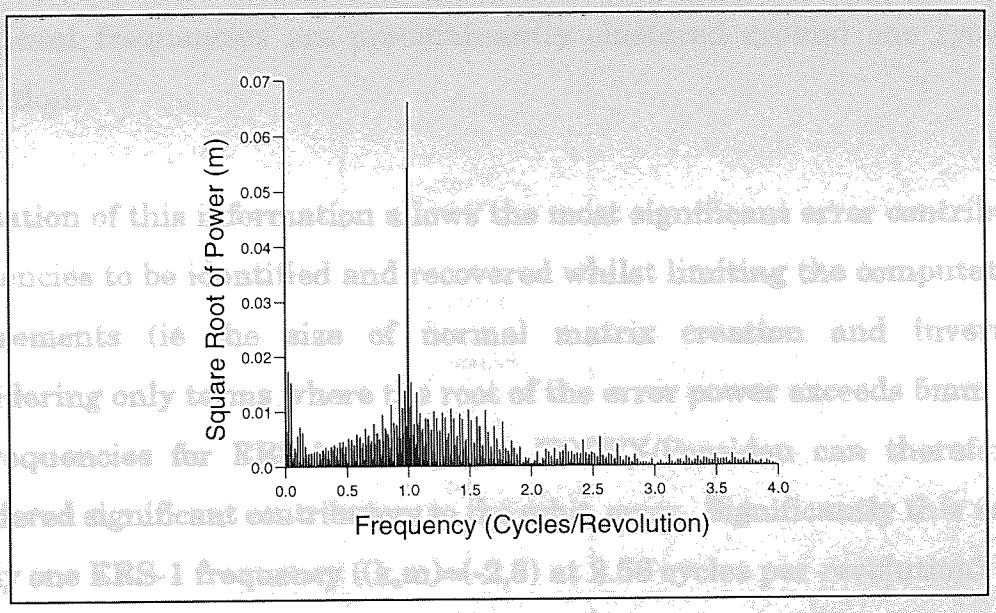

Figure 7.1 Error Powers for ERS-1

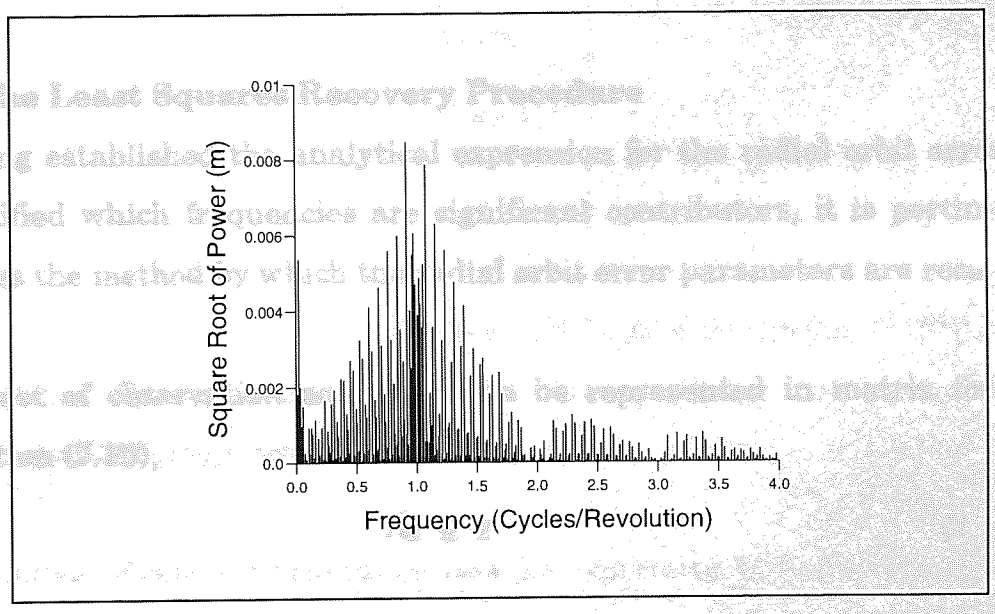

Figure 7.2 Error Powers for TOPEX/POSEIDON

Plots of the square root of the power of the expected error signal due to the JGM-2 gravity field (sine term squared plus cosine term squared) against frequency for ERS-1 and TOPEX/Poseidon are shown in figures 7.1 and 7.2. Clearly, as would be expected, the ERS-1 errors are much larger, and the

significant frequencies are predominantly clustered around one cycle per revolution.

Utilisation of this information allows the most significant error contributing frequencies to be identified and recovered whilst limiting the computational requirements (ie the size of normal matrix creation and inversion). Considering only terms where the root of the error power exceeds 5mm some 76 frequencies for ERS-1 and 10 for TOPEX/Poseidon can therefore be considered significant contributors to the orbit error. Significantly this results in only one ERS-1 frequency ((k,m)=(-2,8) at 2.56 cycles per revolution) being outside the two cycles per revolution domain whilst 7 ERS-1 frequencies, where m >43 ((k,m)=(3,57), (4,43), (3,43), (4,44), (2,43), (2,44) and (5,57)), ignored by Moore and Ehlers [1993], require recovery.

7.4 The Least Squares Recovery Procedure

Having established the analytical expression for the radial orbit error and identified which frequencies are significant contributors, it is pertinent to discuss the method by which the radial orbit error parameters are recovered.

The set of observation equations can be represented in matrix form by equation (7.10),

$$A\underline{x}-\underline{b}=\underline{v} \tag{7.10}$$

where $\underline{v}$ is the noise vector, $\underline{x}$ the vector of parameters recovered and A the transformation matrix where the i^{th} row is given by equation (7.11),

$$A^T = \begin{bmatrix} \vdots \\ \cos\Psi_{km}^{T/P}(t) \\ \sin\Psi_{km}^{T/P}(t) \\ \vdots \\ \Delta^{TOPEX} \\ \Delta^{Poseidon} \\ t^{T/P} - t_*^{T/P} \\ (t^{T/P} - t_*^{T/P})\sin M^{T/P} \\ \vdots \\ \cos\Psi_{km}^{E1}(t) \\ \sin\Psi_{km}^{E1}(t) \\ \vdots \\ t^{E1} - t_*^{E1} \\ (t^{E1} - t_*^{E1})\sin M^{E1} \\ \vdots \end{bmatrix} \qquad (7.11)$$

In equation (7.11) $\Delta^{\text{TOPEX}} = 1$ for TOPEX - ERS-1 dual crossovers, $\Delta^{\text{Poseidon}} = 1$ for Poseidon - ERS-1 dual crossovers and both are equal to zero otherwise and for single satellite crossovers.

The method of least squares minimises the expression Q, defined by equation (7.12),

$$Q = \underline{v}^T W \underline{v} \qquad (7.12)$$

where W is a diagonal weight matrix having the i^{th} value,

$$W_{ii} = \frac{1}{\sigma_{obs}^2}$$

if σ_{obs} is the standard deviation of observation i.

The least squares solution for $\underline{x}$ is then,

$$(A^T W A)\underline{x} = A^T W \underline{\hat{b}} \tag{7.13}$$

which is often written in the form,

$$N\underline{x} = \underline{\hat{b}} \tag{7.14}$$

N being the normal matrix, and N^{-1} the covariance matrix.

By analysis of the eigenvalues of the covariance matrix several authors ie Moore and Ehlers [1993], Carnochan et al [1994] have shown that the recovered solution is not particularly reliable for large sets of parameters. For this reason constraints based upon the expected errors (as shown in figures 7.1 and 7.2) have been utilized. The inclusion of constraints reduces the eigenvalues of the covariance matrix (which are a measure of the error ellipse's semi major axis [Bomford, 1980]) as observed by Moore and Ehlers [1993]. In addition the eigenvectors yield the linear contribution of parameters leading to ill-conditioning. The utilisation of constraints requires that Q be redefined as,

$$Q = \underline{v}^T W \underline{v} + \underline{s}^T W' \underline{s} \tag{7.15}$$

where $\underline{s}$ is a subset of $\underline{x}$ with known standard deviation $\underline{\sigma}$ and W' is a diagonal weight matrix with the i^{th} element,

$$W'_{ii} = \frac{1}{\sigma_i^2}$$

σ_i being the expected error in the i^{th} term.

The resultant solution equation is,

$$(A^T WA + W')\underline{x} = A^T W\hat{\underline{b}} \qquad (7.16)$$

7.5 The Initial ERS-1 Orbits

Using the force models in table 7.3, ephemerides for ERS-1 have been computed using the Aston university orbit determination software described in chapter 4.

Table 7.3 Force Models for SATAN-A Orbit Determination Software

Gravity Field Model	JGM-2 [1] (degree and order 70)
Thermospheric Model	MSIS-83 [2]
Surface Force Model	Aston University Model [3]

1 - [Nerem et al, 1994] , 2 - [Hedin, 1983], 3 - [Ehlers, 1993]

Within the orbit determination the parameters recovered were initial state vector, six hour drag scale factors, a solar reflectivity factor and an empirical once per revolution along track acceleration. The drag scale factors were each given the constraint, C, defined by equation (7.17),

$$C = \overline{C_D} \pm 1.0 \qquad (7.17)$$

where $\overline{C_D}$ is the mean value of the drag scale factors over the arc. Similarly the reflectivity scale factor was given a constraint of 1±0.2.

For test purposes the period analysed, MJD 49006 - MJD 49041, corresponded to cycle 9 of ERS-1's multi-disciplinary phase, and the orbits were converged using crossover and laser range data. Both data types were assigned unit weights and each arc was typically six days in length with consecutive arcs

having a one day overlap, except close to orbital manoeuvres.

Table 7.4 Corrections Used for the ERS-1 Altimetry.

Ocean Tide Model	CSR 3.0 [1]
Ionospheric Correction	BENT Model[2]
Wet and Dry Troposphere	OPR Correction
Solid Earth Tides	OPR Correction
Inverse Barometer Correction	Applied (derived from dry troposphere)
Sea State Bias	5.95% $h_{1/3}$ (derived in chapter 5)
Sea Surface Topography	JGM-2 Geosat Model (deg & order 15)
Geoid Model	JGM-2[3] (degree & order 70) OSU91A[4] (degrees and orders 70 - 360)
Altimeter Range Bias	-75.0cm

1 - [Eanes R, 1995] , 2 -[Llewellyn and Bent, 1973], 3- [Nerem et al, 1994], 4 - [Rapp et al, 1991]

The models used for the various ERS-1 altimetric corrections are given in table 7.4 and the TOPEX/Poseidon altimetry was similarly corrected with the following exceptions. For sea state bias the Gaspar 4 parameter model [Gaspar et al, 1994] (expressed by equation(5.6)) was used. Also the dual frequency ionospheric correction was deemed more accurate than that given by the BENT model. As the DORIS tracking data was not readily available to allow the determination of sufficiently accurate in-house TOPEX/Poseidon orbits the orbit heights used were the NASA JGM-2 orbit heights given on the AVISO CDROM.

Computation of the orbits for cycle 9 enabled the determination of all the single and dual crossover locations, and corresponding residuals. On imposing a maximum time difference of five days between the two epochs, so

that any ocean signal is not observed, the data distributions presented in figures 7.3 and 7.4 are obtained.

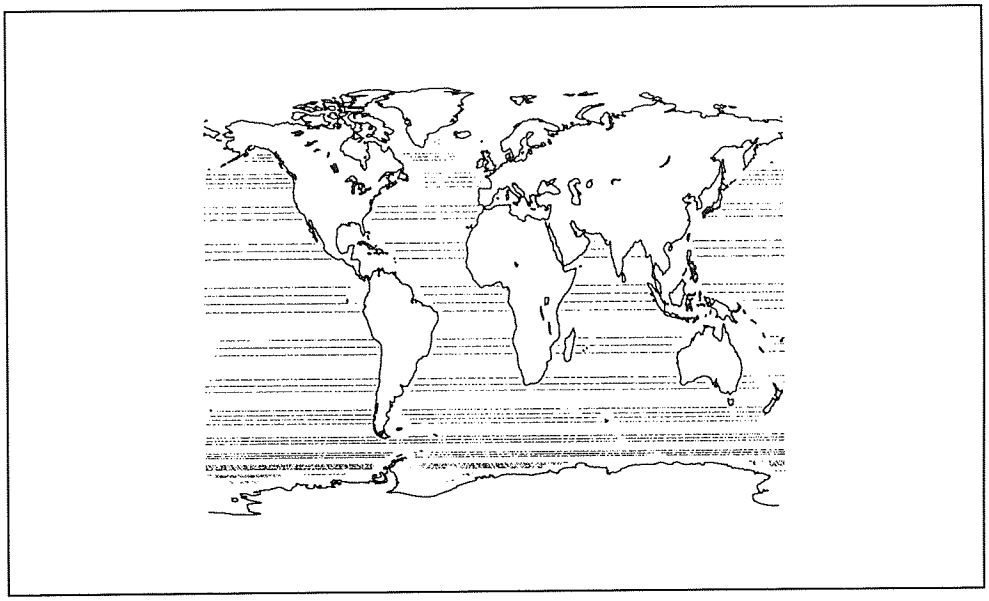

Figure 7.3 Single Satellite Crossover Distribution for Cycle 9

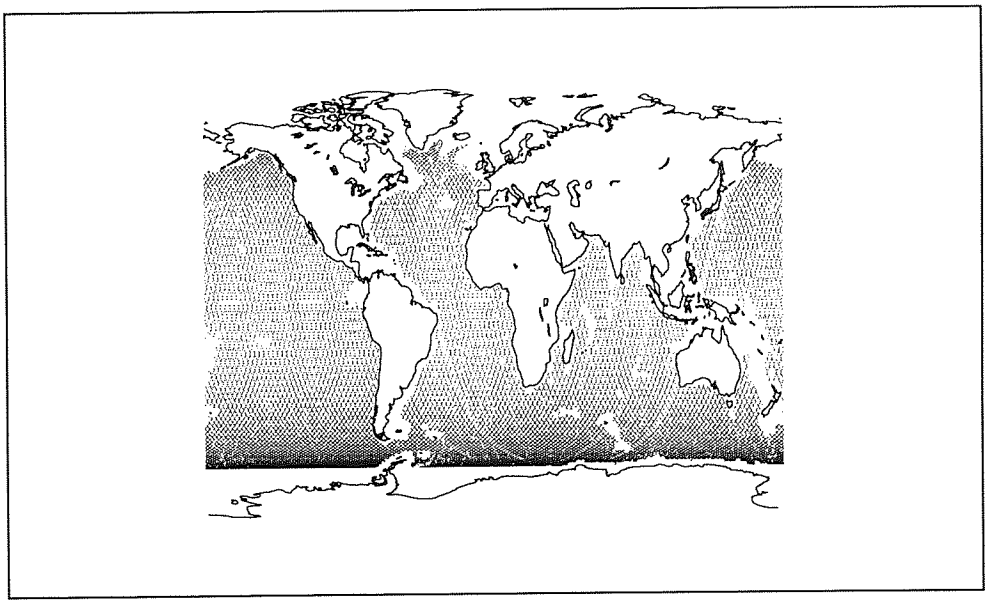

Figure 7.4 Dual Crossover Data Distribution for Cycle 9

The improved distribution of dual crossovers is a consequence of the 5 day time restriction limiting the single satellite crossovers to specific latitudes. The high inclination of ERS-1 causes the concentration of single satellite crossovers to be at high latitudes which are predominantly over ice or land such that they are of no use as satellite tracking data.

Table 7.5 Rms Fits to the Crossover and Altimeter Datasets for Cycle 9.

DATES (MJD)	SXO Rms (cm)	DXO Rms (cm)	Alt Rms (cm)
49005 - 49011	14.5 (0.7%)	12.0 (0.2%)	25.2 (1.0%)
49010 - 49016	13.0 (1.4%)	14.4 (0.6%)	22.9 (1.2%)
49015 - 49022	14.0 (0.7%)	12.2 (0.1%)	23.3 (1.3%)
49022 - 49027	14.3 (4.4%)	13.2 (2.2%)	24.7 (3.1%)
49026 - 49032	14.0 (0.7%)	12.2 (0.5%)	23.9 (1.5%)
49031 - 49037	14.5 (1.2%)	13.0 (0.7%)	23.9 (1.4%)
49036 - 49042	15.8 (0.7%)	12.8 (0.4%)	24.4 (1.1%)

On employing a rejection criterion of 40cm for crossovers and 70cm for altimetry (with respect to an *apriori* relative range biases of 30.2/45.0cm for TOPEX/Poseidon dual crossovers) yielded the rms fits to the crossover and altimeter datasets as given in table 7.5 where the numbers in parenthesis are the percentage of observations rejected.

As a comparison the fits of the TOPEX single satellite crossovers are provided in figure 7.5 which show the typical rms value to be 7.5cm

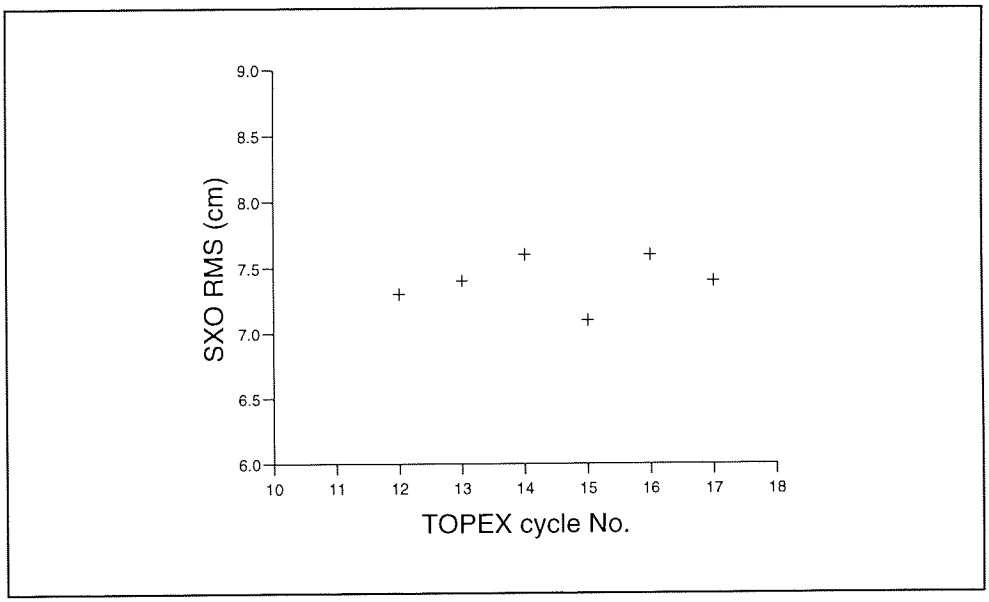

Figure 7.5 TOPEX Single Satellite Crossover Residual Rms Values

As a signal of 1.7cm rms in the TOPEX single satellite crossovers can be attributed to the variable component of the geographically correlated orbit error [Moore et al, 1996(a)] the remaining signal due to altimetric correction and non conservative force mis modelling radial errors can be estimated as 5.0cm rms.

As would be expected the ERS-1 orbital fits are significantly poorer than those for TOPEX/Poseidon. If the dual crossover is considered as a measure of the ERS-1 radial error, and signals of 5.0cm rms are removed for both the error contributions of TOPEX (altimetric and non conservative force mis modelling) and ERS-1 (altimetric errors) the ERS-1 radial accuracy can be approximated to 10.4cm rms. It should be noted that this is only an estimate as the accuracy of the ERS-1 altimeter measurement is unknown. However, the assumption that the ERS-1 altimeter accuracy is less than that of TOPEX is founded on the use of the less accurate BENT ionosphere and sea state bias models.

7.6 The Orbit Refinement

Early work [Carnochan et al, 1994] using the GEMT2 [Marsh et al, 1989] gravitational field for the derivation of both ERS-1 and TOPEX/Poseidon orbits revealed that the recovery of error terms for TOPEX/Poseidon as well as ERS-1 provided the optimal solution. This solution strategy also employed ERS-1 single satellite crossovers to extend the latitude range of data provided by the dual crossovers. However, with the creation of the JGM [Nerem et al, 1994] gravity fields, and the resulting improvements in the TOPEX/Poseidon orbits, as observed in the crossover residuals typically approximating 7.5 cm rms, it was deemed that the TOPEX/Poseidon orbit error signal (3-4cm rms in the radial direction) was too small to be identified without absorbing other signals. This has therefore resulted in the ERS-1 parameters being the only parameters solved for. Several solution strategies, employing both dual and single satellite crossover residuals, are now described in the subsequent sections.

7.7 The Thirty Five Day Solution

In the first instance one solution for the entire 35 day cycle was obtained, using both the single and dual crossover datasets and the constraints outlined in section 7.3. By eliminating periods of overlap and using equation (7.2) to model the radial error for ERS-1 some 210 parameters were recovered. This total of 210 parameters comprised of 76 frequencies which are defined by a cosine and sine term, 7 sets of 8 arc dependent parameters and two constants. Initially recovery of both TOPEX and Poseidon constants for each of the arcs was attempted, however, this resulted in large correlations to the extent that the recovered solution was unreliable.

The initial and post correction fits to the crossover datasets subject to a 40cm prior to correction and 30cm post correction rejection levels are presented in table 7.6 and the recovered ERS-1 error shown in figure 7.6 .

Table 7.6 Pre and Post Correction Rms Fits to the Crossover Datasets.

	SXO Rms (cm)	DXO Rms (cm)
Initial ERS-1 Orbits	14.5 (1.6%)	12.6 (0.6%)
Corrected ERS-1 Orbits	11.0 (1.1%)	10.1 (0.6%)

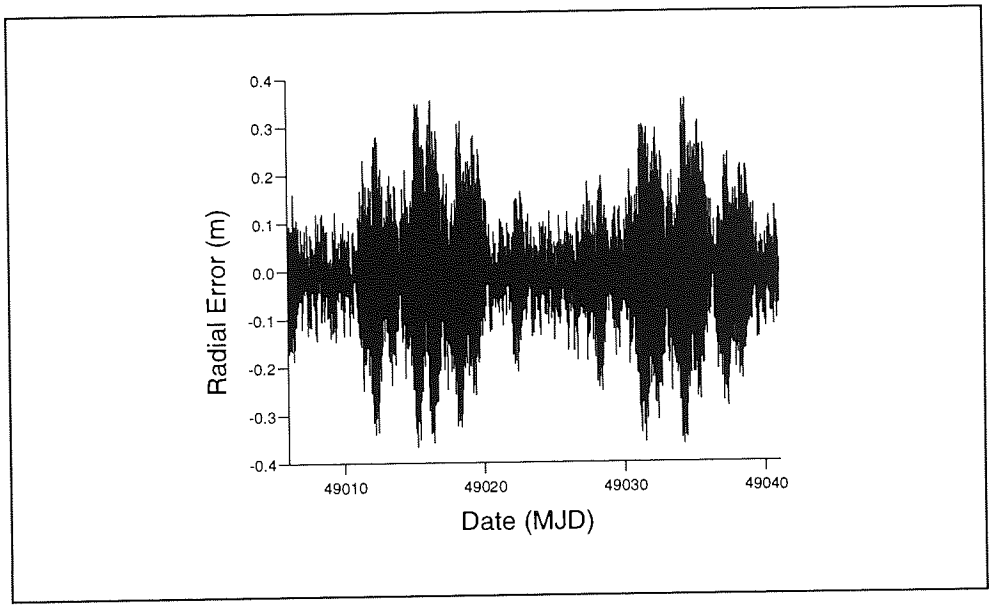

Figure 7.6 Recovered Error for the 35 Day Solution

Evidence for reduction in the radial error is seen as both single and dual satellite crossover residuals have been reduced whilst more single satellite crossover observations have been accepted.

Again using the dual crossover as a measure of the ERS-1 radial accuracy and assuming that the signal removed by the correction procedure is purely ERS-1 orbit error, the accuracy of the corrected ERS-1 orbits is 7.2cm rms (after the removal of 7.5cm rms).

The recovered error signal, shown in figure 7.6 , has an rms of 11.0cm and exhibits peaks where certain arcs are less well defined. This suggests that

the recovered signal is not a complete representation of the orbit error as the dual and single satellite crossover residuals should exhibit a more significant reduction than the 7.5cm rms obtained.

To check the validity of the solution the eigenvalues and eigenvectors of the covariance matrix were analysed to determine possible errors in the recovered solution. The eigenvalues are plotted in figure 7.7, and show that none of the recovered terms cause a serious degradation in the solution as the maximum eigenvalue is only 5.3cm.

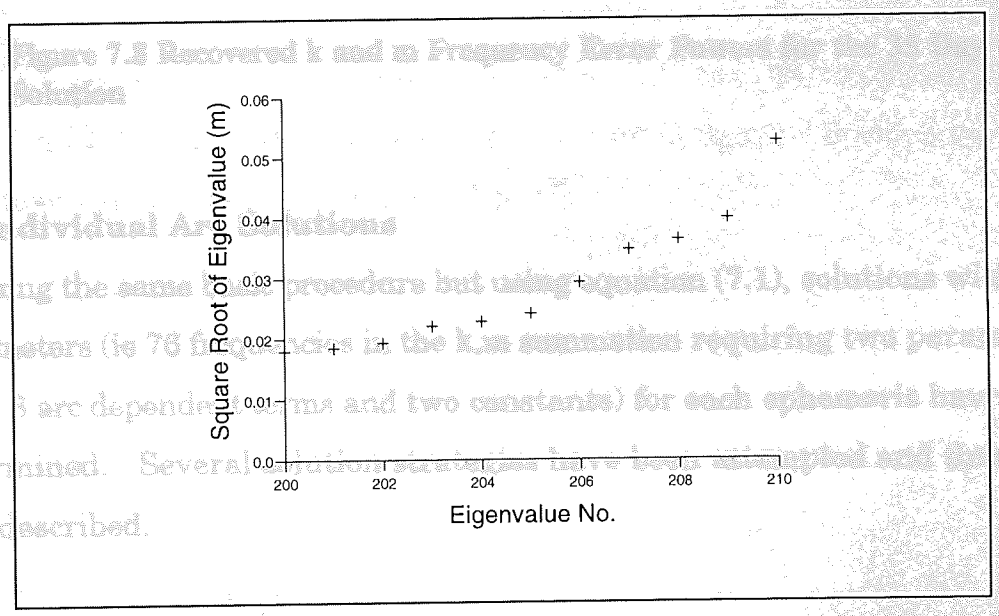

Figure 7.7 Recovered Eigenvalues for the 35 Day Solution

The powers of the k and m frequencies recovered are shown in figure 7.8 to have similar values to those in figure 7.1. This therefore suggests that the strategy is not optimal for the error model derived and solutions have therefore been determined for each arc.

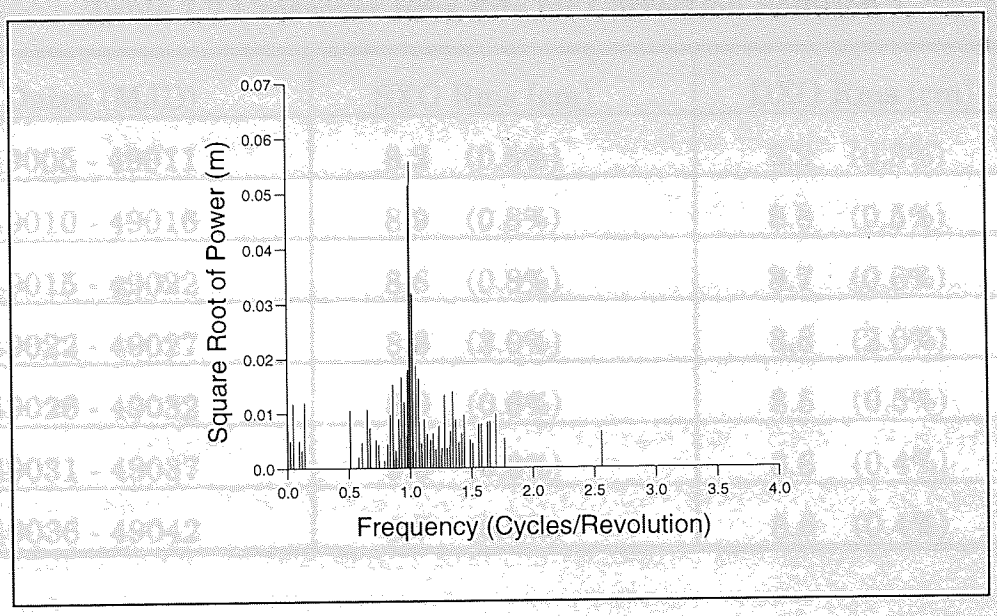

Figure 7.8 Recovered k and m Frequency Error Powers for the 35 Day Solution

7.8 Individual Arc Solutions

Utilising the same basic procedure but using equation (7.1), solutions with 162 parameters (ie 76 frequencies in the k,m summation requiring two parameters each, 8 arc dependent terms and two constants) for each ephemeris have been determined. Several solution strategies have been attempted and these are now described.

7.8.1 Solution 1: Recovery of All Terms

Recovering all the ERS-1 terms in equation (7.1) for each individual arc resulted in the post correction rms fits to the crossover datasets as those presented in table 7.7 when rejection levels of 30cm for both datasets were employed.

Table 7.7 Crossover Rms Fits for Correction Solution 1.

Dates (MJD)	SXO Rms (cm)	DXO Rms (cm)
49005 - 49011	8.2 (0.5%)	8.2 (0.3%)
49010 - 49016	8.9 (0.8%)	8.8 (0.5%)
49015 - 49022	8.6 (0.8%)	8.7 (0.6%)
49022 - 49027	8.8 (3.0%)	8.8 (2.0%)
49026 - 49032	8.9 (0.6%)	8.5 (0.5%)
49031 - 49037	9.0 (0.3%)	8.6 (0.4%)
49036 - 49042	8.7 (0.6%)	8.6 (0.4%)

The recovered constant terms, measures of the TOPEX/ERS-1 and Poseidon/ERS-1 relative range biases are plotted in figure 7.9 which result in the mean values presented in table 7.8.

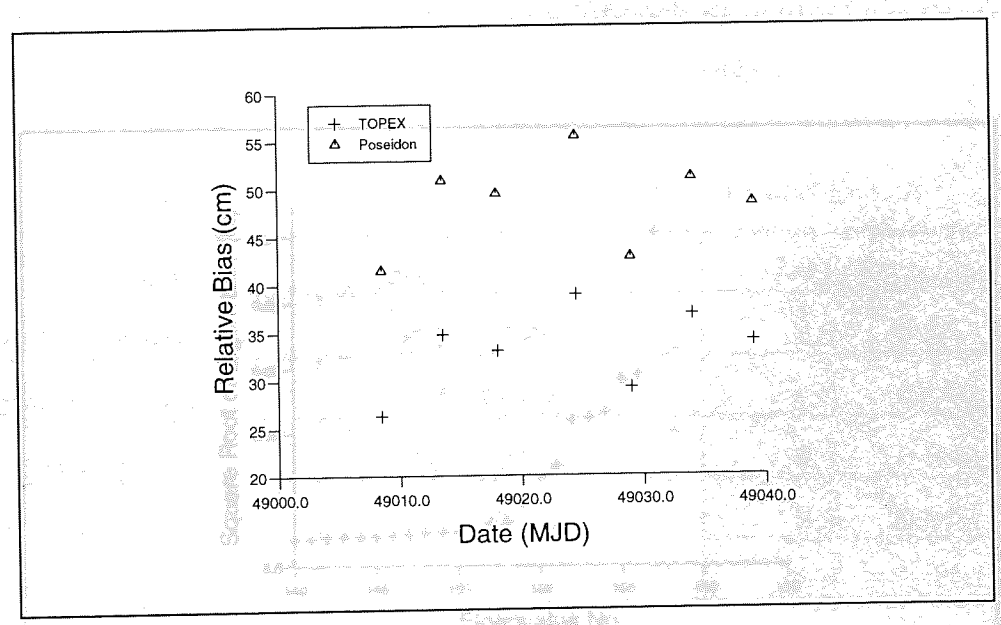

Figure 7.9 Recovered Relative Altimeter Range Biases for Cycle 9

Table 7.8 Relative Altimeter Biases for Cycle 9

Altimeters	Relative Range Biases
TOPEX / ERS-1	33.3 ± 4.0 cm
Poseidon/ ERS-1	48.5 ± 4.5 cm

Clearly the resultant values for the TOPEX/Poseidon - ERS-1 relative range biases are noisy. This is most likely caused by the absorption of some orbit error and or sea state bias errors into the recovered parameters.

The solution strategy, however, results in the fits to the single and dual satellite crossovers being significantly reduced, thus indicating a sizeable reduction in orbit error. The mean dual crossover residual of 8.6cm suggests that a signal of 9.2 cm has been removed such that the accuracy of the ERS-1 orbits is now 4.9cm rms.

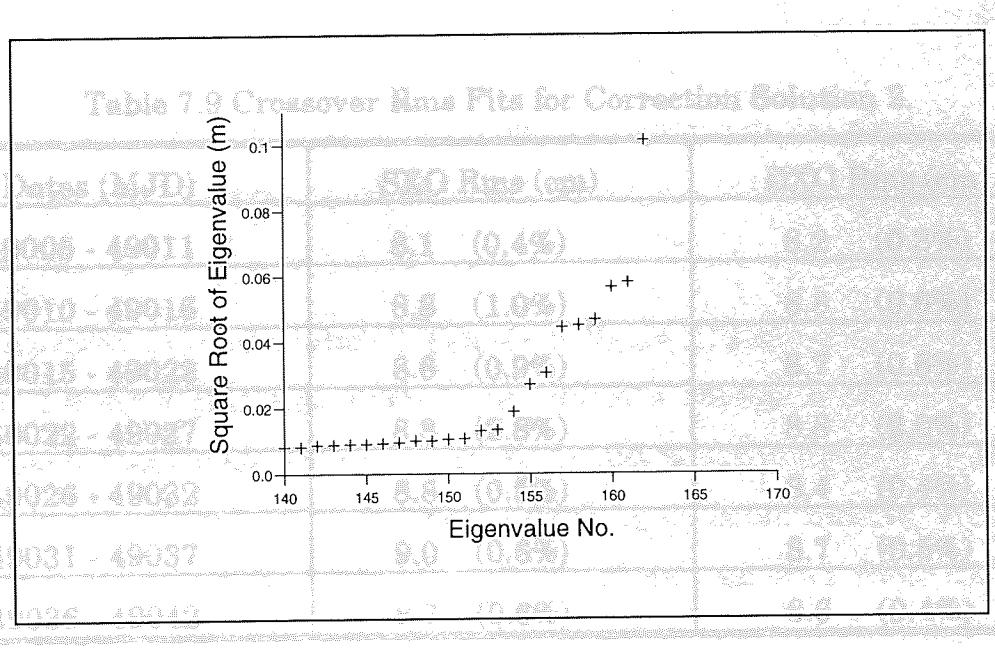

Figure 7.10 Eigenvalues of Solution 1 for the Arc MJD 49026-49032

Analysis of the eigenvalues (those recovered for the arc MJD 49026 - MJD 49032 are shown in figure 7.10) of the covariance matrix reveals that some terms are highly correlated resulting in a degradation of the solution.

The recovered eigenvectors suggest that the terms responsible for the largest eigenvalues (10.1cm, 5.8cm and 5.7 cm) are the constant terms ($C_1^{T/P}$ and C_1^{Pos}), the once per revolution terms (C_6 and C_7) and the frequencies where (k,m) are equal to (2,43) and (4,43). Now the constant terms are important to model the relative altimeter biases which are approximately 30cm for TOPEX - ERS-1 and 45cm for Poseidon - ERS-1 dual crossover, whilst the terms with frequencies at and close to one cycle per revolution are expected to contribute significant errors. For this reason it was decided to investigate two other solution strategies which are now described.

7.8.2 Solution 2: Suppression of the Constant Terms

Using the constant terms obtained for the 35 day solution and suppressing their recovery during the error estimation for each individual arc resulted in the post correction crossover rms fits presented in table 7.9.

Table 7.9 Crossover Rms Fits for Correction Solution 2.

Dates (MJD)	SXO Rms (cm)	DXO Rms (cm)
49005 - 49011	8.1 (0.4%)	8.2 (0.3%)
49010 - 49016	8.8 (1.0%)	8.8 (0.6%)
49015 - 49022	8.6 (0.9%)	8.7 (0.6%)
49022 - 49027	8.8 (2.8%)	8.8 (2.0%)
49026 - 49032	8.8 (0.5%)	8.4 (0.4%)
49031 - 49037	9.0 (0.6%)	8.7 (0.5%)
49036 - 49042	8.7 (0.6%)	8.6 (0.4%)

Clearly the suppression of the constant terms has resulted in no degradation of the fits to the crossover data as the mean dual crossover fit of 8.6cm suggests a radial accuracy of 4.9cm rms.

The eigenvalues of the covariance matrix for this solution corresponding to the arc MJD 49026 - 49032 are given in figure 7.11 and show that the maximum eigenvalue, of 10.1cm, has been removed and that a significantly more reliable solution has been obtained.

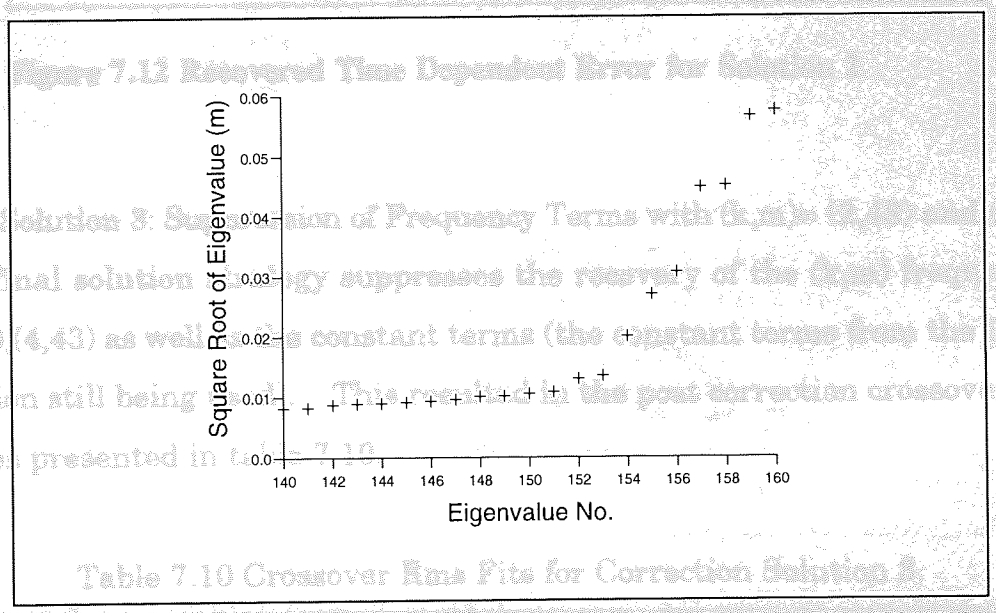

Figure 7.11 Eigenvalues of Solution 2 for the Arc MJD 49026-49032

The recovered error for solution 2 is shown in figure 7.12 and comparisons with figure 7.6 show that this strategy results in a similar error recovery as obtained for the 35 day solution. However, the peaks in figure 7.12 are not as noisy and this results in the overall error signal being smaller having an rms of 9.2 cm, which is identical to the signal removed from the dual crossovers.

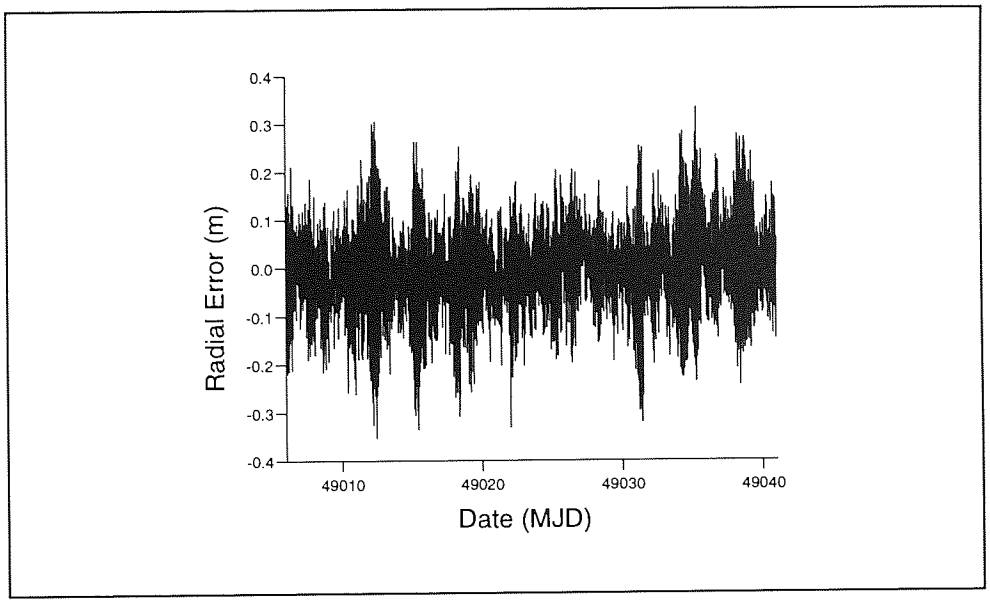

Figure 7.12 Recovered Time Dependent Error for Solution 2

7.8.3 Solution 3: Suppression of Frequency Terms with (k,m)= (2,43) and (4,43)
The final solution strategy suppresses the recovery of the (k,m) frequencies (2,43),(4,43) as well as the constant terms (the constant terms from the 35day solution still being used). This resulted in the post correction crossover rms values presented in table 7.10.

Table 7.10 Crossover Rms Fits for Correction Solution 3.

Dates (MJD)	SXO Rms (cm)	DXO Rms (cm)
49005 - 49011	8.9 (0.5%)	8.5 (0.3%)
49010 - 49016	8.8 (1.0%)	8.8 (0.6%)
49015 - 49022	8.8 (1.1%)	8.9 (0.6%)
49022 - 49027	8.8 (3.3%)	8.9 (2.2%)
49026 - 49032	8.9 (0.8%)	8.4 (0.5%)
49031 - 49037	9.2 (0.5%)	8.7 (0.4%)
49036 - 49042	9.2 (0.6%)	8.9 (0.5%)

The mean dual crossover rms value of 8.7cm reveals that the suppression of the frequencies close to one cycle per revolution has resulted in a less significant improvement. The approximate radial accuracy of the ERS-1 orbits using this solution strategy is therefore only 5.1cm rms.

Analysis of the covariance matrix eigenvalues (figure 7.13) shows that the possible error in the error solution is now less than 3.5cm.

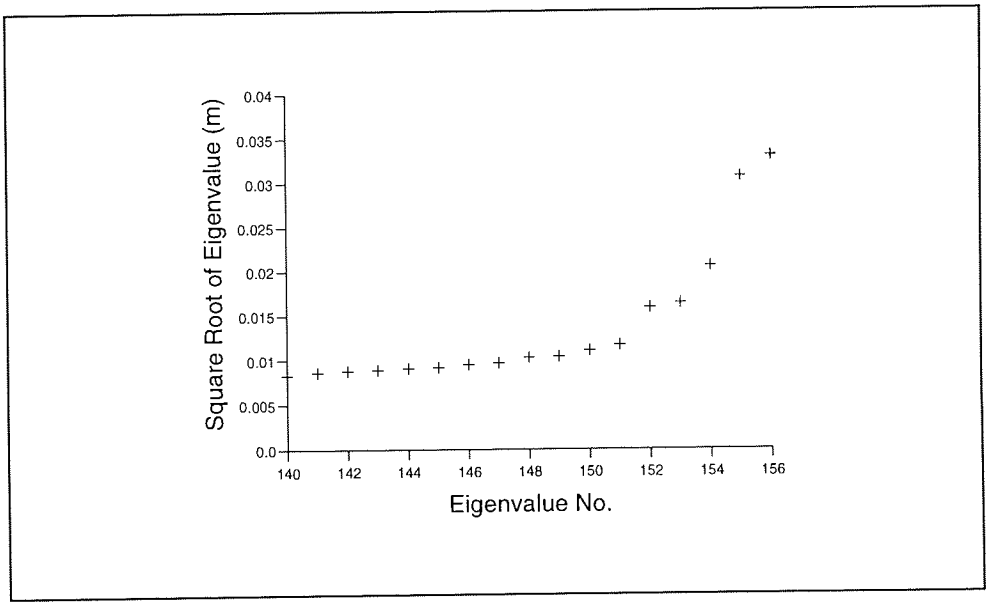

Figure 7.13 Eigenvalues of Solution 3 for the Arc MJD 49026-49032

7.9 Analysis of Error Recovery Strategies

Clearly the suppression of the constant terms has provided a more reliable solution in that the largest eigenvalue (and hence possible error in the recovered solution) has been removed. This is of even more significance when arcs outside cycle 9 are considered as the maximum eigenvalue associated with the two constant terms was observed to be as high as 40cm, most likely because of the shortage of Poseidon data. The suppression of the terms with frequency close to one cycle per revolution has reduced the maximum

eigenvalue but as these frequencies are significant contributors to the radial orbit error it remains to be seen as to whether the suppression of these terms is beneficial.

Analysis of tables 7.7, 7.9 and 7.10 shows that the suppression of the constant terms does not significantly alter the reduction in the crossover rms fits, however, by suppressing those frequencies close to one cycle per revolution the crossover rms reduction is marginally lower.

The rms values of the recovered error signals, the suggested signal removed from the dual crossover residual improvement and the estimated ERS-1 radial accuracies for each of these strategies are given in table 7.11.

Table 7.11 Error Signal Removed by Each Correction Procedure.

Correction Procedure	Error Signal Rms	DXO Signal Removed	ERS-1 Radial Accuracy
35 day Solution	11.0 cm	7.5 cm	7.2 cm
Solution 1	9.2 cm	9.2 cm	4.9 cm
Solution 2	9.2 cm	9.2 cm	4.9 cm
Solution 3	8.8 cm	8.8 cm	5.1 cm

7.10 Application of the Error to the Altimeter Datasets

Whilst the significant reduction of the dual and single satellite rms fits is encouraging, the use of these datasets within the radial orbit error recovery implies that this cannot be taken as total validation of radial orbit error removal. For this reason an independent data set in the form of 30 second normal altimeter residuals has been calculated for each of the recovered error solutions using the same geophysical corrections as outlined in table 7.4.

Table 7.12 Altimeter Fits for the Various Orbit Correction Strategies.

ERS-1 Orbit	Altim Rms (cm)
Original	24.1 (1.5%)
Corrected - 35 day Solution	23.9 (1.5%)
Corrected - Solution 1	23.6 (1.4%)
Corrected - Solution 2	23.6 (1.4%)
Corrected - Solution 3	23.6 (1.5%)

The fits to this altimeter data set are given in table 7.12 where it can be seen that the signals removed for the 35day and individual arc corrections are 3.1cm and 4.9cm respectively. These signals are much lower than those suggested by the single and dual crossover reductions.

Analysis of the pre- and post-correction altimeter residual fits when the error from solution 2 is applied for each individual arc as shown in table 7.13 suggests that the sea surface topography used is poor.

Table 7.13 Altimeter Rms Values for Solution 2

Dates (MJD)	Orig Altim Fit Rms	Corr Altim Fit Rms
49005 - 49011	25.2 (1.0%)	23.7 (0.9%)
49010 - 49016	22.9 (1.2%)	23.0 (1.3%)
49015 - 49022	23.3 (1.3%)	23.2 (1.1%)
49022 - 49027	24.7 (3.1%)	23.6 (2.7%)
49026 - 49032	23.9 (1.5%)	23.9 (1.6%)
49031 - 49037	23.9 (1.4%)	23.7 (1.4%)
49036 - 49042	24.4 (1.1%)	24.0 (1.1%)

Indeed the corrected rms values for some arcs are higher than the uncorrected values suggesting that the sea surface topography errors are masking the initial orbit error and hence the improvement in radial position.

For this reason a degree and order 15 sea surface topography with respect to the geoid defined in table 7.4, h_{sst}, has been derived from TOPEX data covering the period MJD 49006 - 49041. Equation (7.18) describes the sea surface recovered,

$$h_{sst}=\sum_{l=1}^{l=15}\sum_{m=0}^{m=l}(C_{lm}^{sst}\cos m\lambda+S_{lm}^{sst}\sin m\lambda)\overline{P_{lm}}(\sin\Phi) \qquad (7.18)$$

where C_{lm}^{sst} and S_{lm}^{sst} are the normalized harmonic coefficients, P_{lm} are the normalized polynomials, λ is the longitude and Φ the latitude.

The rms fits of the original and corrected altimeter residuals with this more accurate independently determined sea surface are shown in table 7.14.

Table 7.14. Altimeter Fits to the Derived TOPEX Sea Surface.

ERS-1 Orbit	Altim Rms (cm)
Original	19.1 (1.2%)
Corrected - 35 day solution	18.0 (1.2%)
Corrected - solution 1	17.6 (1.2%)
Corrected - solution 2	17.6 (1.2%)
Corrected - solution 3	17.6 (1.2%)

The reductions in each of these datasets suggest the removal of 6.4cm rms for the 35 day solution and 7.4cm rms for each of the individual arc solutions. Whilst these values are still slightly lower than the signals removed from the crossover datasets the values are much closer than those obtained with the GEOSAT sea surface.

7.11 Conclusions

The solution strategy of estimating the radial orbit error for the full cycle has not worked as well as determining the error for individual arcs. This is of course due to the fact that more parameters are used to define the radial error and the k and m frequency terms can therefore absorb some of the non-gravitational orbit error. Clearly the suppression of the constant terms and frequencies close to once per revolution has little impact on the models ability to recover the ERS-1 radial orbit error for individual arcs. With the largest eigenvalue due to the correlation between constant terms sometimes rising as high as 40cm it would appear prudent to use the constant terms derived by the 35 day solution and suppress their recovery when determining the error for each arc.

The suppression of the frequency terms close to one cycle per revolution (k,m) = (2,43) and (4,43) , however, results in a less significant improvement in the crossover fits. As these terms are expected to contribute significantly to the orbit error as the ERS-1 orbit is near resonance for m=43 the suppression of these terms is not considered beneficial. The solution strategy adopted is therefore solution 2.

Chapter 8

Validation of Radial Orbit Error Removal and Accuracy Assessment of the Corrected ERS-1 Orbits

8.1 Introduction

In chapters 6 and 7 the radial orbit error model was derived and applied to cycle 9 of ERS-1's multi-disciplinary phase. This chapter describes validation procedures used to confirm that the radial orbit error has been reduced, thus enabling a unification of the TOPEX and ERS-1 altimeter datasets, and to assess the accuracy of the corrected orbits for 13 cycles of ERS-1 data. The chapter is subsequently split into four sections : recovery of the ERS-1 relative range biases with respect to TOPEX and Poseidon; mean sea surface and variability comparisons between ERS-1 and TOPEX; calculation of the geographically correlated mean and variable (variation about the mean) components of the ERS-1 radial orbit error and comparisons of the Aston University ERS-1 orbital refinement with those corrected by cubic splines [Le Traon, 1995].

8.2 The ERS-1 Orbits and Data Preparation

Using the orbit determination software outlined in chapter 4 and the models outlined in chapter 7, orbits have been generated for 13 cycles (cycle 6 - cycle 18) of ERS-1's multi-disciplinary phase. This corresponds to some 440 days of data covering the period MJD 48901 - 49343 (6th October 1992 - 22nd

December 1993). Both laser range and single satellite crossover tracking data was utilised to determine the baseline ERS-1 orbits which were then corrected using the model derived in chapter 6 and the methodology described in chapter 7. The resulting mean pre- and post- correction rms fits to the crossover (single and dual satellite) and altimeter datasets for each cycle are those given in tables 8.1 and 8.2 when the *apriori sea* surface model used is the GEOSAT derived model described in chapter 7 and rejection levels of 40/30cm and 70cm are used for the original/corrected crossover and altimetry data sets respectively.

Table 8.1 Rms Fits for the Original ERS-1 Orbits.

Cycle No.	Δ_{SXO} (cm)	Δ_{DXO} (cm)	Δ_{ALT} (cm)
6	12.8 (2.4%)	12.8 (2.4%)	24.7 (1.3%)
7	13.4 (0.8%)	12.4 (0.4%)	23.5 (1.1%)
8	13.6 (1.6%)	12.7 (0.8%)	24.7 (1.4%)
9	14.5 (1.6%)	12.6 (0.6%)	24.1 (1.5%)
10	13.0 (0.8%)	11.7 (0.6%)	24.4 (1.6%)
11	13.1 (1.2%)	12.3 (0.8%)	24.4 (1.4%)
12	13.3 (1.2%)	12.4 (0.7%)	24.4 (1.2%)
13	13.6 (4.0%)	12.5 (1.7%)	24.7 (2.7%)
14	13.2 (0.7%)	12.1 (0.6%)	24.1 (1.1%)
15	13.1 (1.1%)	12.3 (0.7%)	24.0 (1.5%)
16	13.0 (0.6%)	11.5 (0.3%)	23.5 (1.2%)
17	12.9 (2.1%)	11.8 (1.0%)	23.3 (1.4%)
18	12.9 (0.8%)	11.6 (1.7%)	23.7 (1.1%)

On taking the mean of the dual crossover values of table 8.1 and assuming 5.0cm contributions from TOPEX altimetric and orbit errors and a 5.0 cm

contribution from ERS-1 altimetric errors the radial accuracy of ERS-1 for the 13 cycles can be estimated as 9.9 cm rms.

Table 8.2 Rms Fits for the Corrected ERS-1 Orbits.

Cycle No.	Δ_{SXO} (cm)	Δ_{DXO} (cm)	Δ_{ALT} (cm)
6	8.9 (0.8%)	9.0 (0.8%)	23.2 (1.2%)
7	8.6 (0.6%)	8.8 (0.7%)	22.9 (1.0%)
8	8.4 (0.6%)	8.6 (0.6%)	23.0 (1.2%)
9	8.7 (0.9%)	8.6 (0.7%)	23.6 (1.4%)
10	9.1 (0.7%)	8.7 (0.7%)	23.7 (1.6%)
11	9.3 (1.2%)	9.4 (1.0%)	23.6 (1.3%)
12	9.0 (0.8%)	9.3 (1.0%)	23.3 (1.1%)
13	8.7 (4.6%)	9.1 (2.6%)	23.2 (2.5%)
14	8.8 (0.7%)	8.9 (1.0%)	23.5 (0.9%)
15	8.0 (0.7%)	8.5 (0.7%)	22.9 (1.4%)
16	8.3 (0.3%)	8.5 (0.7%)	22.8 (1.1%)
17	8.5 (1.6%)	8.6 (1.0%)	22.8 (1.4%)
18	8.5 (0.5%)	8.3 (0.6%)	22.9 (1.0%)

Using the assumptions outlined in chapter 7 regarding the error contributions from TOPEX (altimetric and orbit) and ERS-1 (altimetric) the mean dual crossover fit of 8.8cm indicates a radial accuracy 5.2cm rms if ERS-1 orbit error is the only signal removed. This value is slightly higher than that obtained for cycle 9 in chapter 7 because the geographical distribution of crossovers varies throughout the year and cycle 9 gives a particularly good distribution due to the epochs corresponding to the southern hemisphere summer.

8.3 Recovery of the Relative Altimeter Range Biases

An important component in unifying different altimeter datasets is the removal of relative altimeter range biases. The constant terms in the recovery of the radial orbit error model are predominantly due to these relative biases (hence the recovery of two constants - one for TOPEX and one for Poseidon). It should be noted, however, that with the movement of the reference time to the middle of the arc for the arc dependent parameters (C_1 ... C_9) some of the constant term will be due to orbit error of an originally secular nature. Similarly, any error in the ERS-1 (or TOPEX/Poseidon) sea state bias will result in an offset that contributes to the recovered relative range bias, particularly as the dual crossovers are concentrated in the southern oceans where high wave heights (and hence errors in the sea state bias) are often observed. These additional signals, however, should only take the size of a few centimetres and only contribute noise to the relative biases recovered over the 13 cycles as the full annual cycle of wind and waves is sampled. As the solution procedure adopted involves suppressing the recovery of the constant term when recovering the error for each arc (as described by solution 2 in chapter 7), solutions for each of the 35 day cycles have been obtained.

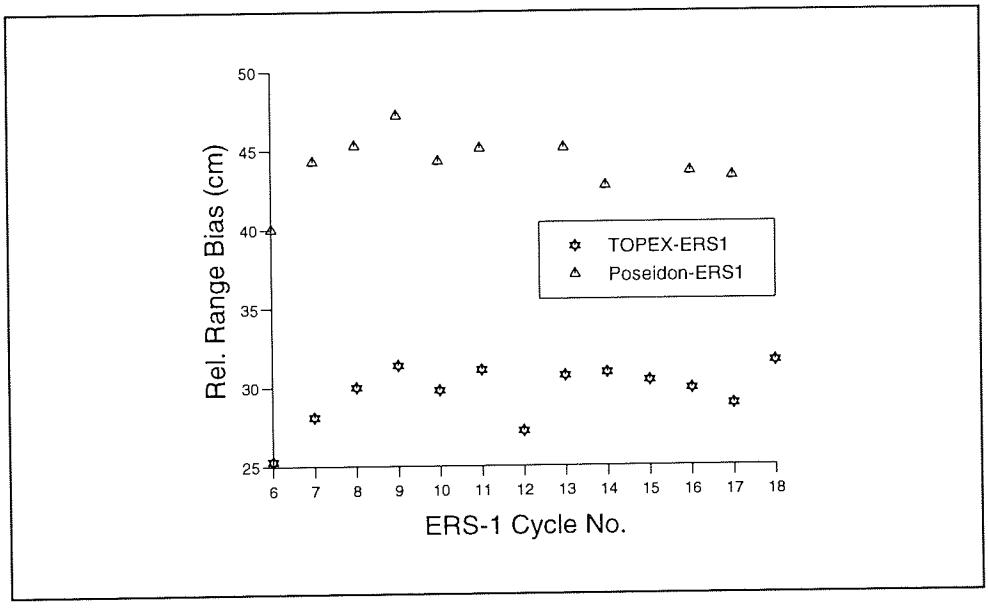

Figure 8.1 The TOPEX/Poseidon - ERS-1 Relative Range Biases

The 13 relative bias values obtained are shown in figure 8.1 which on averaging give the relative biases shown in table 8.3.

Table 8.3 Mean TOPEX/Poseidon - ERS-1 Relative Range Biases.

Altimeters	Relative Range Bias (cm)
TOPEX - ERS-1	30.2 ±1.8
Poseidon - ERS-1	45.0 ±1.9

The values in table 8.3 compare with the absolute range bias values of -39.3 ± 5.0 cm , -17.3 ± 3.0 cm and -0.3 ± 3.0 cm obtained for ERS-1, TOPEX and Poseidon through short arc analysis by Murphy et al [1996]. Using the absolute values of range bias the relative range biases obtained are 22.0 ± 6.0 cm and 39.0 ± 6.0 cm for TOPEX/ERS-1 and Poseidon/ERS-1 respectively. Some difference between the relative range biases observed is obvious, however, the error bars do overlap (just).

8.4 Mean Sea Surface and Annual Variability Comparisons

To validate the removal of radial obit error and unification of the ERS-1 and TOPEX altimeter datasets in a consistent manner, mean sea surfaces and sea surface variability studies have been performed with both datasets. This is an important element of validating the removal of orbit error as the ultimate purpose is to improve the accuracy of the ERS-1 altimetry to a level comparable with that of TOPEX/Poseidon.

8.4.1 Mean Sea Surface Comparisons

Mean sea surfaces of degree and order 15, with respect to the geoid outlined in table 7.4, have been determined for both ERS-1 (original and corrected orbits) and TOPEX altimeter datasets for the period MJD 48901 - MJD 49343, corresponding to cycles 6-18 of ERS-1's multi-disciplinary phase. Altimeter

residuals in the form of 30 second normal points have been used to model the mean sea surface by using the spherical harmonic expansion given in equation (7.18).

The mean sea surface derived for the baseline ERS-1 orbits is shown in figure 8.2, whilst the rms fits of the altimeter residuals for both the baseline and corrected orbits with respect to their corresponding mean sea surfaces, are given in table 8.4.

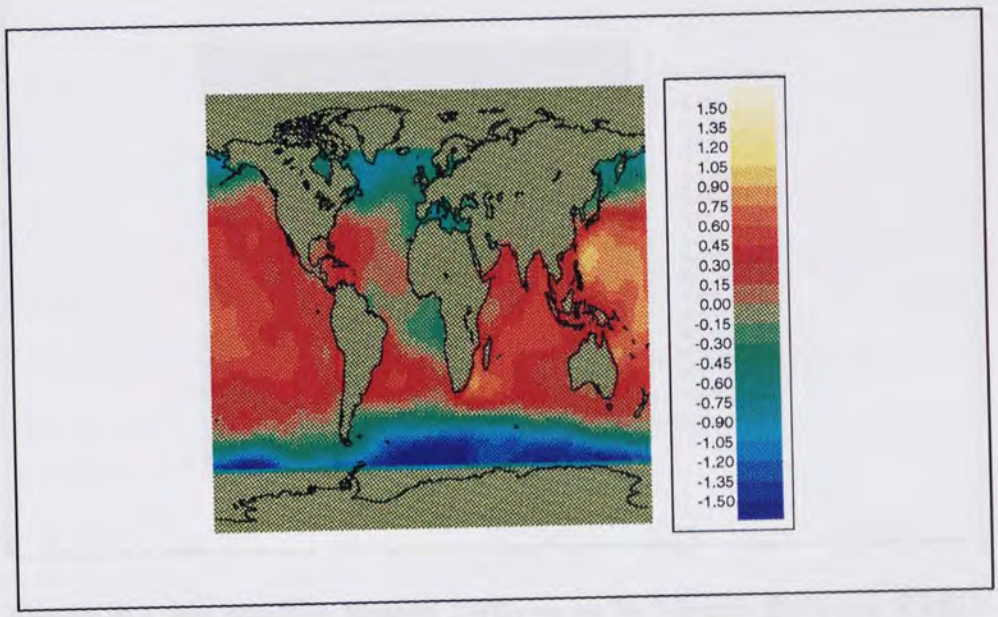

Figure 8.2 Mean Sea Surface Height in Meters Derived from Original ERS-1 Orbits

Table 8.4 Altimeter Fits to the ERS-1 Mean Sea Surfaces.

ERS-1 Orbits and Sea Surface	Altim Rms Fit (cm)
Original	18.6
Corrected	17.6

As shown in table 8.4 the corrected sea surface topography and ERS-1 orbits

provide the better fit to the altimetry data with the removal of 6.0 cm rms from the residuals.

Comparisons of the actual sea surface topographies reveals little as the TOPEX and ERS-1 sea surfaces are all very similar. However, by removing the mean TOPEX sea surface from the two ERS-1 surfaces some significant features can be observed.

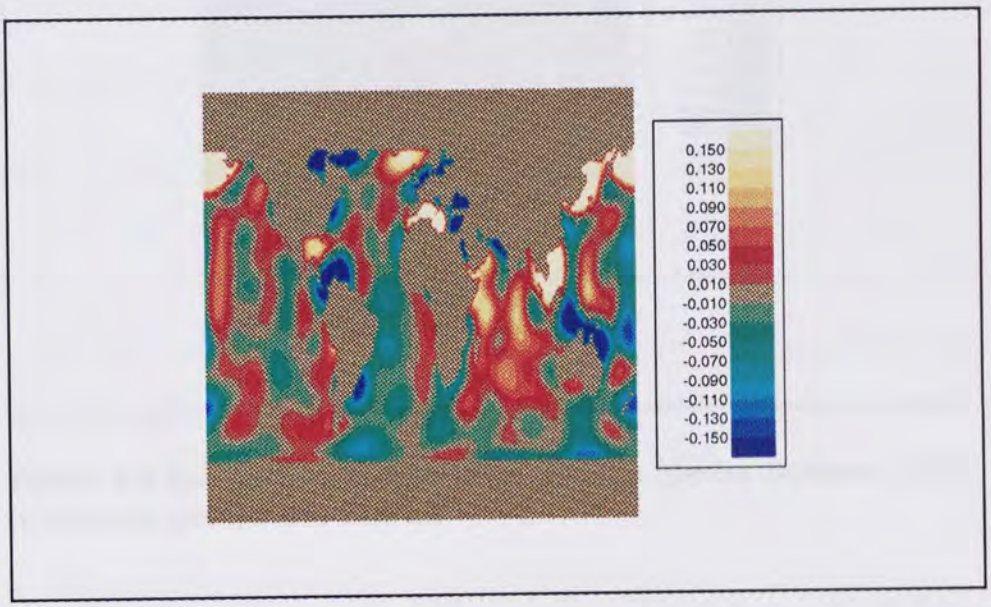

Figure 8.3 Sea Surface Height Differences in Meters Between ERS-1 (Original Orbits) and TOPEX

Figure 8.3 plots the differences between the mean sea surfaces derived from the original ERS-1 and TOPEX altimeter data sets whilst figure 8.4 shows the differences between the corrected ERS-1 and TOPEX mean sea surfaces. Both figures reveal the areas of largest differences (denoted as yellows and blues) to be in coastal and shallow water regions , such as the Mediterranean, around Indonesia, Japan, Gulf of Mexico and Hudson Bay, where the tide model is deficient and the altimetry data is rejected during processing (figures 7.3 and 7.4 show that for cycle 9 no dual or single satellite crossovers are accepted in

these areas). Figure 8.3 , however, also outlines some areas of significant difference, between the original ERS-1 and TOPEX sea surfaces, in the Indian and Pacific Oceans where there is an abundance of altimetry data. Examination of figure 8.4 shows that with the corrected ERS-1 orbits these differences are reduced.

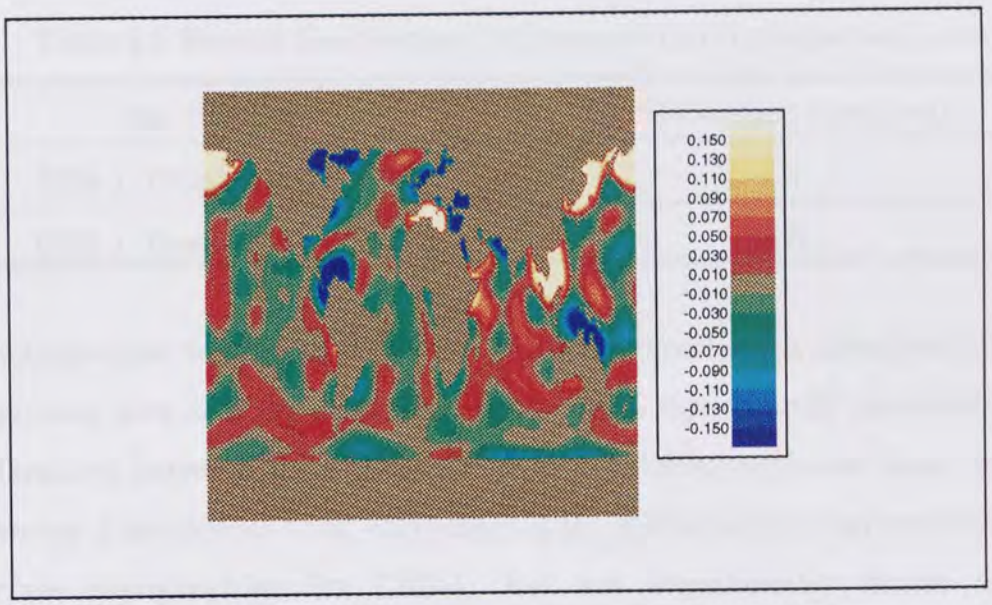

Figure 8.4 Sea Surface Height Differences in Meters Between ERS-1 (Corrected Orbits) and TOPEX

Comparisons of the sea surface differences at each 2 degree by 2 degree grid location between latitudes of ±65 degrees gives the rms variations shown in table 8.5 when no rejection criteria are utilised.

Table 8.5 Rms of Sea Surface Differences (No Rejections)

Sea Surfaces	Difference Rms (cm)
ERS-1 (Original) - TOPEX	9.4
ERS-1 (Corrected) - TOPEX	8.8

This confirms that the corrected ERS-1 sea surface is closer to that derived by

TOPEX with the use of the corrected ERS-1 orbits resulting in an erroneous signal of 3.3cm rms being removed from the sea surface topography. When all grid locations with differences greater than ±15cm (ie the coastal and shallow water areas) are rejected the rms differences between the sea surfaces are those presented in table 8.6.

Table 8.6 Rms of Sea Surface Differences (15 cm Rejection Level)

Sea Surfaces	Difference Rms (cm)
ERS-1 (Original) - TOPEX	4.7
ERS-1 (Corrected) - TOPEX	3.6

It is important to note that the use of a long wavelength spherical harmonic expansion acts as a low pass filter to the data, significantly underestimating differences between the datasets that are of wavelength less than 2600km. However it is evidence that correction of the ERS-1 orbits has resulted in sea surface topographies for ERS-1 that are significantly closer to those determined by TOPEX.

8.4.2 Annual Sea Surface Variability Comparisons

In order to compare the sea surface variabilities observed by both TOPEX and ERS-1, spherical harmonic sea surfaces of degree and order 15 for each ERS-1 35 day period have been determined. This has resulted in 13 sea surfaces being derived for each of the two ERS-1 and the TOPEX altimeter datasets. Subtraction of the corresponding mean surface from each of these near monthly solutions provides a measure of the sea surface variability, with respect to the mean, for each 35 day period. Amplitudes and phases for signals corresponding to a constant, annual, semi annual (six monthly), tri annual (four monthly) and seasonal (three monthly) frequencies have been recovered for every sea surface bin of dimension 2 degrees by 2 degrees.

The recovered amplitudes and phases for the dominant annual variability are shown in figures 8.5 and 8.8 for the original ERS-1 ,figures 8.6 and 8.9 for the TOPEX and figures 8.7 and 8.10 for the corrected ERS-1 altimeter datasets.

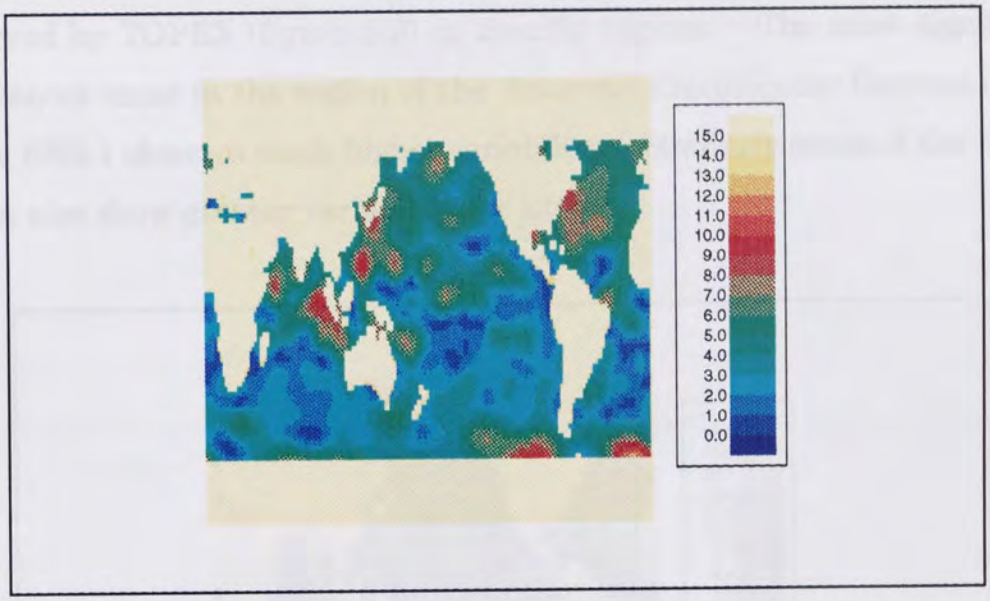

Figure 8.5 Annual Variability Amplitudes in Centimeters for the Original ERS-1 Orbits

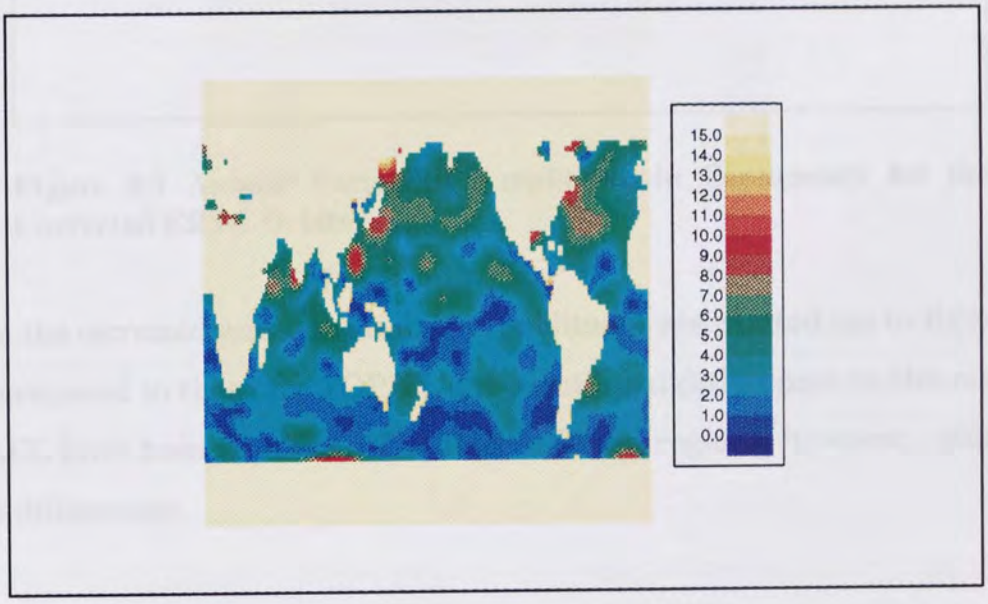

Figure 8.6 Annual Variability Amplitudes in Centimeters for TOPEX

The phases are plotted as monthly values of the peak of the annual cycle,

relative to January 1st.

Figure 8.5 reveals that the amplitudes of the annual variability observed by the original ERS-1 altimeter data set are significantly different from those observed by TOPEX (figure 8.6) in specific regions. The most significant differences occur in the region of the Antarctic Circumpolar Current (ACC) where ERS-1 observes much higher variability. Similarly areas of the Pacific Ocean also show greater variability for ERS-1.

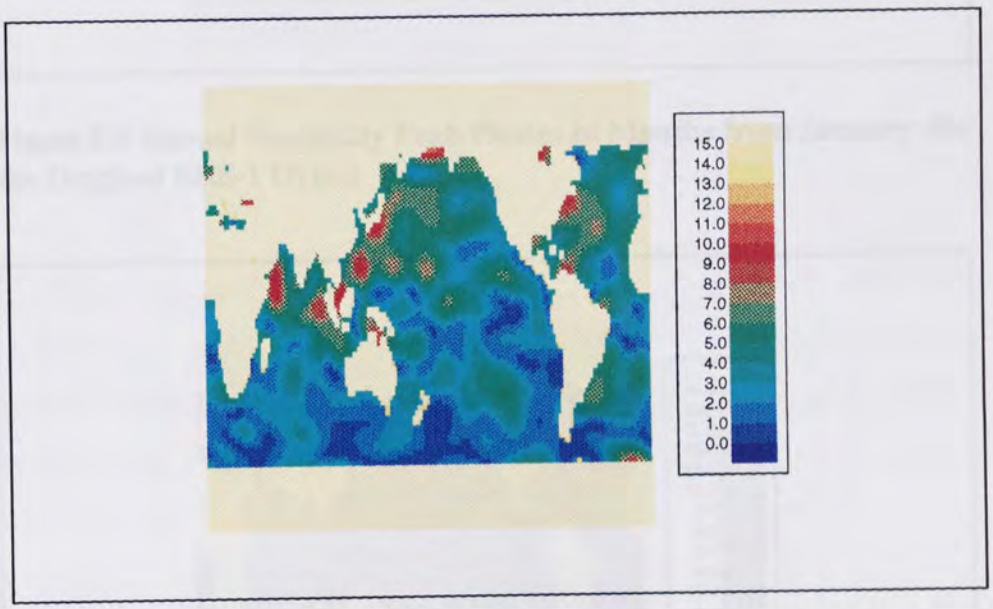

Figure 8.7 Annual Variability Amplitudes in Centimeters for the Corrected ERS-1 Orbits

When the corrected annual variability amplitudes are plotted (as in figure 8.7) and compared to those for TOPEX, the significant differences in the region of the ACC have been removed. The Pacific Ocean regions, however , still show some differences.

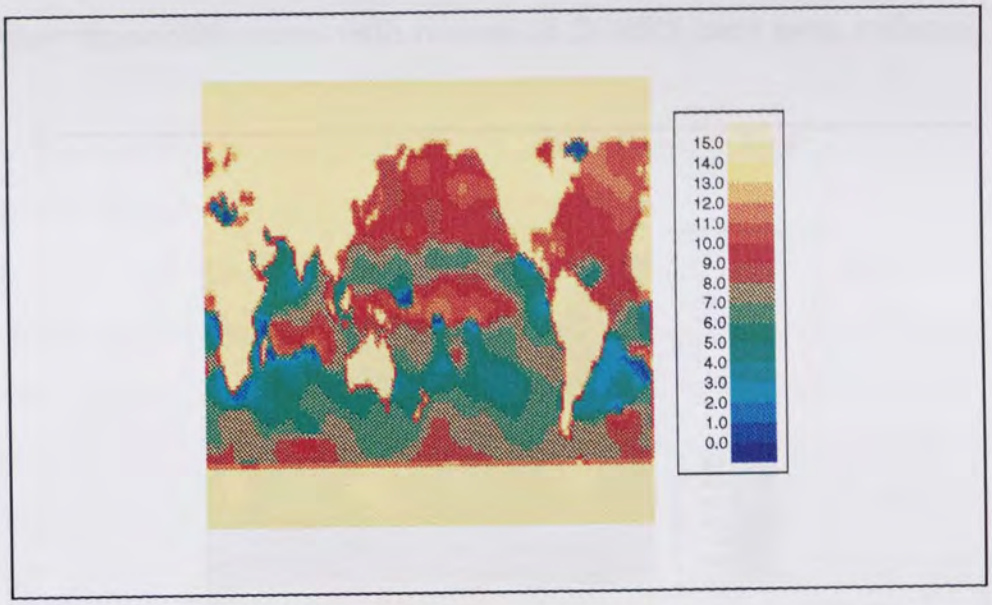

Figure 8.8 Annual Variabilty Peak Phases in Months from January for the Original ERS-1 Orbits

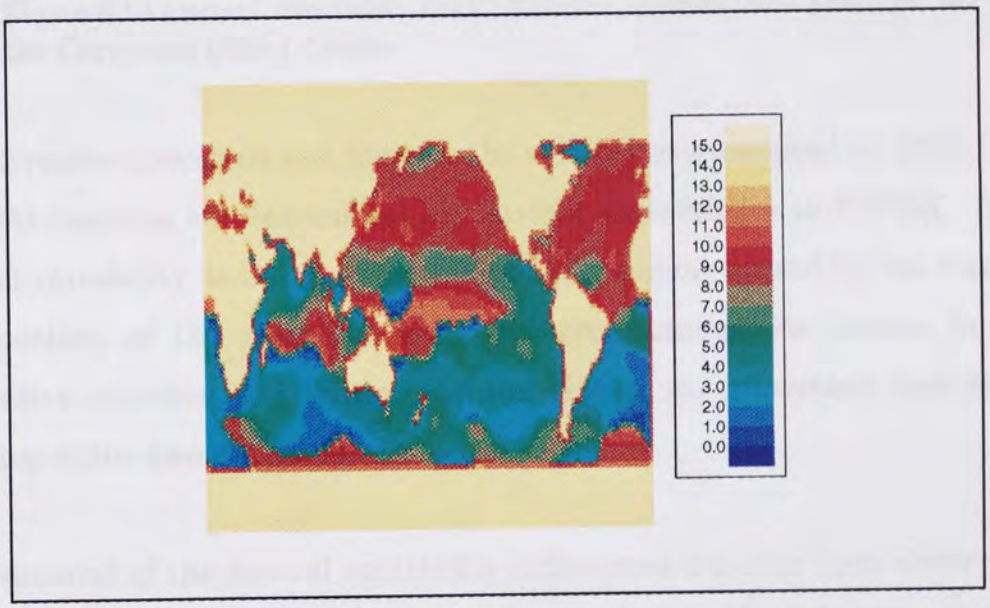

Figure 8.9 Annual Variability Peak Phases in Months from January for TOPEX

Figures 8.8 and 8.9 also demonstrate similar problems with the uncorrected ERS-1 variability peak phases, as regions close to the ACC show significant differences when compared to those derived from TOPEX. The annual variability peak phases for the corrected ERS-1 orbits, in figure 8.10 , again

show that these differences with respect to TOPEX have been reduced.

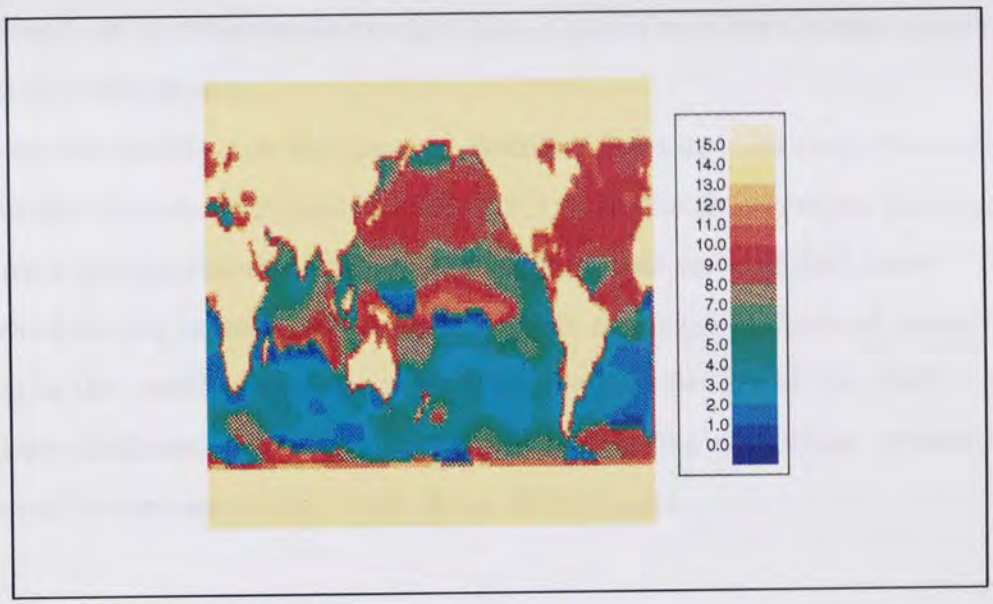

Figure 8.10 Annual Variability Peak Phases in Months from January for the Corrected ERS-1 Orbits

The correction procedure can therefore be said to have produced an ERS-1 data set that observes similar annual sea surface variabilities to TOPEX. As the annual variability is the dominant variability signal caused by the warming and cooling of the northern and southern hemisphere oceans in their respective summer and winter months this is an important test for the merging of the two data sets.

This removal of the annual variability differences has also been observed by Moore [1996(a)] who derived sea surface time series for the TOPEX and ERS-1 (original and corrected) datasets. By differencing the ERS-1 and TOPEX time series and using empirical orthogonal functions the variability differences were broken down into the various contributing modes. Comparison of the original ERS-1 data set to TOPEX provided a greater number of significant modes and a higher variation in variability than the corrected ERS-1 data set. It was also shown that the annual signal was removed as the dominant mode in the

corrected data set.

8.5 Study of the Geographically Mean and Variable Components of the Radial Orbit Error

This section is split into two parts. Both sections use the dual crossover data set for the 13 cycles outlined in section 8.2 . In the first section the mean and variable geographical orbit error is determined on a global basis. This is followed in the second part by a harmonic analysis performed over latitude bands in the southern oceans to determine which orders of the JGM-2 gravity field are deficient for ERS-1 and confirm that the correction procedure has removed errors associated with these deficiencies.

8.5.1 The Global Analysis

Tapley and Rosborough [1985], Rosborough [1986] and Klokocnik et al [1993] define the radial orbit error for a satellite pass as the sum of two components,

$$\Delta r = \Delta f + \delta_{AD} \Delta v \qquad (8.1)$$

where Δf and Δv are the mean geographically correlated error and the geographically correlated variation about the mean and can be expressed in terms of Kaula's inclination functions [Kaula, 1966] and the satellite latitude and longitude [Tapley and Rosborough, 1985; Schrama, 1992; and Klokocnik et al, 1993]. δ_{AD} is defined by,

$$\delta_{AD} = \begin{matrix} 1 - ascending \\ -1 - descending \end{matrix}$$

A single satellite crossover residual , being the combination of an ascending and descending arc, can therefore be defined by,

$$\Delta_{SXO} = \pm 2 \Delta v \qquad (8.2)$$

with the sign being dependent upon whether the first crossover epoch

corresponds to the ascending or descending pass. The single satellite crossover is therefore only a measure of the variable component of the geographically correlated orbit error and, as discussed in section 7.21, is not capable of describing the radial orbit error in its entirety.

The TOPEX/Poseidon - ERS-1 dual crossover residual, however is dependent upon two different satellites and thus described by equation (8.3),

$$\Delta_{DXO}=\Delta f^{T/P}+\delta_{AD}^{T/P}\Delta\nu^{T/P}-(\Delta f^{E1}+\delta_{AD}^{E1}\Delta\nu^{E1}) \tag{8.3}$$

where the superscript T/P and E1 refer to TOPEX/Poseidon and ERS-1 respectively.

By assuming the contribution from TOPEX/Poseidon is negligible, and dropping the E1 superscript for ease of notation, equation (8.3) can be simplified such that the dual crossover residual is defined in terms of the mean and variable components of the ERS-1 orbit error.

$$\Delta_{DXO}=-\Delta f-\delta_{AD}\Delta\nu \tag{8.4}$$

On considering dual crossover residuals for descending and ascending ERS-1 passes the mean and variable components for 2 degree latitude by 4 degree longitude bins are defined by equation (8.5) [Moore et al, 1996(a)],

$$\Delta f=-\frac{1}{2N_{dual}^{A}}\sum_{i=1}^{i=N_{dual}^{A}}\Delta_{DXO}^{A}-\frac{1}{2N_{dual}^{D}}\sum_{i=1}^{i=N_{dual}^{D}}\Delta_{DXO}^{D} \tag{8.5a}$$

$$\Delta\nu=-\frac{1}{2N_{dual}^{A}}\sum_{i=1}^{i=N_{dual}^{A}}\Delta_{DXO}^{A}+\frac{1}{2N_{dual}^{D}}\sum_{i=1}^{i=N_{dual}^{D}}\Delta_{DXO}^{D} \tag{8.5b}$$

where N^{A}_{dual} is the number of dual crossovers within the region with ascending arcs of residual $\Delta_{DXO}{}^{A}$ and the superscript D similarly denotes descending arcs.

Using the dual crossover residuals for the entire 13 cycles, with time differences of less than 10 days , the ERS-1 mean and variable components of the radial orbit error for bins with a minimum of 25 dual crossovers have been recovered. These are shown in figures 8.11 - 8.14.

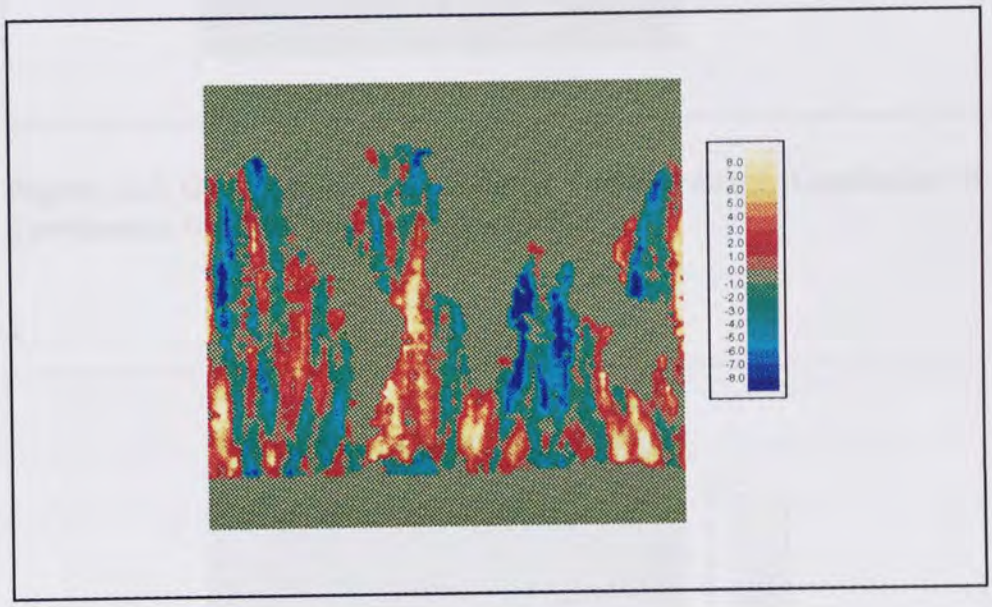

Figure 8.11 Geographically Correlated Mean Error Amplitudes in Centimeters for the Original ERS-1 Orbits

Figures 8.11 and 8.12 demonstrate that the areas of high error, in both the mean and variable components, for the uncorrected ERS-1 orbits are predominantly in the southern hemisphere, resulting in a north south slope. This is gravity field error with the greater accuracy in the northern hemisphere due to the predominance of laser range tracking data there.

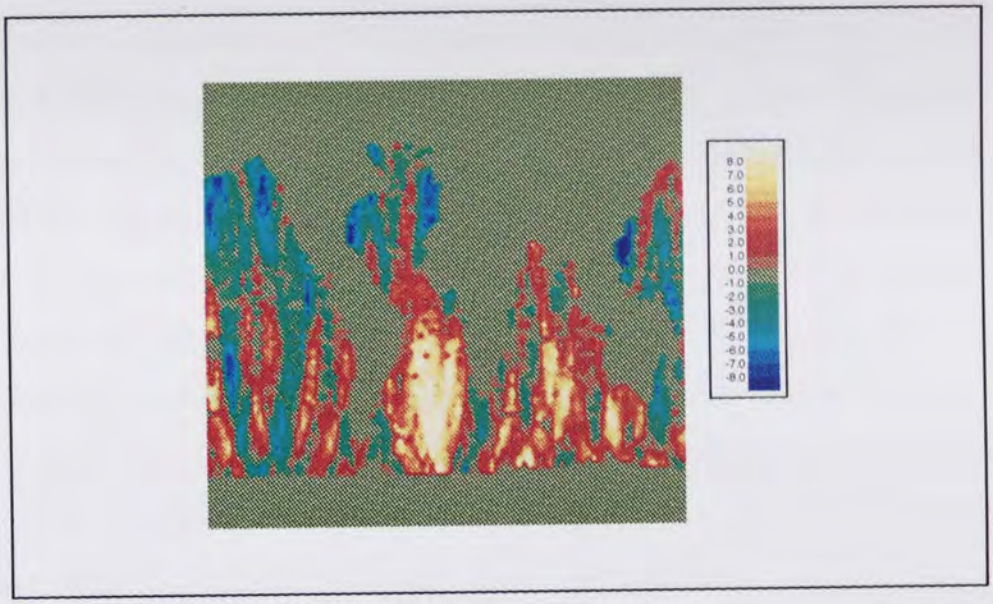

Figure 8.12 Geographically Correlated Variable Error Amplitudes in Centimeters for the Original ERS-1 Orbits

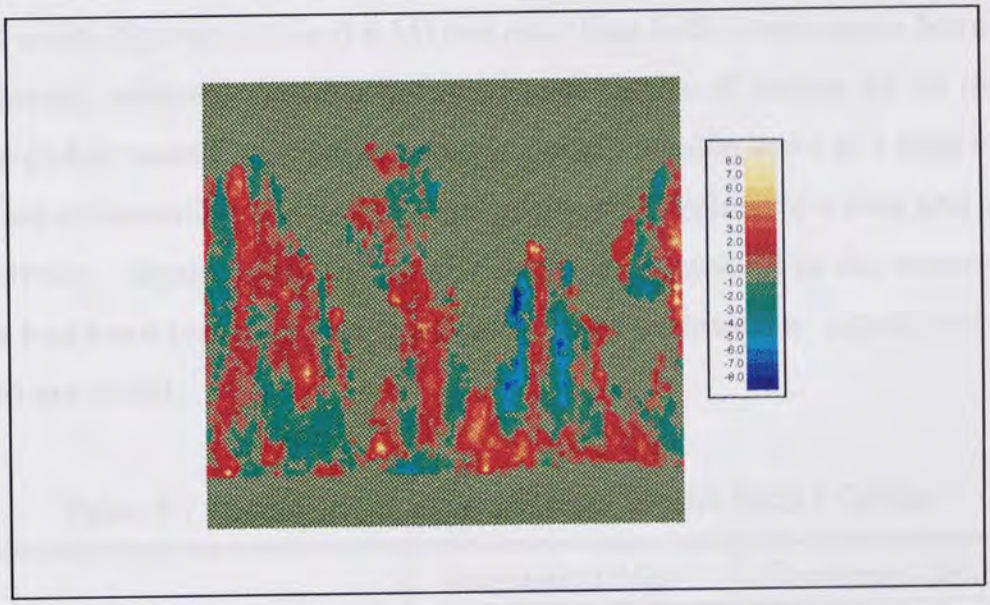

Figure 8.13 Geographically Correlated Mean Error Amplitudes in Centimeters for the Corrected ERS-1 Orbits

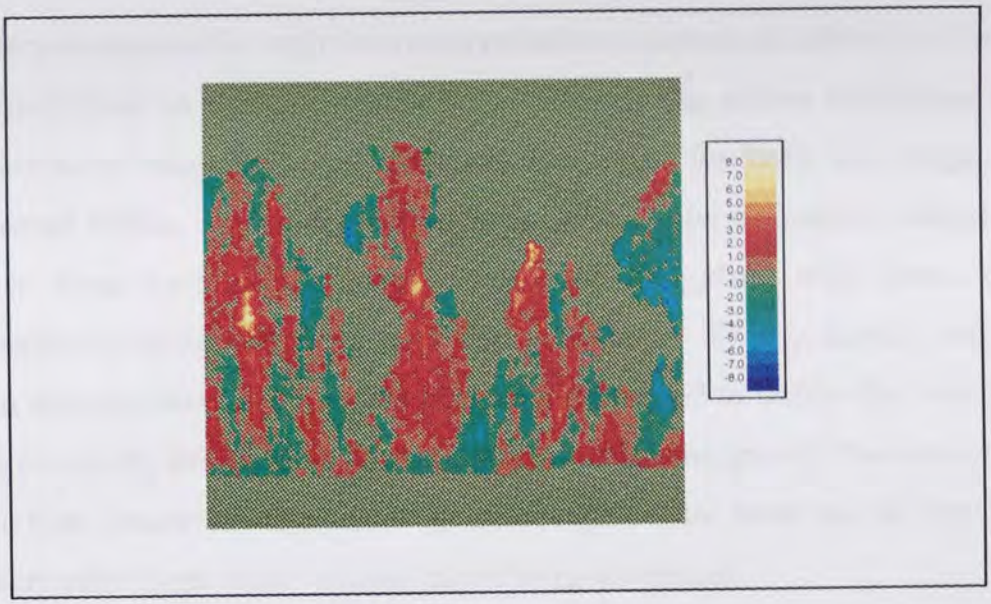

Figure 8.14 Geographically Correlated Variable Error Amplitudes in Centimeters for the Corrected ERS-1 Orbits

Upon analysis of the mean and variable error components for the corrected ERS-1 orbits (figures 8.13 and 8.14) it is clear that both components have been significantly reduced. Taking the root mean square of values for all regions gives a global mean error of 2.2cm and a global variable error of 1.9cm for the corrected orbits whilst the uncorrected orbits yield values of 4.2cm and 4.0cm respectively. Significantly the north - south slope present in the uncorrected orbits has been removed and those areas that maintain a significant error (>6cm) are small.

Table 8.7 Radial Orbit Error Sources for the ERS-1 Orbits

	Original Orbits	Corrected Orbits
Radial Accuracy	9.9cm rms	5.2cm rms
Mean Geog. Correlated	4.2cm rms	2.2cm rms
Variable Geog. Correlated	4.0cm rms	1.9cm rms
Non Cons. Force Mis-Mod.	8.0cm rms	4.3cm rms

The error sources for both the uncorrected and corrected orbits can therefore be quantified as shown in table 8.7. Clearly the errors attributed to non conservative force mis-modelling are dominant for both the original and corrected orbits. The correction procedure whilst definitely reducing the errors from each of the error sources is struggling with those due to atmospheric drag and solar radiation pressure. This is hardly surprising when one considers the number of parameters used to define the non gravity field errors (8) compared to those used to model the gravity field error (152). If further improvements are to be made the radial error model for the non conservative force error sources must be re-examined.

8.5.2 Harmonic Analysis of Dual Crossovers in the Southern Hemisphere

From Rosborough [1986] the radial orbit error may be expanded in terms of the geopotential coefficients such that the error due to a given geopotential order m can be expressed as,

$$\Delta r = \sum_{m=0}^{m=L} \Delta r_m \tag{8.6}$$

where Δr_m is defined by equation (8.7),

$$\Delta r_m = \Delta f_m + \delta_{AD} \Delta v_m \tag{8.7}$$

and,

$$\Delta f_m = E_m cosm\lambda + F_m \sin m\lambda \tag{8.8a}$$

$$\Delta v_m = \delta_{AD}(G_m \sin m\lambda - H_m \cos m\lambda) \tag{8.8b}$$

on assuming constant values for the inclination and latitude functions given by Tapley and Rosborough [1985], Schrama [1992] and Klokocnik et al [1993]. Moore et al [1996(a)] describes the terms E_m,F_m,G_m and H_m as,

$$E_m = \sum_{l=\max(m,2)}^{l_{\max}} \sum_{p=0}^{p=l} \Lambda_{lmp} \Xi^f_{lmp} \Delta C_{lm} \qquad (8.9a)$$

$$F_m = \sum_{l=\max(m,2)}^{l_{\max}} \sum_{p=0}^{p=l} \Lambda_{lmp} \Xi^f_{lmp} \Delta S_{lm} \qquad (8.9b)$$

$$G_m = \sum_{l=\max(m,2)}^{l_{\max}} \sum_{p=0}^{p=l} \Lambda_{lmp} \Xi^v_{lmp} \Delta C_{lm} \qquad (8.9c)$$

$$H_m = \sum_{l=\max(m,2)}^{l_{\max}} \sum_{p=0}^{p=l} \Lambda_{lmp} \Xi^v_{lmp} \Delta S_{lm} \qquad (8.9d)$$

where the expressions Λ_{lmp} , Ξ^f_{lmp} and Ξ^v_{lmp} are those of Klokocnik et al [1994].

E_m, F_m, G_m and H_m depend upon latitude, but for a given satellite are assumed constant across a narrow latitude band. Using the 13 cycles of dual crossover residuals within the latitude range of -41 degrees and -66 degrees ,to provide a near continuous data set uncorrupted by land masses , the amplitudes E_m, F_m, G_m and H_m have been recovered for latitude bands of width 1 degree and 1.5 degrees. The latitude band width changes from 1.0 degrees south of -56 degrees to 1.5 degrees in order to compensate for the sparser distribution of dual crossovers at latitudes closer to the equator.

The recovered parameters for each latitude band have been used to determine the mean power of the variable and mean error components (P_m^v and P_m^f) for each harmonic of order m by using equation (8.10).

$$(P_m^f)^2 = \frac{1}{N_{bands}} \sum_{i=1}^{i=N_{bands}} (E_m^2 + F_m^2) \qquad (8.10a)$$

$$(P_m^v)^2 = \frac{1}{N_{bands}} \sum_{i=1}^{i=N_{bands}} (G_m^2 + H_m^2) \qquad (8.10b)$$

The recovered powers for the original and corrected ERS-1 orbits are presented in figures 8.15 - 8.18.

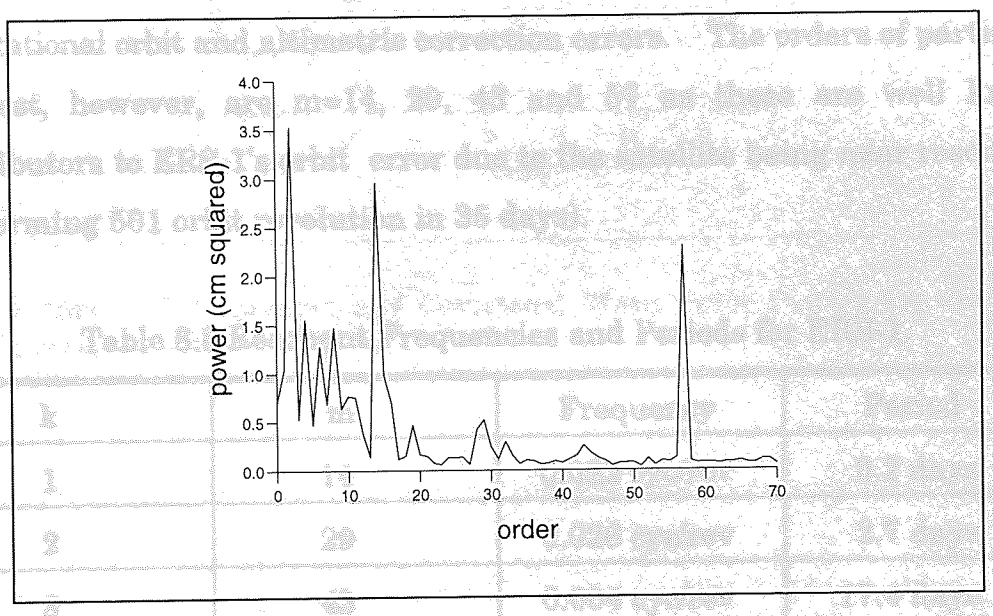

Figure 8.15 Geographically Correlated Mean Error Powers for the Original ERS-1 Orbits

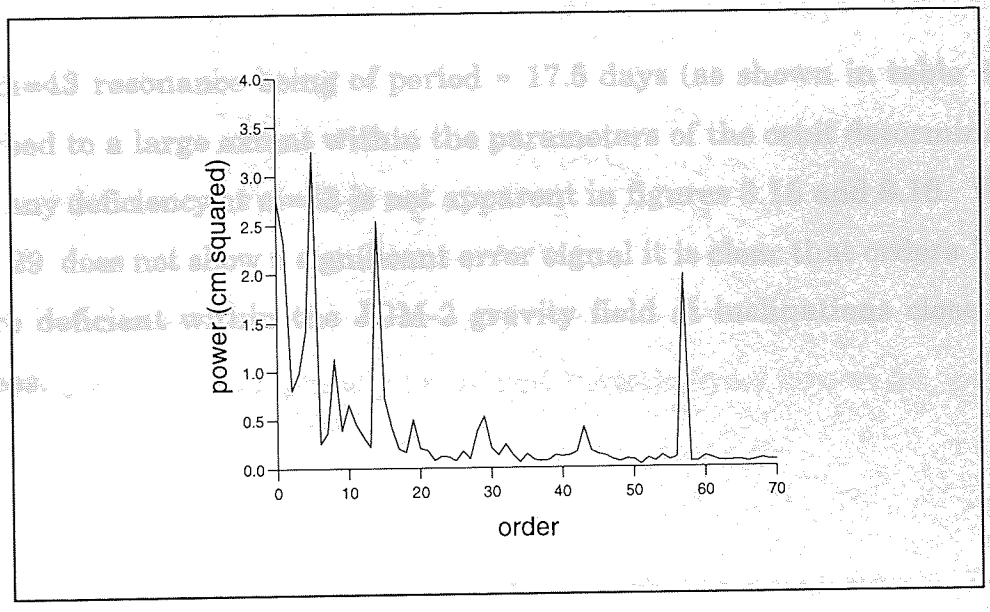

Figure 8.16 Geographically Correlated Variable Error Powers for the Original ERS-1 Orbits

Although the powers recovered for the uncorrected orbits are contaminated to some extent due to the presence of other signals such as non-gravitational orbit error, figures 8.15 and 8.16 provide a very good indicator of the orders of the JGM-2 gravity field which are deficient for satellites in high inclination orbits such as ERS-1. Clearly there are strong low order (m<10) signals, some of which are due to the gravity field whilst others are probably due to non-gravitational orbit and altimetric correction errors. The orders of particular interest, however, are m=14, 29, 43 and 57 as these are well known contributors to ERS-1's orbit error due to the satellite being near resonance (performing 501 orbit revolution in 35 days).

Table 8.8 Resonant Frequencies and Periods for ERS-1.

k	m	Frequency	Period
1	14	0.022 cyc/rev	3.2 days
2	29	0.026 cyc/rev	2.7 days
3	43	0.004 cyc/rev	17.4 days
4	57	0.018 cyc/rev	3.9 days

The m=43 resonance being of period $\approx$ 17.5 days (as shown in table 8.8) is absorbed to a large extent within the parameters of the orbit determination. Thus any deficiency at m=43 is not apparent in figures 8.15 and 8.16. Whilst order 29 does not show a significant error signal it is clear that orders 14 and 57 are deficient within the JGM-2 gravity field at inclinations close to 98 degrees.

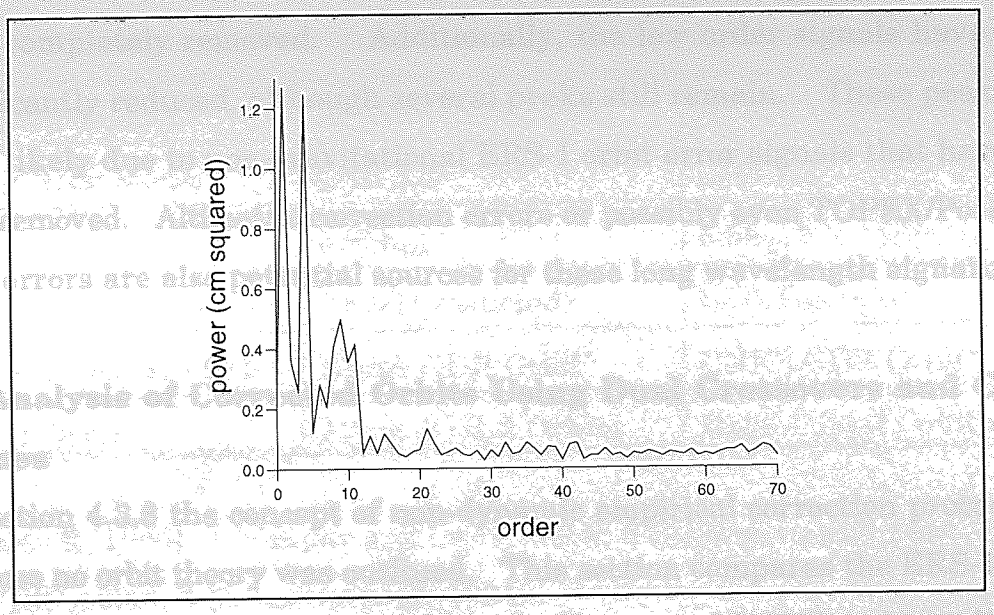

Figure 8.17 Geographically Correlated Mean Error Powers for the Corrected ERS-1 Orbits

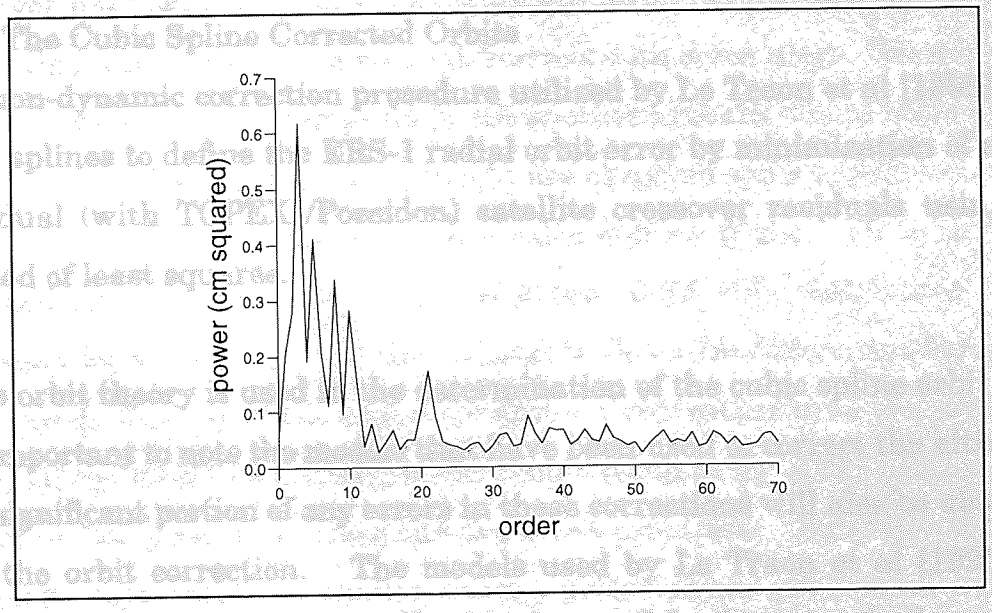

Figure 8.18 Geographically Correlated Variable Error Powers for the Corrected ERS-1 Orbits

Analysis of figures 8.17 and 8.18, which show the mean powers for the corrected orbits, reveals that the error signals due to orders 14 and 57 have

been completely removed. Additionally, the low order signals have been significantly reduced, although several peaks still remain. These peaks are most likely due to non-gravitational ERS-1 orbit error signals that have not been removed. Altimetric correction errors or possibly even TOPEX/Poseidon orbit errors are also potential sources for these long wavelength signatures.

8.6 Analysis of Corrected Orbits Using Dual Crossovers and Cubic Splines

In section 4.3.3 the concept of non-dynamic empirical correction procedures that use no orbit theory was outlined. This section compares the ERS-1 dual crossover corrected orbits generated by Le Traon et al [1995] and supplied by AVISO, using such a method, with those determined using the theory and methodology developed in chapters 6 and 7.

8.6.1 The Cubic Spline Corrected Orbits

The non-dynamic correction procedure utilized by Le Traon et al [1995] uses cubic splines to define the ERS-1 radial orbit error by minimisation of single and dual (with TOPEX /Poseidon) satellite crossover residuals using the method of least squares.

As no orbit theory is used in the determination of the cubic spline orbit error it is important to note the models that have been used to correct the altimetry as a significant portion of any errors in these corrections will also be absorbed into the orbit correction. The models used by Le Traon et al [1995] are essentially the same as those outlined in chapter 7 for the Aston dual crossover data set; however, there are some differences and these are given in table 8.9.

Table 8.9 Differences Between the AVISO and Aston Altimeter Corrections.

Correction/Orbit	ASTON Crossovers	AVISO Crossovers
Ocean Tide Model	CSR 3.0[1]	CSR 1.2[1]
Sea State Bias	$5.95h_{1/3}$	$5.5h_{1/3}{}^{2}$
Ionospheric Correction	BENT(predicted)[3]	BENT(actual)
TOPEX/Poseidon Orbit	NASA GDR Orbit[4]	CNES GDR Orbit[4]
ERS-1 Orbit	Aston JGM-2 Orbits	Delft JGM-2 Orbits[5]

1-[Eanes R, 1995], 2-[Gaspar and Ogar, 1994], 3-[Llewellyn and Bent, 1973], 4-[AVISO,1992], 5-[Scharroo et al, 1994].

Of the differences between the AVISO and Aston dual crossover datasets the most significant is probably the different sea state bias models. If the crossover data set was evenly distributed in latitude and variation in wave height this would result in a mean difference with some noise. However, as the crossovers are predominantly in the southern oceans where large values and variation of significant wave height are observed some additional signal will undoubtedly be absorbed by the cubic splines if the 5.95 % model is assumed correct. Whilst a difference of near 0.5% only contributes a 1cm difference for wave heights of 2m, at heights above 7m differences exceeding 3.5cm exist. The use of the actual sunspot activity rather than the predicted values for the BENT ionospheric model should result in the AVISO ionospheric correction being more accurate and cause few problems. Similarly the CSR 1.2 and 3.0 tide models are similar and few problems are anticipated with the use of these models.

In the cubic spline error estimation [Le Traon et al, 1995], some 2500 spline knots mainly positioned at the northern and southernmost TOPEX - ERS-1 dual crossovers are typically used for each cycle. Those arcs that result in the two knots being further than 10,000km apart and which have a minimum of

20 dual crossovers have an additional knot placed in the middle of the arc. This then requires the recovery of some 2500 parameters (number of knots +4) in the least squares recovery procedure. In comparison the Aston procedure uses a minimum of 1134 parameters to define the error for a cycle containing 7 arcs and a maximum of 1458 parameters for a cycle with 9 arcs.

To assess the accuracy of the orbits and the cubic spline correction the initial JGM-2 orbits (as supplied by Delft University) and those improved with corrections supplied by AVISO have been applied to 7 cycles (cycles 6 -12) of the Aston dual and single satellite crossover data sets. The rms fits to these data sets are presented in tables 8.10 and 8.11 when means of -41.8 cm (TOPEX) and -26.8cm (Poseidon) have been removed from the uncorrected dual crossovers and -11.7cm (TOPEX) and 3.4 cm (Poseidon) have been removed from the corrected dual crossovers to account for the relative range biases and differences in reference ellipsoids.

Table 8.10 Delft ERS-1 Orbit Fits to Aston Crossover Datasets.

Cycle No.	ΔSXO Rms (cm)	ΔDXO Rms (cm)
6	20.1 (3.5%)	15.8 (0.7%)
7	21.4 (2.6%)	15.1 (0.3%)
8	21.3 (0.9%)	17.0 (4.7%)
9	16.0 (0.4%)	13.1 (0.2%)
10	18.6 (3.4%)	15.0 (1.4%)
11	19.5 (1.2%)	14.6 (0.2%)
12	15.3 (0.2%)	12.8 (0.1%)

Table 8.11 AVISO Corrected ERS-1 Orbit Fits to Aston Crossover Datasets.

Cycle No.	ΔSXO Rms (cm)	ΔDXO Rms (cm)
6	8.3 (0.1%)	8.0 (0.3%)
7	8.3 (0.3%)	7.7 (0.3%)
8	7.6 (0.3%)	7.7 (0.4%)
9	7.9 (0.5%)	7.8 (0.4%)
10	8.0 (0.4%)	8.0 (0.4%)
11	9.2 (1.1%)	9.0 (0.7%)
12	9.0 (0.6%)	9.1 (0.5%)

The rms fits for the Delft orbits (subject to a 50cm rejection level) are higher than those for the baseline Aston orbits as the former were determined using laser ranges as the only satellite tracking data set. The corrected orbits, however, provide lower rms values (subject to a 30cm rejection level) than the corrected Aston orbits. Using the same assumptions outlined earlier regarding the error signals from TOPEX/Poseidon and ERS-1 the mean dual crossover fits of 14.8cm and 8.2cm indicate radial accuracies of 13cm and 4.2 cm for the uncorrected and corrected orbits respectively. As it is assumed that none of the signal removed is anything but ERS-1 orbit error the estimate of 4.2cm is definitely optimistic. However, it is almost impossible to ascertain how much of these other signals has been absorbed.

8.6.2 Analysis of the Delft and AVISO Orbits

Using the methodology outlined in 8.5.1 the mean and variable components of the orbit error have been determined for the Delft and AVISO ERS-1 orbits. Analysis of the seven cycles (6-12) results in the derived mean and variable components plotted in figures 8.19 - 8.22.

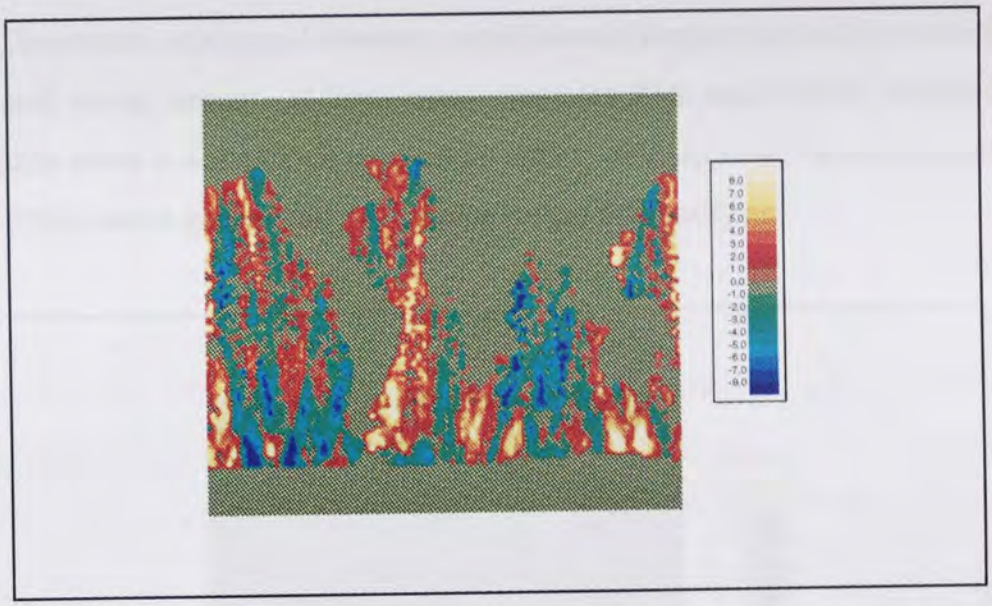

Figure 8.19 Geographically Correlated Mean Error Amplitudes in Centimeters for the Delft ERS-1 Orbits

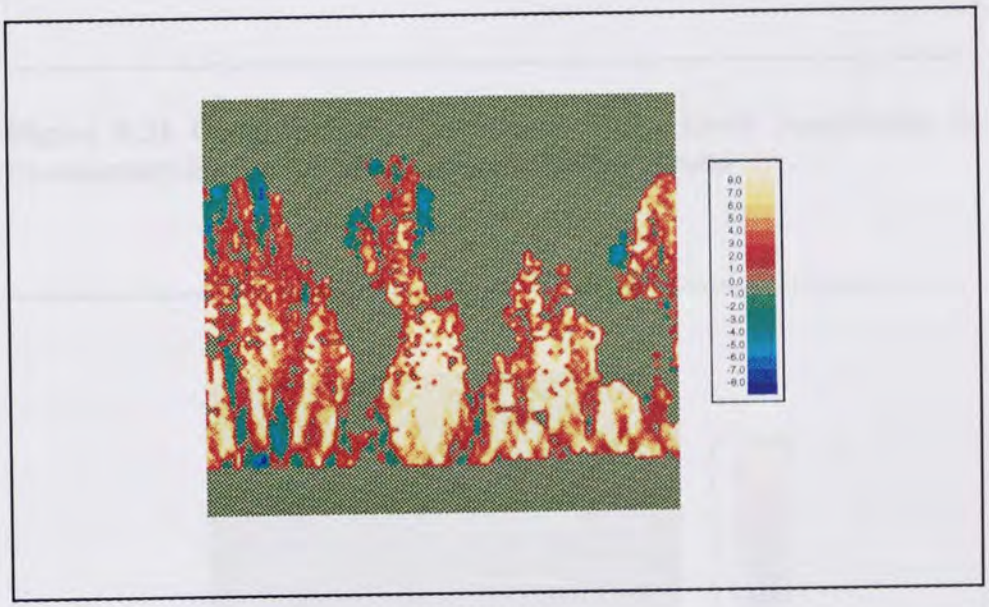

Figure 8.20 Geographically Correlated Variable Error Amplitudes in Centimeters for the Delft ERS-1 Orbits

The mean and variable components of the JGM-2 orbits supplied by Delft University show similar errors to those obtained for the original ERS-1 orbits generated at Aston (figures 8.11 and 8.12). The variable component for the

Delft University orbits is, however, significantly larger (variable error=5.7cm rms and mean error = 4.2cm rms) than for the equivalent Aston orbits (variable error = 4.0cm rms and mean error= 4.2 cm rms) again because the Delft orbits were generated with laser range data only.

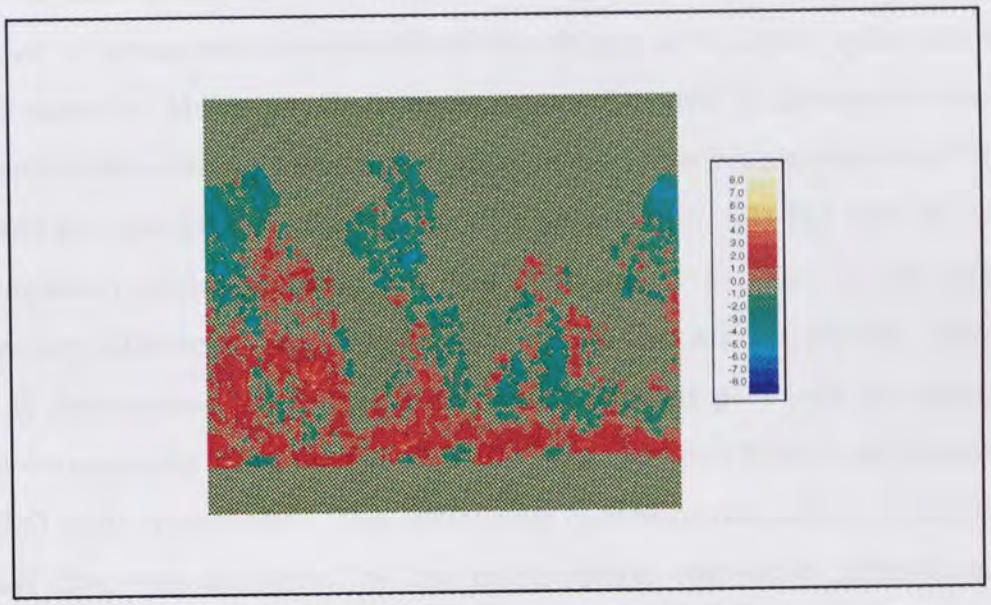

Figure 8.21 Geographically Correlated Mean Error Amplitudes in Centimeters for the AVISO Corrected ERS-1 Orbits

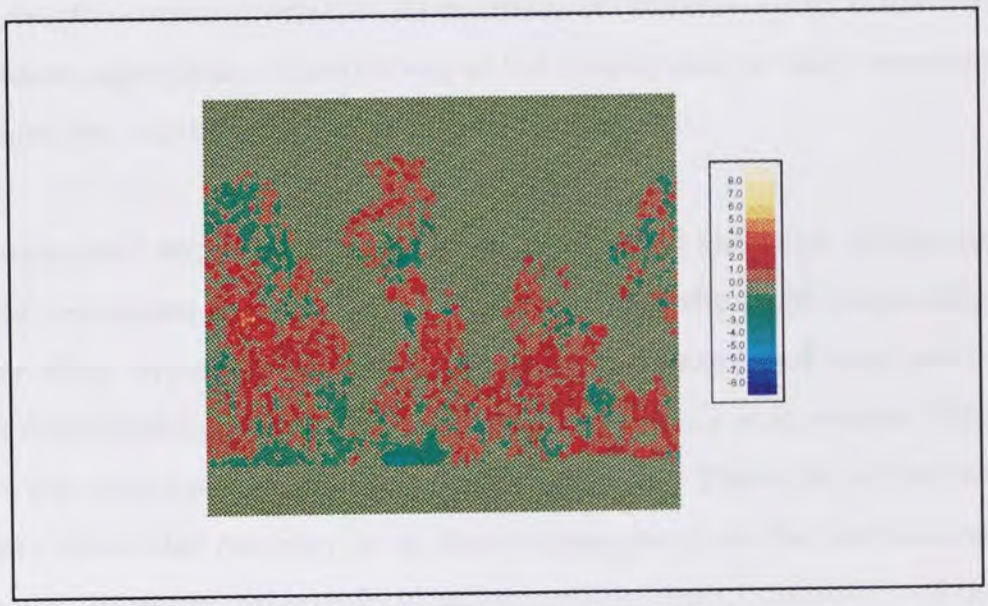

Figure 8.22 Geographically Correlated Variable Error Amplitudes in Centimeters for AVISO Corrected ERS-1 Orbits

The mean and variable components for the cubic spline corrected orbits show a significant reduction. In fact the mean values (mean error of 1.9cm rms and variable error of 1.3cm rms) indicate that a larger error has been removed than in the correction procedure employed at Aston (mean error of 2.2cm rms and variable error of 1.9cm rms). This is not surprising due to the high number of parameters recovered and the ability of the cubic splines to absorb other signals. However, the remaining north-south tilt present in the mean component is a cause for concern as this should have been completely removed (as was the case for the Aston correction procedure). At the time of study no explanation could be found for this phenomena as none of the altimeter correction differences were expected to reveal this kind of signal. Only later was it determined [Le Traon, 1996] that different pole tide corrections had been erroneously used for the TOPEX/Poseidon and ERS-1 altimetry in the AVISO dual crossovers. This difference therefore resulted in a north-south signal that was absorbed by the cubic spline correction procedure. On applying the corrected orbits to the Aston altimeter datasets the pole tide discrepancy was reinstated. This highlights the main problem with non-dynamic, empirical, correction procedures as extreme care must be taken when applying the corrected orbits to other altimeter datasets which utilise different correction algorithms. Ideally if any of the geophysical or tidal corrections are changed the orbit correction should be recomputed.

The estimated error components for the uncorrected and cubic spline corrected orbits are shown in table 8.12. Unsurprisingly the Delft University orbits suffer from larger variable geographically correlated and non conservative force mis-modelling errors than the Aston equivalents as crossover differences have not been used in the orbit determination. The cubic spline corrected orbits show better recovery in all three categories than the methodology used at Aston, however, this again is not surprising due to the ability of the cubic splines to absorb signals other than the orbit error.

Table 8.12 Radial Error Sources for the Delft and AVISO Corrected ERS-1 Orbits.

	Original Orbits	Corrected Orbits
Radial Accuracy	13.0cm rms	4.2cm rms
Mean Geog. Correlated	4.2cm rms	1.9cm rms
Variable Geog. Correlated	5.7cm rms	1.3cm rms
Non Cons. Force Mis-Mod.	10.9cm rms	3.5cm rms

Figures 8.23 - 8.26 show the mean harmonic powers recovered when a harmonic analysis of data in the southern hemisphere using the Aston crossovers datasets with the Delft and AVISO orbits is carried out using the methodology outlined in 8.5.2.

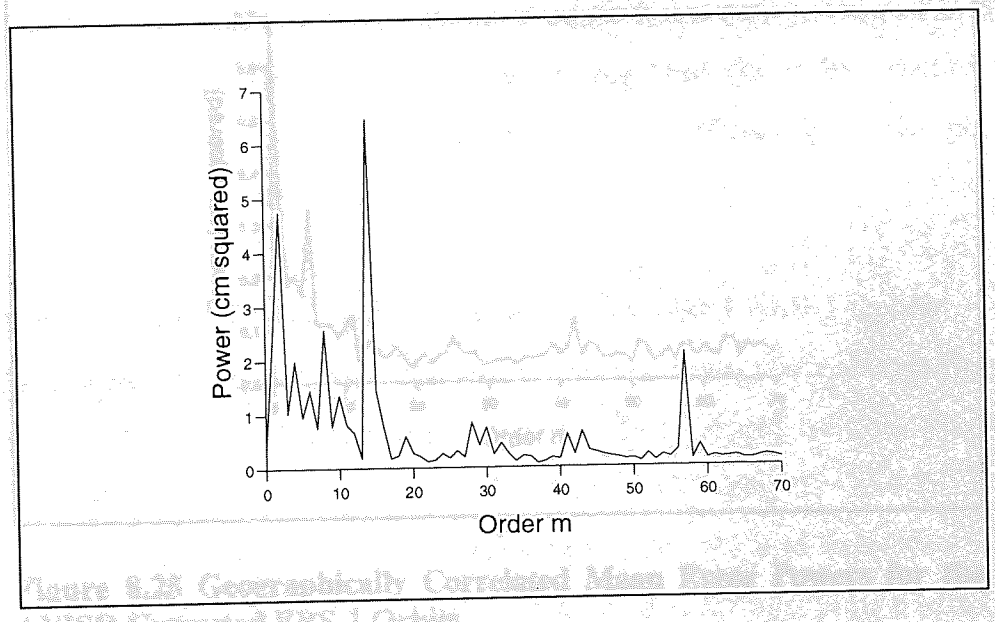

Figure 8.23 Geographically Correlated Mean Error Powers for the Delft ERS-1 Orbits

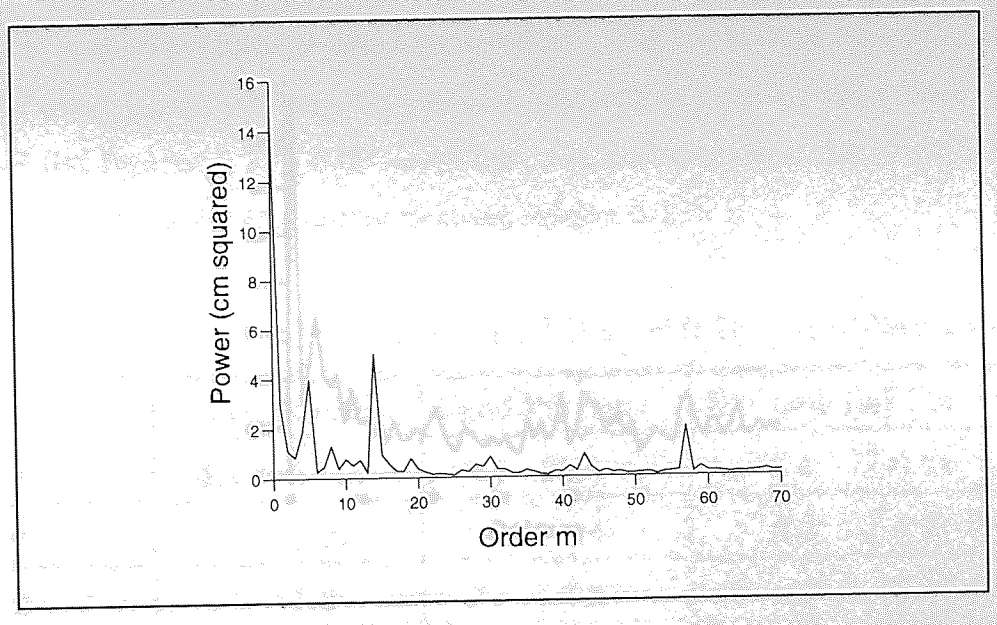

Figure 8.24 Geographically Correlated Variable Error Powers for the Delft ERS-1 Orbits

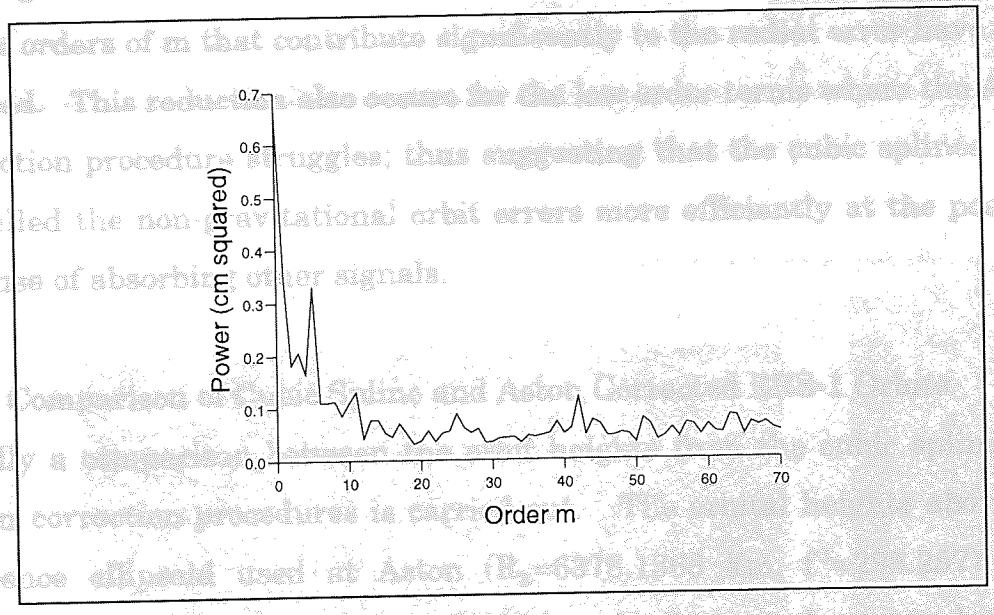

Figure 8.25 Geographically Correlated Mean Error Powers for the AVISO Corrected ERS-1 Orbits

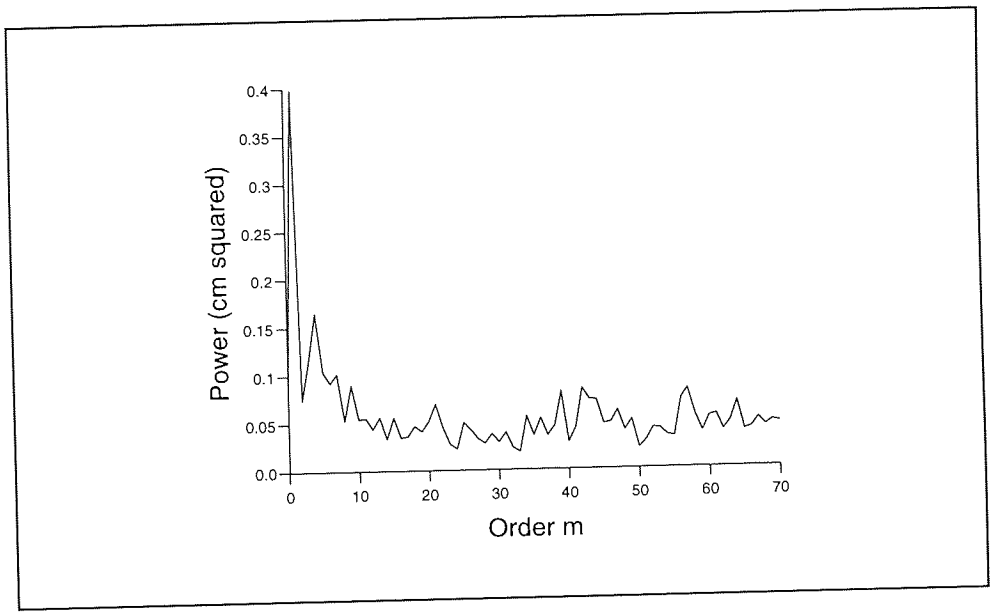

Figure 8.26 Geographically Correlated Variable Error Powers for the AVISO Corrected ERS-1 Orbits

Once again the cubic splines ability to recover the radial error is demonstrated as the orders of m that contribute significantly to the radial error have been reduced. This reduction also occurs for the low order terms where the Aston correction procedure struggles; thus suggesting that the cubic splines have modelled the non-gravitational orbit errors more efficiently at the possible expense of absorbing other signals.

8.6.3 Comparison of Cubic Spline and Aston Corrected ERS-1 Orbits

Finally a comparison between the orbit heights from the cubic spline and Aston correction procedures is carried out. The orbital heights above the reference ellipsoid used at Aston (R_E=6378.1363 km, f^{-1}=298.257) were calculated at 30 second intervals and split into land, sea and extreme latitude categories. The points over land were determined by applying a land filter whilst those with latitudes beyond ±65 degrees were defined as extreme latitude (beyond the latitude range of the dual crossovers). Those points classed as over sea were then checked to see if altimetry data and associated corrections were present so that shallow water regions and periods when the

altimeter was inoperational could be rejected. The mean and rms differences for this comparison (the means being in parenthesis) are presented in table 8.13 whilst figures 8.27 - 8.30 show the rms differences in the orbit heights over land and sea for the entire dataset (cycles 6-12).

Table 8.13 Aston-AVISO Corrected ERS-1 Orbit Height Differences.

Cycle No.	Ocean Pts (cm)	Land Pts (cm)	Extreme Lat Pts (cm)
6	4.5 (0.2)	8.1 (0.8)	7.4 (-0.4)
7	4.6 (-0.2)	9.4 (-1.4)	8.0 (-1.0)
8	5.1 (1.2)	9.9 (-1.8)	8.2 (0.3)
9	4.8 (1.0)	8.7 (-1.5)	7.3 (-0.3)
10	5.1 (0.6)	9.1 (-1.0)	7.7 (-1.5)
11	5.5 (0.1)	9.8 (-0.4)	8.3 (-0.3)
12	2.2 (0.7)	9.2 (1.8)	8.2 (1.2)
6-12	5.0 (0.5)	9.2 (-0.5)	7.9 (-0.4)

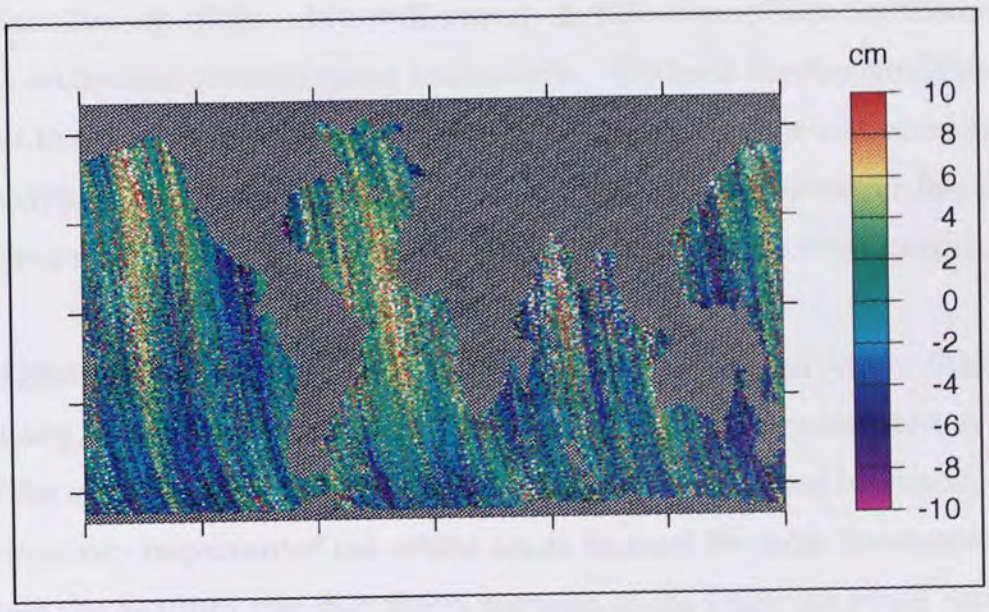

Figure 8.27 Orbit Height Differences for Ascending Arcs Over the Ocean

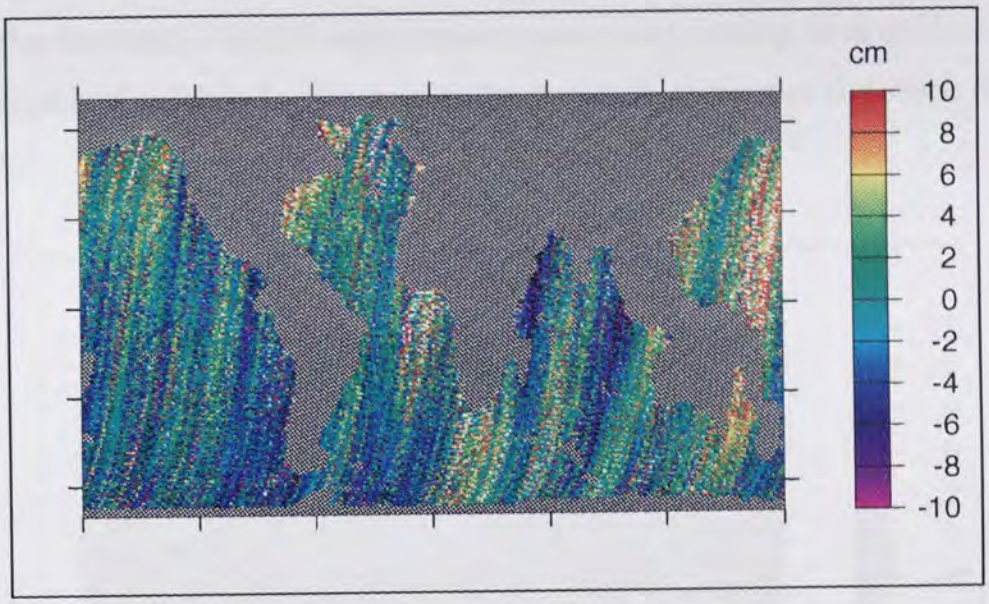

Figure 8.28 Orbit Height Differences for Descending Arcs Over the Ocean

The differences over the oceans show that the orbits agree reasonably well, such that the radial difference between the solutions is approximately 5cm rms. By considering the radial accuracies estimated for both orbits (5.2cm rms and 4.2cm rms for the Aston and AVISO corrected orbits respectively) differences of up to 6.7cm rms can be expected. However, as any error consistent to each of the orbits will cancel, a difference of 5cm for the quoted orbital accuracies would appear reasonable. Without further analysis it is difficult to say which orbit is more accurate as the cubic spline corrected orbits, whilst giving lower geographically correlated and non conservative force mis-modelling errors, will have absorbed other signals into the orbit height.

The higher differences over land and the extreme latitudes where there are few, if any, crossover observations to correct the orbits suggests that at least one of the methodologies provides poor orbital heights for these locations. This is particularly important if the orbits are to be used for polar ice studies. To ascertain the accuracy over non ocean portions of the globe the study could be repeated with ERS-2 altimetry with the orbits at extreme latitudes and over

land checked with PRARE observations once this tracking data set has been calibrated and validated. Such a study, however, is beyond the scope of this thesis.

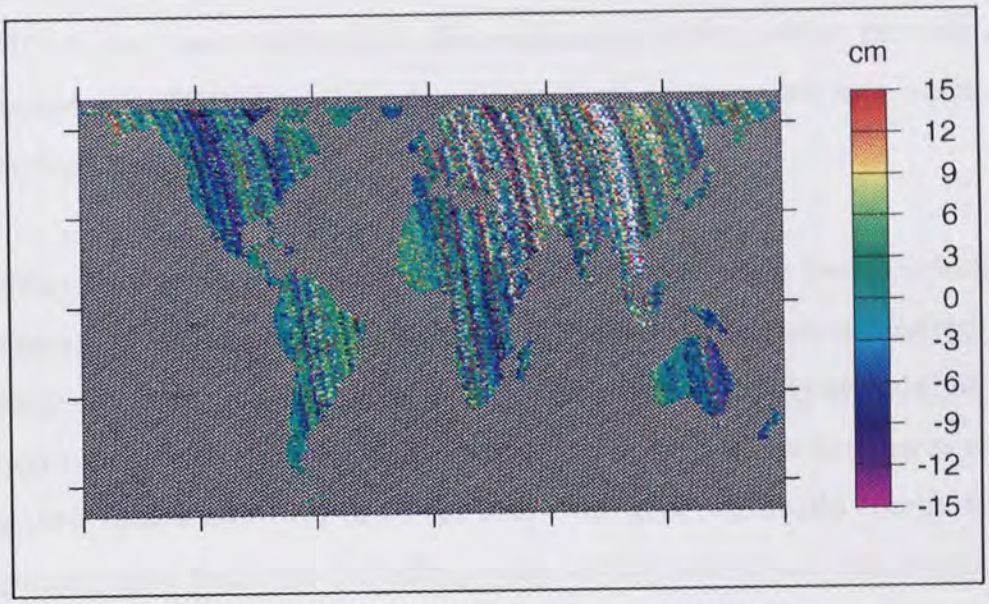

Figure 8.29 Orbit Height Differences for Ascending Arcs Over Land

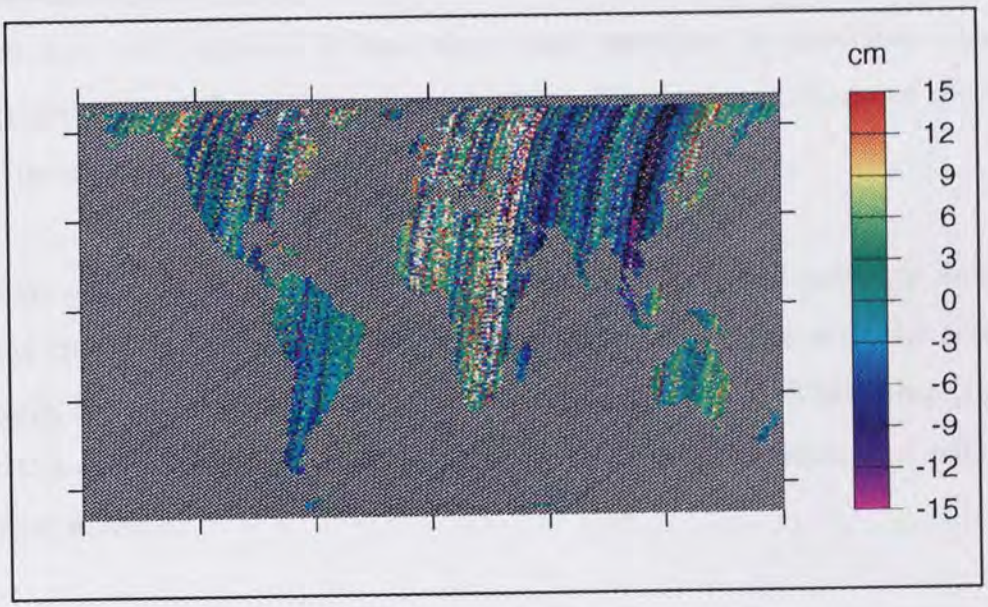

Figure 8.30 Orbit Height Differences for Descending Arcs Over Land

8.7 Conclusions

This chapter has attempted to verify possible unification of the ERS-1 and TOPEX/Poseidon altimeter datasets through refinement of orbital positioning and assessment of the accuracy of the corrected orbits. Clearly the orbit error for ERS-1 has been reduced as the enhanced ERS-1 orbits provide closer agreement with TOPEX in the determination of mean sea surface and annual sea surface variability.

Analysis of the mean and variable geographical orbit error has also validated the removal of orbit error, with the corrected orbits having an estimated radial accuracy of 5.2cm rms, comprising of 2.9cm geographically correlated errors and non-conservative mis-modelling errors of 4.3cm. This compares with an estimated radial accuracy of 9.9cm rms with geographically correlated and non-conservative force mis-modelling errors of 5.8 and 8.0 cm rms respectively for the uncorrected orbits.

By considering dual crossovers in the southern hemisphere between latitudes of -66 and -41 degrees it has also been possible to establish that the gravitational error frequencies that most significantly contribute to the radial error have been well recovered.

Finally, comparison of orbits corrected by the Aston methodology and cubic splines has allowed an estimation of the radial difference over the oceans to be made, the rms difference being approximately 5.0cm. This compares well with the estimate made when comparing the radial accuracies of each orbit (5.2 and 4.2cm).

Chapter 9

Altimeter Calibration Exercise for ERS-2

9.1 Introduction

With the launch of ERS-2 on the 21st April 1995, ESA has two structurally identical satellites operating in the same orbit, separated by some 20 minutes within the orbital plane. This has allowed some interesting uses of ERS-1/ERS-2 altimetry that previously have not been possible eg. the study of differential aerodynamic forces. In order to fully realise the potential this situation offers it is necessary to calculate the sea state (the reader is referred to chapter 5 where the sea state bias of ERS-1 is recovered) and range biases for the ERS-1 and ERS-2 altimeters thus allowing the data sets to be merged.

This chapter outlines some of the work undertaken at Aston University in an estimation of these biases for ERS-2 as a contribution to the ERS-2 Radar Altimeter and Microwave Radiometer Commissioning Working Group set up by the European Space Agency.

9.2 Precise Orbits Used

The period of the ERS-2 mission analysed consisted of one partial and three full 35 day repeat cycles. The first partial ERS-2 cycle was 12 days long and began on MJD 49840 and the last cycle ended on MJD 49957. The four cycles have been split into arcs that are typically five days in length overlapping at the start and finish (overlaps being one day in length) except where manoeuvres are present. As a consequence some 30 ERS-1 and 29 ERS-2

orbits have been determined.

The force models used throughout the orbit determination procedure are given in table 9.1 and the parameters recovered are: drag scale factors for nodes six hours apart; a solar reflectivity coefficient; initial state vector ;an empirical once per revolution along track acceleration and an altimetric time tag bias. The drag scale and solar reflectivity coefficients were constrained by the constraints outlined in chapter 7.

Table 9.1 Force Models Used in Orbit Determination.

Gravity Field Model	JGM-3
Thermospheric Model	MSIS-83[1]
Surface Force Model	Aston University Model[2]

1-[Hedin, 1983], 2-[Ehlers, 1993]

In addition to the laser range data, crossover data, with epoch differences less than five days to minimise aliasing of any oceanographic signal, have been utilised in order to better define the satellite's position. The use of crossovers as a tracking data set has been required because of the poor global coverage offered (predominantly Europe and North America) by the laser range stations.

Table 9.2 Rms Fits for the ERS-1 Orbits.

DATES (MJD)	No. Orb.	SLR Rms	SXO Rms	Alt Rms
49838 - 49852	3	8.2 ± 0.7cm	10.4 ± 0.2cm	22.3 ± 0.4cm
49851 - 49888	9	9.5 ± 1.6cm	10.1 ± 0.4cm	22.3 ± 0.3cm
49887 - 49923	9	10.6 ± 1.6cm	10.1 ± 0.5cm	22.2 ± 0.2cm
49922 - 49957	9	11.1 ± 1.4cm	10.1 ± 0.8cm	22.6 ± 0.4cm

Table 9.3 Rms Fits for the ERS-2 Orbits.

Dates (MJD)	No. Orb.	SLR Rms	SXO Rms	ALT Rms
49838 - 49855	3	8.7 ± 1.6cm	10.7 ± 0.3cm	23.2 ± 0.4cm
49854 - 49887	8	9.9 ± 1.5cm	10.3 ± 0.5cm	22.5 ± 0.5cm
49886 - 49923	9	10.4 ± 0.9cm	10.0 ± 0.6cm	22.1 ± 0.2cm
49922 - 49958	9	11.3 ± 1.6cm	10.3 ± 0.7cm	22.7 ± 0.7cm

The crossover and laser observations were given the same weighting and a rejection level close to the 3σ level (30cm) employed, resulting in the mean rms fits and variations presented in tables 9.2 and 9.3.

Altimetric data was also included within the orbit determination but was given zero weight so as not to influence the solution. This enabled long arc altimeter range biases to be recovered from the 15 second normal altimeter observations.

9.3 The Altimeter Dataset

The altimetry data used in the orbit determination (and subsequently the relative range, sea state and daily time tag bias determination) was the Ocean Product (OPR) supplied by ESA as part of the calibration and validation of ERS-2. The corrections applied are those given on the OPR CDROM [CERSAT, 1996] with the exceptions listed in table 9.5 and the altimeter data was screened for unreliable data by using the editing criteria outlined in table 9.4.

Table 9.4 Altimeter Data Editing Criterion.

Altimeter Range	$\sigma < 25$cm
Significant Wave Height ($h_{1/3}$)	$h_{1/3} < 10$m
Backscatter Coefficient (σ_0)	$6\text{dB} < \sigma_0 < 21\text{dB}$

Table 9.5 Altimeter Range Measurement Corrections.

Ocean Tide Model	CSR 3.0[1]
Pole Tide	Applied
Inverse Barometer Correction	Applied
Sea State Bias	5.5% $h_{1/3}$ [2]
Significant Wave Height	Modified[3]
Geoid Height	JGM-2[4] (deg & order 70) OSU91A[5] (deg & order 70-360)
Sea Surface Topography	Aston[6] (deg and order 15)
Processing Errors	Corrected[7]
USO Drift	Corrected[7]
Altimeter Bias Jumps	Corrected[8]

1-[Eanes R, 1995], 2-[Gaspar and Ogar, 1994], 3-[Cotton and Challenor, 1996], 4-[Nerem et al, 1994], 5-[Rapp et al, 1991], 6-[Moore, 1996(b)], 7-[Stum, 1996], 8-[Loial, 1996]

Table 9.5 outlines several corrections :the modification of the significant wave height; correction for altimeter bias jumps; correction for drift in the ultra stable oscillator and corrections for mistakes in the OPR processing, which are not given as explicit corrections on the OPR data set and warrant some discussion.

9.3.1 Modification of the Significant Wave Height

Comparisons of the significant wave heights as measured by ERS-1 with measurements made at buoy locations has shown that ERS-1 significantly underestimates the heights of ocean waves. Cotton and Challenor [1996] have derived relationships to correct the ERS-1 and ERS-2 significant wave heights such that they are consistent with buoy measurements. The relationships

derived by Cotton and Challenor [1996] for ERS-1 are given by equations (9.1)

$$h_{\frac{1}{3}}^{corr} = 1.156 h_{\frac{1}{3}}^{OPR} + 0.322 \qquad h_{\frac{1}{3}} < 0.92m \tag{9.1a}$$

$$h_{\frac{1}{3}}^{corr} = 0.932 h_{\frac{1}{3}}^{OPR} + 0.527 \qquad h_{\frac{1}{3}} > 0.92m \tag{9.1b}$$

whilst equations (9.2) gives the relationships for ERS-2.

$$h_{\frac{1}{3}}^{corr} = 1.169 h_{\frac{1}{3}}^{OPR} - 0.007 \qquad h_{\frac{1}{3}} < 1.24m \tag{9.2a}$$

$$h_{\frac{1}{3}}^{corr} = 0.955 h_{\frac{1}{3}}^{OPR} + 0.268 \qquad h_{\frac{1}{3}} > 1.24m \tag{9.2b}$$

The value of 5.5% of significant wave height to model the sea state bias was used in preference to that derived in chapter 5 (5.95%) because of the use of these modified wave heights. It was felt that if underestimation of the wave heights had been compensated for by using equations (9.1) and (9.2) 5.95% would be too high and would significantly affect the long arc range biases determined during the orbit determination process

9.3.2 Correction of Altimeter Bias Jumps

Preliminary studies [Moore et al, 1996(b)] of the QLOPR (Quick Look Ocean Product) altimeter data sets revealed that the ERS-1 and ERS-2 altimeters have been experiencing bias jumps. These bias jumps have subsequently been shown to be associated with on board anomalies [Roca and Francis, 1996] which cause the altimeter to be switched off resulting in a drop in instrument temperature and a change in the altimeter's steady state. Analysis of SPTR (Single Point Target Response) data [Loial, 1996] has allowed corrections to account for these bias jumps to be determined and these have subsequently

been applied to both altimeter data sets.

The bias jumps for ERS-1 and ERS-2, as derived from the SPTR data, are shown in figure 9.1.

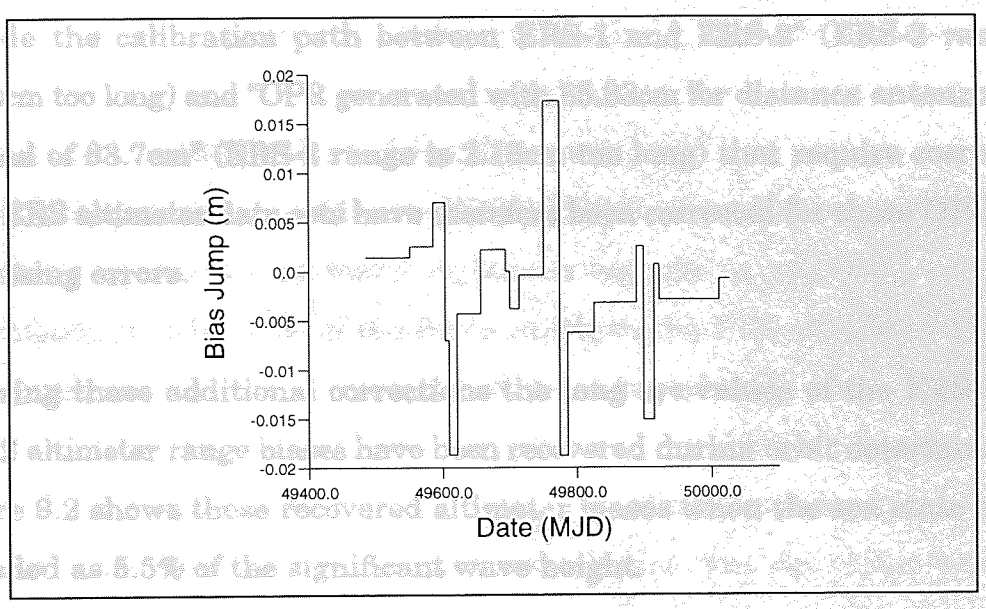

Figure 9.1 Range Bias Jumps for ERS-1 and ERS-2

9.3.3 Correction for Ultra Stable Oscillator Drift

The ultrastable oscillator frequencies onboard ERS-1 and ERS-2 are drifting from their assumed value used during the altimeter data processing by CERSAT [Stum, 1996]. As a consequence the range measurements for these two satellites are drifting such that the absolute and relative altimeter biases do not appear to remain constant over a period of time. As of the middle of 1995 (which corresponds to the period concerned) the ERS-1 range measurements are short by some 2.5cm whilst the ERS-2 range measurements are long by 0.7cm. These corrections have been applied so that the ultra stable oscillator drift does not add to the absolute or relative range biases determined.

9.3.4 Corrections for Data Processing Errors

Several range biases have been artificially introduced into the ERS altimeter measurements during the processing of the data. Stum [1996] reported that these processing errors were caused by "use of bad file for OPR generation" (ERS-1 range is 1.57cm too long), "differences of the group delay of the RF path outside the calibration path between ERS-1 and ERS-2" (ERS-2 range is 40.92cm too long) and "OPR generated with 85.83cm for distance antenna/CoG instead of 83.7cm" (ERS-2 range is 2.13cm too long) that require correction. Both ERS altimeter data sets have therefore been corrected for these OPR data processing errors.

Utilizing these additional corrections the long arc values of the ERS-1 and ERS-2 altimeter range biases have been recovered during orbit determination. Figure 9.2 shows these recovered altimeter biases when the sea state bias is modelled as 5.5% of the significant wave height.

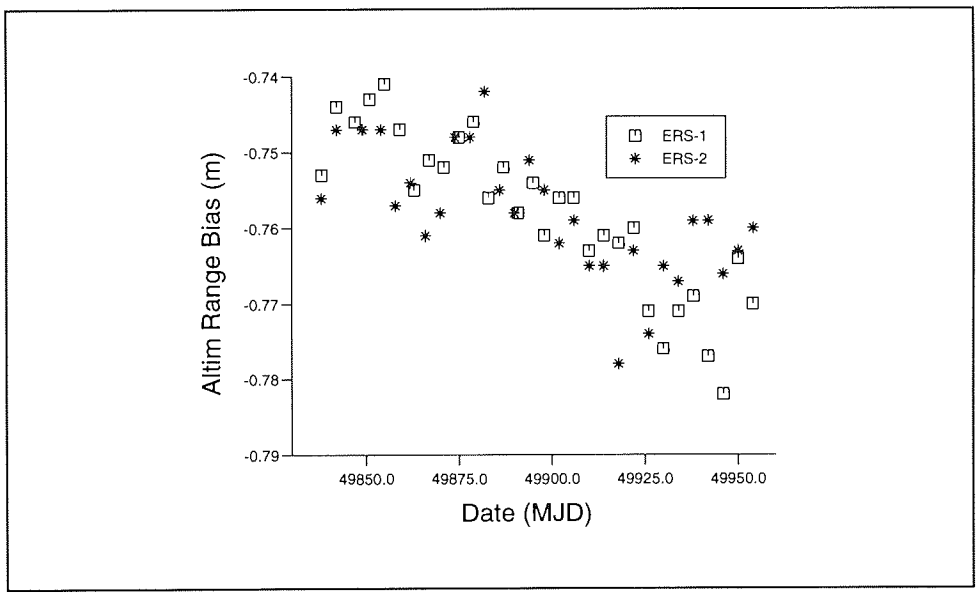

Figure 9.2 Altimeter Range Biases for the ERS Satellites Determined During Orbit Determination

The means of the long arc bias values shown in figure 9.2 are -75.8 ± 1.1 cm and -75.8 ± 0.8 cm for ERS-1 and ERS-2 respectively. Subtraction of the ERS-2 value from that obtained for ERS-1 gives a preliminary relative range bias of 0.0 ± 1.4 cm. As the sea state bias values used in the determination of this value have not been validated no real conclusions can yet be drawn other than the two altimeters appear to be behaving similarly, as would be expected.

9.4 Time Tag and Sea State Bias Recovery

Before determining the relative ERS-1/ERS-2 altimeter range bias it is important to remove as many erroneous signals as possible. This is particularly true because of the haste in which the ERS altimeter datasets were produced (several processing errors have already been identified). Analysis of the ERS-2 QLOPR data [Moore et al, 1996] [Scharroo ,1996] revealed severe problems with the time tags of data processed by ground stations other than Kiruna as the time tag bias was not stable and was frequently as high as ±10ms. To ensure that time tag biases are not absorbed into the ERS orbits an altimetric time tag bias has been recovered from the crossover data during the orbit determination. Subsequently any time tag bias present in the OPR datasets will still be present in the crossover datasets and requires removal before the determination of any relative range bias.

As the significant wave heights have been modified thus causing the sea state biases for the ERS datasets to be unknown it is necessary to determine these corrections. The sea state bias model used is the simple linear relationship with significant wave height described by equation (5.1).

9.4.1 The Time Tag Bias

A time tag bias, τ, results in the altimeter time tag, t, being wrong such that T the correct time tag is defined by equation (9.3),

$$T = t + \tau \qquad (9.3)$$

The altimeter height, h^{alt}, at time t can therefore be expressed by [Lam, 1994],

$$h^{alt}(t)=h^{alt}(T-\tau)=h^{alt}(T)-(\frac{dh^{alt}}{dt})\tau+O(\tau^2) \qquad (9.4)$$

where the error in the altimeter height measurement due to the time tag bias is,

$$\Delta h^{alt}=-(\frac{dh^{alt}}{dt})\tau \qquad (9.5)$$

Wagner and Klokocnik [1994] describe the altimetric height error caused by a constant time tag bias for a near circular orbit above an oblate spheroid Earth as,

$$\Delta h^{alt}=\tau a_e \sin^2 i(f+\frac{C_{20}a_e}{2a})sin2U\frac{dU}{dt} \qquad (9.6)$$

where U is the argument of latitude, i and a are the orbital inclination and semi major axis and a_e , f and C_{20} are the Earth's mean equatorial radius, coefficient of flattening and un-normalized zonal harmonic of degree 2.

The erroneous signal caused by a time tag bias can therefore be identified as a signal of frequency twice per revolution. Significantly this means that if any time tag bias was present in the ERS-1 data set used for chapters 7 and 8 it will have been removed by the correction procedure as a twice per revolution signal was recovered.

9.4.2 The Least Squares Recovery

Using the method of least squares recovery outlined in section 7.4 each of the crossover and repeat pass datasets have been used to determine the sea state, daily time tag and relative range bias values for ERS-1 and ERS-2.

Equation (9.7) defines the i^{th} row of the transformation matrix A where Δ^{rel} is 1 for dual satellite crossovers and ERS-1/ERS-2 repeat pass tracks and zero for single satellite crossovers, $h_{1/3}^{sati}$ is the corrected significant wave height for satellite i (set to zero for TOPEX) and $(dh^{alt}/dt)^i$ is the rate of change in altimeter height with respect to time for satellite i. $(dh^{alt}/dt)^i$ is set to zero for TOPEX, as it is assumed that there is no time tag bias in the TOPEX altimetry, and when the crossover epoch is not within the specified time period for the relevant ERS daily time tag bias.

$$A^T = \begin{bmatrix} \Delta^{rel} \\ h_{\frac{1}{3}}^{sat1} \\ -h_{\frac{1}{3}}^{sat2} \\ -\left(\frac{dh^{alt}}{dt}\right)_{first}^{sat1} \\ \vdots \\ -\left(\frac{dh^{alt}}{dt}\right)_{last}^{sat1} \\ \left(\frac{dh^{alt}}{dt}\right)_{first}^{sat2} \\ \vdots \\ -\left(\frac{dh^{alt}}{dt}\right)_{last}^{sat2} \end{bmatrix} \qquad (9.7)$$

9.4.3 Time Tag and Sea State Bias Determination

To determine the sea state and time tag biases of ERS-1 and ERS-2 prior to recovery of relative range biases, the single satellite crossovers for both of the ERS satellites have been analysed. By considering those points where the time difference is less than ten days scatter plots of the crossover residuals with respect to the first epoch can be constructed and are shown in figures 9.3 and 9.4.

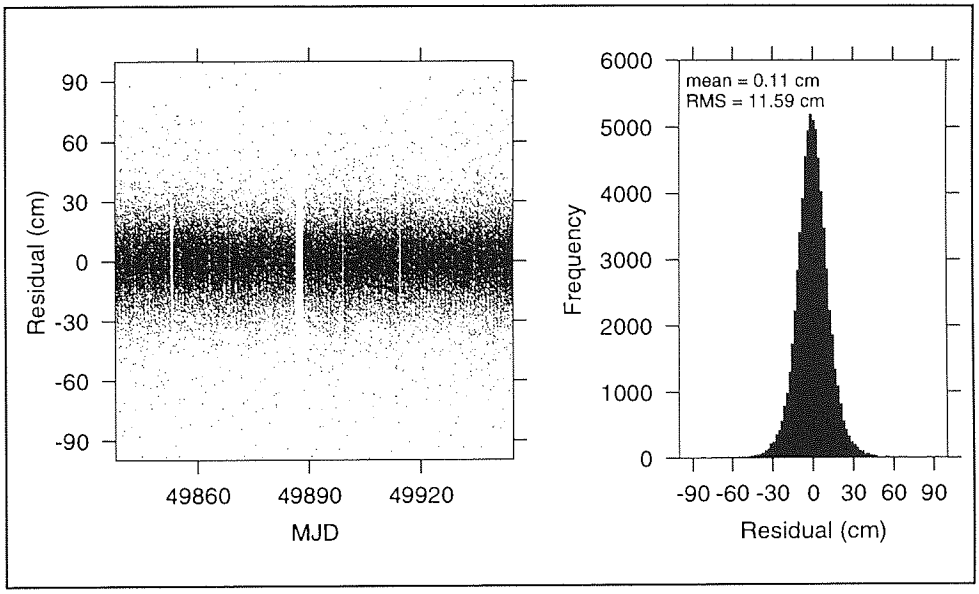

Figure 9.3 ERS-1 Single Satellite Crossover Residuals

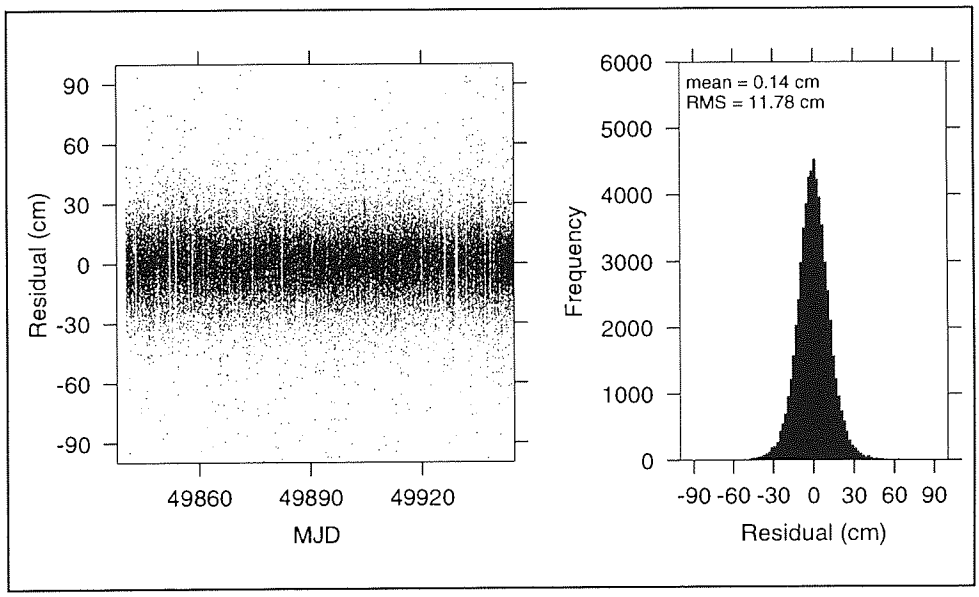

Figure 9.4 ERS-2 Single Satellite Crossover Residuals

Analysis of figures 9.3 and 9.4 shows that the crossover residuals of ERS-1 are slightly lower than the crossover residuals of ERS-2, however, this difference is only marginal and no significance can be attached.

Using the single satellite crossovers plotted in figures 9.3 and 9.4 the sea state and daily time tag biases have been recovered using the method of least squares and suppressing the recovery of the constant term (Δ^{rel}).

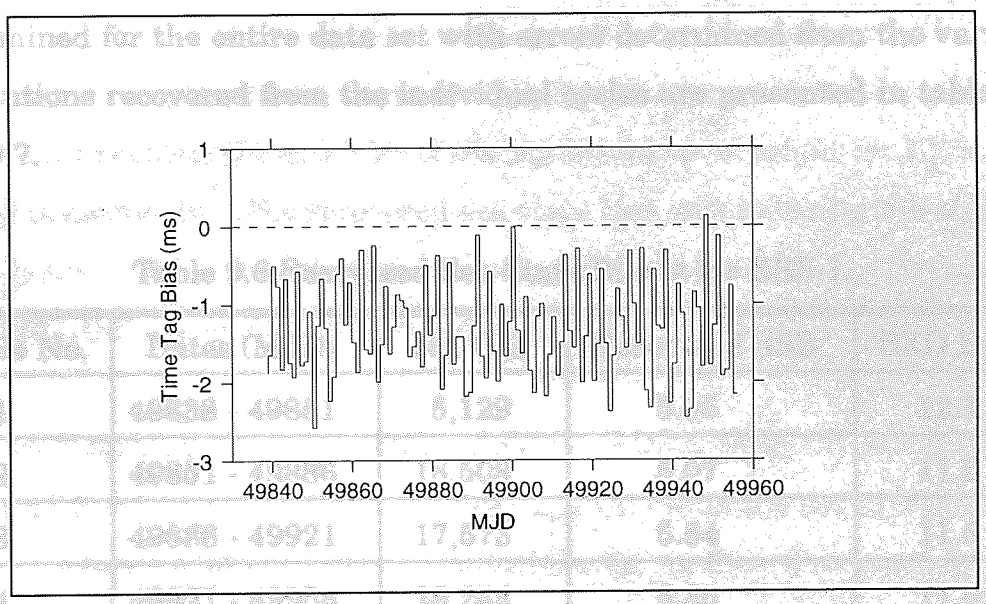

Figure 9.5 Recovered Daily Time Tag Biases for ERS-1

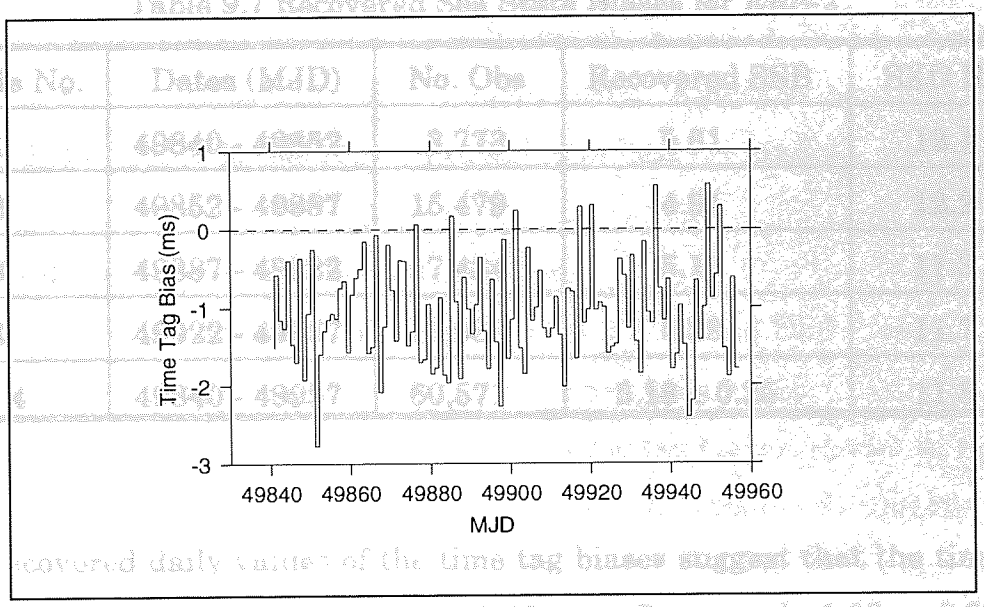

Figure 9.6 Recovered Daily Time Tag Biases for ERS-2

After determining the sea state and daily time tag biases for the entire data set (cycles 1-4) each individual cycle was analysed. This analysis consisted of using the daily time tag biases previously recovered and shown in figures 9.5 and 9.6 and suppressing their recovery whilst the values of sea state bias were recalculated. The sea state biases, as percentages of significant wave height, determined for the entire data set with errors determined from the variance in solutions recovered from the individual cycles are presented in tables 9.6 and 9.7.

Table 9.6 Recovered Sea State Biases for ERS-1.

Cycle No.	Dates (MJD)	No. Obs	Recovered SSB	SXO Rms
1	49838 - 49851	5,129	5.05	12.1
2	49851 - 49886	18,508	5.07	11.5
3	49886 - 49921	17,573	5.54	11.5
4	49921 - 49956	19,244	5.30	11.5
1 - 4	49838 - 49956	68,649	5.27 ± 0.20	11.6

Table 9.7 Recovered Sea State Biases for ERS-2.

Cycle No.	Dates (MJD)	No. Obs	Recovered SSB	SXO Rms
1	49840 - 49852	3,773	5.61	12.1
2	49852 - 49887	15,479	4.94	12.2
3	49887 - 49922	17,434	5.17	11.3
4	49922 - 49957	15,986	5.29	11.7
1 - 4	49840 - 49957	60,571	5.18 ± 0.25	11.8

The recovered daily values of the time tag biases suggest that the time tag biases for ERS-1 and ERS-2 are -1.23 ± 0.17 ms and -1.06 ± 0.30 ms

respectively (where the values are added to the altimeter time tag against the convention of subtracting biases). The source of this bias is as of this moment unclear, however, processing errors and or orbit error of signal two cycles per revolution are possible contributors.

Preliminary studies of the QLOPR (Quick Look Ocean Product) and OPR data sets using the original wave heights resulted in the recovered sea state biases being approximately 6% and 5.5% of the significant wave height for ERS-1 and ERS-2 respectively. The recovered sea state bias values, using the modified wave heights, show that there has been some unification of the data sets in that both ERS-1 and ERS-2 have similar sea state biases.

The lower significant wave height parameters recovered for the sea state bias values, as compared to previous studies, has validated the use of the 5.5% in preference to the 5.95% model of sea state bias during the orbit determination. If a global mean of 2m for the significant wave height is assumed the derived sea state bias would result in the long arc altimeter biases for ERS-1 and ERS-2 as calculated during the orbit determination (figure 9.2) requiring corrections of -5mm and -6mm respectively. Adding these corrections to account for errors in the sea state bias models yields long arc biases of -76.3 ± 1.1 cm and -76.4 ± 0.8 cm for ERS-1 and ERS-2 respectively. A relative bias of 0.1 ± 1.4 cm (ERS-1 - ERS-2) is therefore observed from long arc studies.

9.5 Relative Range Bias Determination

To determine the relative range bias between ERS-1 and ERS-2 several dual satellite crossover and repeat pass datasets have been utilised. All data sets have been corrected by removing the daily time tag biases, shown in figures 9.5 and 9.6 (these values are preferred to values obtained during the orbit determination), and sea state biases of 5.27% and 5.18% for ERS-1 and ERS-2 respectively. In the least squares process the recovery of the sea state and

daily time tag biases was suppressed so that the only term recovered was the relative range bias.

9.5.1 The Dual Crossover Datasets.

Three types of dual satellite crossover are considered, namely; ERS-1/ERS-2, TOPEX/ERS-1 and TOPEX/ERS-2 dual crossovers. No Poseidon data has been used due to the limited timescale of the period analysed and the small amount of Poseidon data available. The TOPEX altimetry data was prepared in exactly the same manner described in chapter 7 except NASA orbit heights determined with respect to the JGM-3 gravitational field, as supplied by AVISO from cycle number 93 onwards, have been used.

Scatter plots and histograms of each of these data sets are shown in figures 9.7 - 9.9 where the dates refer to the first satellite (ie TOPEX in TOPEX/ERS-1 and ERS-1 in ERS-1/ERS-2 dual crossovers) and the recovered relative range biases are presented in tables 9.8 - 9.10 where the errors given are the standard errors from the scatter in solutions for cycles 1-4.

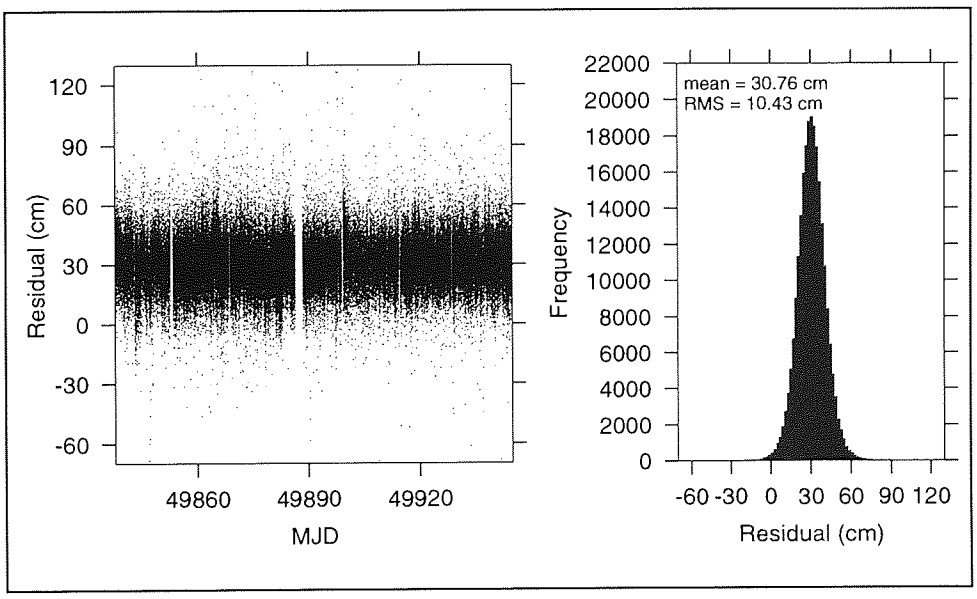

Figure 9.7 TOPEX - ERS-1 Dual Satellite Crossover Residuals

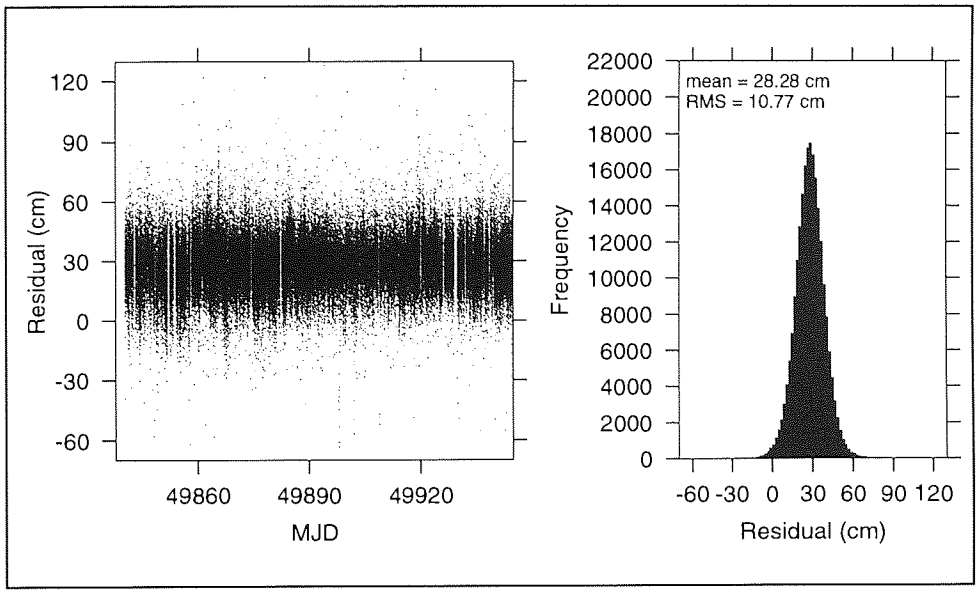

Figure 9.8 TOPEX - ERS-2 Dual Satellite Crossover Residuals

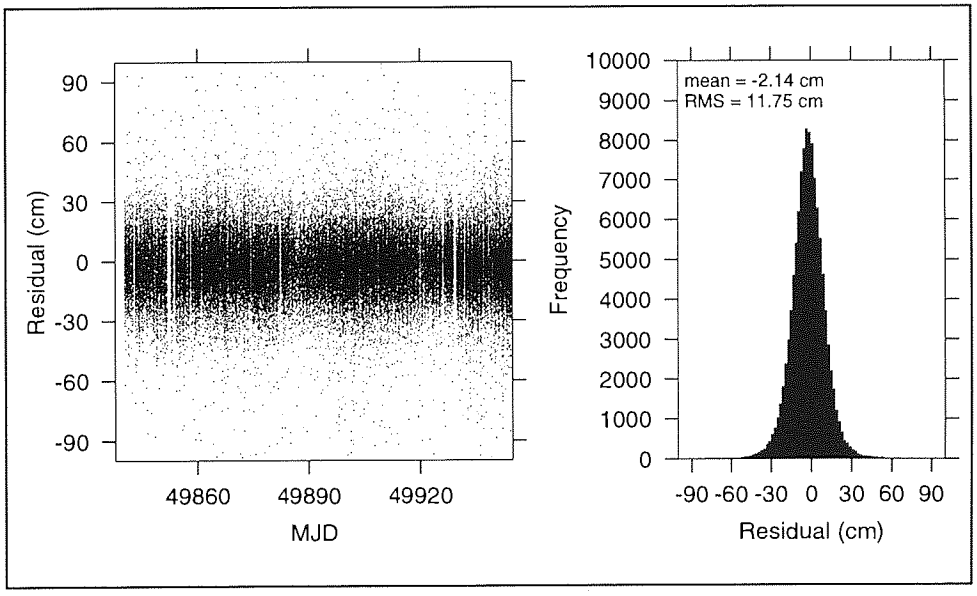

Figure 9.9 ERS-1 - ERS-2 Dual Satellite Crossover Residuals

Table 9.8 Recovered Relative Range Biases from TOPEX - ERS-1 Dual Satellite Crossovers.

Cycle No.	Dates(MJD)	No. Obs	Rel. Range Bias (cm)	Rms (cm)
1	49838-49851	18,910	30.8	11.5
2	49851-49886	87,069	30.3	10.7
3	49886-49921	57,344	30.8	10.2
4	49921-49956	72,522	31.2	10.0
1-4	49838-49956	236,772	30.8 ± 0.3	10.4

Table 9.9 Recovered Relative Range Biases from TOPEX - ERS-2 Dual Satellite Crossovers.

Cycle No.	Dates(MJD)	No. Obs	Rel. Range Bias (cm)	Rms (cm)
1	49840-49852	15,958	26.5	12.3
2	49852-49887	80,653	27.9	11.1
3	49887-49922	60,338	28.9	10.3
4	49922-49957	65,095	28.5	10.3
1-4	49840-49957	222,982	28.3 ± 0.4	10.8

Table 9.10 Recovered Relative Range Bias from ERS-1 - ERS-2 Dual Satellite Crossovers.

Cycle No.	Dates(MJD)	No. Obs	Rel. Range Bias (cm)	Rms (cm)
1	49838-49851	8,253	- 2.7	12.5
2	49851-49886	33,057	- 2.0	11.9
3	49886-49921	34,576	- 2.0	11.6
4	49921-49956	34,477	- 2.6	11.6
1-4	49838-49956	112,291	- 2.2 ± 0.4	11.8

All the dual crossover data sets yield ERS-1 - ERS-2 relative range biases close to -2.0 cm, although a larger scatter is observed for the TOPEX dual crossovers (where the TOPEX - ERS-1 relative range bias is subtracted from the TOPEX - ERS-2 relative range bias). This is hardly surprising as the different media corrections (primarily ionosphere) and non-cancellation of orbit errors will contribute to the TOPEX - ERS relative biases observed.

9.5.2 Repeat Track Analysis.

As ERS-2 follows the ground track of ERS-1 but with a time lag of one day it is possible to use the repeat passes between ERS-1 and ERS-2 as a data set similar to dual satellite crossovers. The repeat tracks from ERS-1 (or ERS-2) every 35 days are not considered because of the growth in ocean signal associated with the large time difference between epochs.

The repeat pass data was constructed by interpolating the altimeter and orbit heights at 0.25 degree latitude intervals for each of the ERS satellites. No cross track corrections for deviation from the reference track were made due to the continual close proximity of the tracks throughout the ERS-2 calibration phase. This results in an extensive global data set which is more evenly distributed throughout the latitudinal bands than the single and dual satellite crossovers.

The scatter plot and histogram of the mean relative bias for each pair of ascending and descending tracks with a minimum of 20 observations are shown in figure 9.10, when sea state biases of 5.27% and 5.18% are applied with the time tag bias values of figures 9.5 and 9.6 and their recovery suppressed. The relative range biases recovered by the least squares procedure are given in table 9.11.

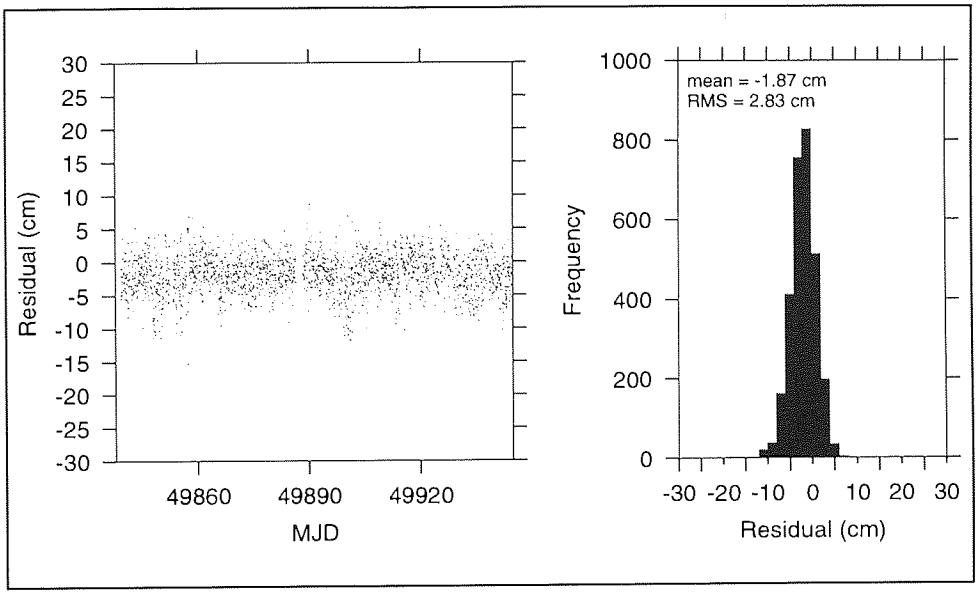

Figure 9.10 Mean Relative Bias for Each Pair of ERS-1 - ERS-2 Repeat Pass Tracks

Table 9.11 Recovered Relative Range Biases from ERS-1 - ERS-2 Repeat Tracks.

Cycle No.	Dates(MJD)	No. Obs	Rel. Range Bias (cm)	Rms (cm)
1	49838-49851	94,122	- 2.3	8.0
2	49851-49856	268,932	- 1.6	7.3
3	49856-49921	269,987	- 1.5	7.4
4	49921-49956	265,271	- 2.2	7.2
1-4	49838-49956	901,530	- 1.8 ± 0.4	7.4

Again an ERS-1 - ERS-2 relative range bias close to -2.0cm is observed. The low rms fits to the repeat pass data is due to the ERS geographically correlated errors (mean and variable) cancelling to the extent that the observations are of accuracies near consistent with TOPEX/Poseidon single satellite crossovers. This data set with it's inherent accuracy and high number of well distributed observations is obviously very powerful.

9.6 An Estimation of the Systematic Errors in the Relative Range Bias

In an attempt to estimate realistic errors (as opposed to the rms variation) for the relative range biases given in tables 9.8 - 9.11 and the long arc range bias values derived during the orbit determination the effect of systematic errors from various sources are considered. These error sources consist of geographically correlated orbit error, centre of gravity and instrumental offset errors, media /tidal correction errors and sea state bias errors.

9.6.1 Geographical Orbit Error

Due to the non uniform distribution of crossover and repeat pass data (data is predominantly southern hemisphere) it is necessary to consider the systematic effects that orbit error might impose upon the relative and absolute range bias recoveries.

Whilst the geographically correlated orbit error will cancel for the repeat pass tracks between the ERS satellites so that there is no obvious systematic error contribution, the same cannot be said for the dual crossover data sets. In the case of ERS-1 - ERS-2 dual crossovers this is due to any systematic errors between the ascending and descending arcs still being observable. The difference in geographically correlated orbit error between the ERS satellites and TOPEX/Poseidon will also cause a systematic bias to be introduced into the relative bias determined from TOPEX - ERS dual crossovers. However, the subtraction of the TOPEX - ERS-1 relative bias from the TOPEX - ERS-2 relative bias should still provide a reasonable measure of the ERS-1 - ERS-2 relative bias due to the systematic errors present in each data set being similar, and therefore cancelling.

The effect of orbit error is perhaps most significant when determining the range biases from long arc analysis. However, as any systematic bias error is likely to be present in both data sets a reasonable relative bias should be

obtainable.

The systematic orbit error is thus quantified by assuming the mean of the single satellite crossover residuals as presented in figures 9.3 and 9.4. The higher value for ERS-2 is taken resulting in a systematic bias of 0.14 cm being adopted for ERS-1 and ERS-2.

9.6.2 Media and Tidal Correction Errors.

The significant media errors are primarily due to mis-modelling of the wet and dry troposphere, the ionosphere, ocean tides and inverse barometer corrections. Stum [1996] reported that a mean bias of 0.7 cm between the ERS-1 and ERS-2 wet tropospheric corrections as measured by the two, slightly different, microwave radiometers could be observed. As the dry tropospheric correction models are the same for both satellites and based upon the same meteorological data, there should be no systematic bias observed in any dual ERS altimeter measurement from this correction. Similarly it is assumed that the models used for the ionospheric (Bent Model) and ocean tide (CSR 3.0) corrections provide no systematic bias in the ERS-1 - ERS-2 dual crossovers and repeat track data. The systematic error for ERS dual measurements (dual satellite crossovers and repeat passes) is therefore defined as 0.7 cm.

TOPEX/Poseidon's ionospheric correction is more accurately determined than ERS-1's due to the use of a dual frequency altimeter. Similarly the microwave radiometer on board TOPEX/Poseidon cannot be assumed to measure the same wet tropospheric correction as measured by the radiometers onboard the ERS satellites. As the ocean tide model used is the same for both satellites no systematic error is assumed. A 1cm systematic error is therefore expected between the ERS and TOPEX altimeter media corrections.

The long arc range bias measurements will contain systematic errors from

each of the altimetric media corrections. Additionally tidal corrections may provide a systematic error so a much larger systematic error of 2cm is assumed for the long arc range bias determination.

9.6.3 Sea State and CoG/Instrumental Errors.

The sea state biases for ERS-1 and ERS-2 are recovered as 5.27 ± 0.20 and 5.18 ± 0.25 percent of the significant wave height (as presented in tables 9.6 and 9.7) where the variation is derived from the scatter of recovered results. The systematic bias due to sea state bias is therefore assumed to be 0.25% of the significant wave height for both ERS-1 and ERS-2. Assuming an average of 2m for the significant wave height results in systematic errors of 0.5 cm due to the sea state bias for each altimeter measurement.

The error due to mis-modelling of the centres of gravity and/or instrumental corrections is assumed to be 0.2cm for each of the ERS satellites.

9.6.4 The Absolute and Relative Range Biases and Errors

Table 9.12 Systematic Errors for Each Dataset.

Data Type	Orbit Error	Media Errors	SSB Errors	CoG Errors
T-ERS DXOs	0.14 cm	1.00 cm	0.50 cm	0.20 cm
E1-E2 DXOs	0.20 cm	0.70 cm	0.70 cm	0.30 cm
Repeat Passes	0.00 cm	0.70 cm	0.70 cm	0.30 cm
Altim Obs	0.14 cm	2.00 cm	0.70 cm	0.20 cm

Table 9.13 Recovered Relative Range Biases with Estimated Errors.

Data set	Rel/Abs Altimeter Range Bias (cm)
TOPEX - ERS-1 Dual Crossovers	30.8 ± 1.1
TOPEX - ERS-2 Dual Crossovers	28.3 ± 1.1
ERS-1 - ERS-2 Dual Crossovers	- 2.2 ± 1.1
ERS-1 - ERS-2 Repeat Pass Tracks	- 1.8 ± 1.0
ERS-1 Altimeter Observations	-76.3 ± 2.1
ERS-2 Altimeter Observations	-76.4 ± 2.1

Table 9.12 summarises the systematic error sources that contribute to each of the datasets and table 9.13 presents the derived absolute and relative range biases, plus errors derived from the error contributions of table 9.12, for each of the data types.

9.7 Conclusions

Upon correction of the ERS altimeter datasets for onboard bias jumps, Ultra Stable oscillator drift, OPR processing errors and underestimation of the wave heights analysis of the single satellite crossovers has resulted in the ERS-1 and ERS-2 sea state biases being determined as 5.27 ± 0.20 and 5.18 ± 0.25 percent of the significant wave height respectively. The closeness of these results suggests that equations (9.1) and (9.2) compensate for ERS-1's and ERS-2's underestimation of wave height reasonably well. Similarly the daily time tag biases recovered for each satellite, -1.23 ± 0.17 ms for ERS-1 and -1.06 ± 0.30 ms for ERS-2, are similar.

The ERS-1 - ERS-2 relative range biases recovered from analysis of the dual satellite crossovers, repeat pass tracks and altimeter observations are summarised in table 9.14, where the errors presented are those derived in section 9.6.

Table 9.14 ERS-1 - ERS-2 Relative Range Biases.

Data set	ERS-2- ERS-1 Relative Bias (cm)
TOPEX - ERS Dual Crossovers	- 2.5 ± 1.6
ERS-1 - ERS-2 Dual Crossovers	- 2.2 ± 1.0
ERS-1 - ERS-2 Repeat Passes	- 1.8 ± 1.0
ERS-1 and ERS-2 Altimeter Obs	0.1 ± 3.0

Taking a weighted mean of the values in table 9.14 results in the ERS-1/ERS-2 relative range bias being -2.1cm, thus indicating that ERS-2 measures 2.1 cm longer than ERS-1.

Chapter 10
Conclusions

10.1 A Review of the Thesis Aims

The aim of this thesis was primarily to reduce the errors present within the ERS-1 (and to a lesser degree ERS-2) altimeter datasets such that they have accuracies commensurate with TOPEX/Poseidon. Whilst the radial orbit error of ERS-1, at the time of study, was identified as the largest discrepancy between the ERS and TOPEX/Poseidon datasets, the recovery of the relative range and sea state biases for ERS-1 was also deemed important for the unification of these datasets.

Progress in this direction has been achieved, firstly, by analysis and removal of the two most significant error sources present in the ERS dataset, namely; the sea state bias and orbit error; and secondly by calibration of the ERS-2 altimeter with respect to ERS-1.

10.2 Reduction of ERS-1 Error due to Sea State Bias

Analysis of several models for the less accurate sea state bias model of ERS-1 (compared to TOPEX/Poseidon) by the minimisation of single satellite crossovers has been carried out in chapter 5. All of the models considered, with terms relating to wind speed and significant wave height, provide considerably better fits to the crossover datasets than the model provided on the OPR dataset. Whilst the most significant improvement was achieved by the four parameter model, similar to that used for TOPEX/Poseidon,

comparisons of the results with those for TOPEX/Poseidon revealed anomalous trends relating to the term involving the square of the ERS-1 significant wave height (ie this parameter took the opposite sign). This discrepancy could only be assigned to the properties of the ERS-1 tracker. Until further analysis and confirmation of this result is carried out it was concluded that models consisting of both significant wave height and wind speed parameters would be unreliable. For this reason the simple linear relationship between sea state bias and significant wave height was adopted where the sea state bias is defined as 5.95% of the significant wave height. The use of this model instead of that provided on the OPR dataset resulted in the ERS-1 single satellite crossover residuals reducing from 16.6 cm rms to 16.1 cm rms. As the OPR sea state bias model is approximately equal to 2% of the significant wave height this represents an error of 8cm at wave heights of 2m (the approximate global average) and significantly larger errors at wave heights of 5m or more.

10.3 Reduction of ERS-1 Error due to Radial Orbit Error

The radial orbit error of ERS-1 was expressed as a finite Fourier expansion series to model the gravitational field based error and additional secular and periodic terms to model errors due to atmospheric density, solar radiation pressure and initial state vector mis-modelling. By analysis of the JGM-2 gravity field's co-variance matrix, the significant gravitational error frequencies were identified and recovered for 13 cycles of ERS-1's multi-disciplinary phase. An optimal strategy for error recovery was devised by analysis of the solution's co-variance matrix eigenvalues and the reduction in the TOPEX/Poseidon - ERS-1 dual crossover residuals. This strategy consisted of recovering 160 out of the 162 dominant error terms for each individual arc, where the two constant terms were taken from the respective 35 day solution (involving the recovery of 210 parameters). This then resulted in the mean TOPEX/Poseidon - ERS-1 dual crossover residual reducing from 12.2cm rms to 8.8cm rms which translates to a radial accuracy improvement

of 8.5cm rms; the original ERS-1 orbits having a radial accuracy of 9.9cm compared with 5.2cm rms for the corrected orbits.

Determination of the mean of the constant offsets in the TOPEX/Poseidon - ERS-1 dual crossover datasets allowed the relative altimeter range biases between TOPEX/Poseidon and ERS-1 to be defined as 30.2 (TOPEX) and 45.0 (Poseidon) cm respectively, which compares favourably with independent results obtained by other authors from absolute range bias determination. This result, however, will change when the mismodelling of the TOPEX USO drift present in the AVISO CDROM data has been corrected. Once corrected the TOPEX and Poseidon altimeters will have similar range (and relative range) biases close to that derived for Poseidon.

The reduction of orbit error was then validated by comparisons of the mean sea surface and annual variability derived from the ERS-1 and TOPEX altimetry datasets. The analysis showed that the errors present in the ERS altimeter dataset have been significantly reduced as the corrected ERS-1 dataset gave results more consistent with TOPEX.

Analysis of dual crossovers to determine the geographically correlated orbit errors for ERS-1 also showed that the correction procedure had reduced the errors present, with the mean and variable components being 2.2cm and 1.9cm respectively compared to 4.2cm and 4.0cm for the uncorrected orbits. Errors associated with the significant near resonance frequencies for ERS-1 in its 35 day repeat phase (ie at orders 14, 29, 43 and 57 in the gravity field) were also shown to have been removed, thus validating the removal of orbit error.

Comparisons of the corrected orbit heights with those of orbits corrected by cubic splines showed the radial differences over the ocean to be 5.0cm, suggesting that both strategies provide orbits of accuracies near the 5cm level.

By analysis of the geographically correlated errors for the cubic spline corrected orbits it was also possible to see that there was still some signal that could be removed as the mean and variable components had values of 1.9cm rms and 1.3cm rms respectively. Comparisons of the error powers, however, suggests that the cubic splines performed better at removing lower order signals which may be associated with media corrections rather than orbit error.

10.4 Reduction of ERS-2 Errors by Calibration with Respect to ERS-1

The last chapter, chapter 9, attempted to calibrate ERS-2 with respect to ERS-1 and TOPEX/Poseidon. This was achieved by analysis of single and dual crossover residuals as well as repeat track data, resulting in a relative bias of -2.1cm (ERS-2 measuring 2.1cm longer) being determined. Additionally it is shown that, when the wave heights for both satellites are calibrated with respect to buoy data, the sea state biases are similar. ERS-1 was determined to have a sea state bias equal to 5.27% of significant wave height compared with 5.18% for ERS-2. As expected the time tag biases of the two altimeters were similar (ERS-1 = -1.23ms and ERS-2 = -1.06ms) thus confirming the similarity in the two altimeters.

10.5 Summary of Conclusions

To summarise the findings of the thesis;

1) The ERS-1 OPR sea state bias is an underestimation and the sea state bias should be defined as 5.95% of the significant wave height.
2) The ERS-1 radial orbit error has been reduced by minimising the single and dual (with TOPEX/Poseidon) crossover residuals such that the accuracies of the uncorrected and corrected orbits can be summarised as in table 10.1.

Table 10.1 ERS-1 Radial Orbit Accuracies

	Orig. ERS-1 Orbits	Corr. ERS-1 Orbits
Radial Error	9.9cm rms	5.2cm rms
Geog. Fixed Error	4.2cm rms	2.2cm rms
Geog. Variable Error	4.0cm rms	1.9cm rms
Non Cons. Force Mod. Error	8.0cm rms	4.3cm rms

3) The near resonant frequency signals for ERS-1 have been removed in the non dynamic correction procedure.

4) In the calibration of ERS-2 with respect to ERS-1 the time tag and sea state biases (using modified wave heights) are those given in table 10.2 and the relative range bias is -2.1cm (ERS-2 measures 2.1cm longer).

Table 10.2 Bias Values for ERS-1 and ERS-2

	ERS-1	ERS-2
Sea State Bias	5.27± 0.20 % Sig. Wave Ht.	5.18 ±0.25 % Sig. Wave Ht.
Time Tag Bias	-1.23 ±0.17 ms	-1.06 ±0.30 ms

10.6 Suggestions for Future Work

Whilst the main aims of the thesis have been met in that an ERS-1 dataset more consistent with that of TOPEX/Poseidon has been developed there are still some areas that could have been investigated had time permitted.

Firstly , the sea state bias models analysed revealed some anomalous trends within the ERS-1 altimeter data. As the ERS-2 altimeter is virtually identical (although the tracking software has been modified slightly) it would have been interesting to see whether the same anomalous characteristics are observed in ERS-2 data. Also, the dependency upon orbit heights used casts some doubt on the value of 5.95% obtained for the linear relationship with

significant wave height. With the launch of ERS-2, and the year's worth of data for the tandem ERS-1/ERS-2 phase, an ideal dataset in the form of ERS-1/ERS-2 repeat tracks exists for the analysis of ERS-1 and ERS-2 sea state biases. As the geographically correlated errors (mean and variable) will cancel the repeat tracks will provide an accurate dataset that may not require the use of crossovers in the orbit determination, thus allowing the sea state bias to be determined with much greater certainty.

The second area that could receive more attention is the non-conservative (drag and solar radiation pressure) force mis-modelling as the model used in this thesis is heavily biased towards the removal of gravitational field errors. With the creation of the JGM gravity fields the errors associated with the gravitational field have been reduced and surface force errors are proportionally more significant. Also, with the availability of PRARE on ERS-2 the correction procedures employed at Aston University and by AVISO could be validated at the extreme latitudes and over land where the most significant differences occur.

Finally, having reduced the errors associated with the ERS-1 orbits and sea state bias the most significant difference remaining in the ERS and TOPEX/Poseidon datasets will be the ionospheric corrections. If TOPEX/Poseidon and ERS altimetry data is to be merged properly this area requires attention.

References

Antreasian P.G and Rosborough G.W (1992),'Prediction of Radian Energy Forces on the TOPEX/Poseidon Spacecraft', Journal of Spacecraft and Rockets, 29(1), pp 81-90.

Asknes K (1976),'Short Period and Long Period Perturbations of a Spherical Satellite due to Direct Solar Radiation', Celestial Mechanics, 13(1), pp 89-104

AVISO (1992),'AVISO User Handbook: Merged TOPEX/Poseidon Products', AVI-NT-02-101-CN, Edition 1.0.

Barrick D.E and Lipa B.J (1985),'Analysis and Interpretation of Altimeter Sea Echo', Advances in Geophysics, 27, pp 61-100.

BNSC (1990), BNSC Factsheet Ref. No. DC-F1-EOS-ED-0001

Bomford (1980),'Geodesy', 4th Edition, Clarendon Press, Oxford.

Born G.H, Richards M.A and Rosborough G.W (1982), 'An Empirical Determination of the Effects of Sea State Bias on Seasat Altimetry', Journal of Geophysical Research, 87, pp 3221-3226.

Carnochan S, Moore P, Ehlers S, Lam C.W and Woodworth P.L (1994), 'Improvement of the Radial Positioning of ERS-1 Through Dual Crossover Analysis with TOPEX/Poseidon', In Proceedings of the Second ERS-1 Symposium, Hamburg, Germany, 11-14 October 1993, ESA SP-361, 2, pp753-758.

Cartwright D.E and Ray R.D (1990),'Oceanic Tides from Geosat Altimetry', Journal of Geophysical Research, 95, pp 3069-3090.

CERSAT (1996),'Altimeter and Microwave Radiometer ERS Products : User Manual', C2-MUT-A-01-1F, version 2.0.

Colombo O.L (1984),'Altimetry, Orbits and Ocean Tides', NASA Technical Memorandum 86180.

Cook G.E (1966),'Perturbations of Near Circular Orbits by the Earth's Gravitational Potential', Planet Space Sciences, 14, pp 433-444, Pergamon Press.

Cotton D. and Challoner P. (1996),'Calibration and Validation of ERS-2 OPR Wind/Wave Measurement', Presented to ERS-2 Radar Altimeter and Microwave Radiometer Commissioning Workgroup, Meeting # 10, ESA - ESRIN, 25 - 26 April 1996.

Douglas B.C and Agreen R.W (1983),'The Sea State Correction for Geos-3 and Sesat Satellite Altimeter Data', Journal of Geophysical Research, 88, pp 1655-1661.

Dumont J.P (1985),'Estimation Optimale des Parametres Altimetriques des Signaux Radar Poseidon', PhD Thesis, Institut National Polytechnique de Toulouse, France, 1985.

Eanes R (1995), Anonymous ftp, (ftp://ftp.csr.utexas.edu/pub/tide)

Ehlers S (1993),'Various Techniques and Procedures for Refining ERS-1 Orbits', PhD Thesis, University of Aston in Birmingham, U.K.

Engelis T. (1988),'On the Simultaneous Improvement of a Satellite Orbit and Determination of Sea Surface Topography using Altimeter Data', Manuscripta Geodetica, 13, pp 180-190.

Francis C.R (1993),'The Height Calibration of the ERS-1 Radar Altimeter', In Proceedings of the First ERS-1 Symposium, Cannes, France, 4-6 November, 1992 ESA SP-359, pp 381-393.

Fu L.L and Glazman R (1991),'The Effect of the Degree of Wave Development on the Sea State Bias in Radar Altimetry Measurements', Journal of Geophysical Research, 96, pp 829-834.

Fu L.L, Christensen E.J, Yamarone C.A, Lefebvre M, Menary Y, Dorrer M and Escudier P (1994), 'TOPEX/Poseidon Mission Overview', Journal of Geophysical Research, 99 (C12), pp 24,369-24,381.

Gaspar P, Ogar F, Le Traon P.Y and Zanife O.Z (1994),'Estimating the Sea State Bias of the TOPEX and Poseidon Altimeters from Crossover Differences', Journal of Geophysical Research, 99, pp 24981 - 24994.

Gaspar P and Ogar F (1994), 'Estimation and Analysis of the Sea State Bias of the ERS-1 Altimeter', Report of Task B1-B2 of IFREMER contract No. 94/2.426016/C.

Glazman R.E, Greysukh A and Zlotnicki V (1994),'Evaluating Models of Sea State Bias in Satellite Altimetry', Journal of Geophysical Research, 99, pp 12581-12591.

Gray R.D (1993),'Global Non-Dynamic Refinement of Radial Orbit Error for Altimetric Earth Satellites', PhD Thesis, University of Aston in Birmingham, U.K.

Hedin A.E (1983), 'A revised Thermospheric Model Based on Mass Spectrometer and Incoherent Scatter Data: MSIS-83', Journal of Geophysical Research , 88 (A12), pp 10170-10188.

Kaula W.M (1966),'Theory of Satellite Geodesy: Applications of Satellites to Geodesy', Blaisdell Publishing Company, Waltham, Masssachusetts, U.S.A.

King-Hele D.G (1987), 'Satellite Orbits in an Atmosphere: Theory and Applications', Blackie, Glasgow.

Klokocnik J, Kostelecky J and Jandova M (1993), 'Altimetry with Dual Satellite Crossovers', Paper presented to IAG General Meeting, Beijing, China.

Klokocnik J, Kostelecky J and Karasova D (1994), 'Satellite Altimetry and its use in Geoscience', Class Text, Research Institute of Geodesy, Topography and Cartography the Czech Republic. (ISBN 80-85881-004)

Lam C.W, Moore P and Woodworth P.L (1993), 'Calibration of ERS-1 Altimetry over the North Sea',In Proceedings of the First ERS-1 Symposium, Cannes, France, 4-6 November, 1992, ESA SP-359, pp 85-90.

Lam C.W (1994), 'Application of ERS-1 and TOPEX/Poseidon Altimetry Using Precise Orbits', PhD Thesis, University of Aston in Birmingham, U.K.

Lerch F.J, Nerem R.S, Putney B.H, Felsentreger T.L, Sanchez B.V, Marshal J.A, Klosko S.M, Patel G.B, Williamson R.G, Chinn D.S, Chan J.C, Rachlin K.E, Chandler N.L, McCarthy J.J, Luthcke S.B, Pavlis N.K, Pavlis D.E, Robbins J.W, Kapoor S and Pavlis F.C (1994), 'A Geopotential Model from Satellite Tracking, Altimeter and Surface Gravity Data: GEM-T3', Journal of Geophysical Research 99(B2), pp 2815-2898.

Le Traon P.Y (1996) "Personal Communication", CLS Space Oceanography Group, Toulouse, France.

Le Traon P.Y, Gaspar P, Bouyssel F and Makhmara H. (1995), 'Using TOPEX/Poseidon Data to Enhance ERS-1 Data', Journal of Atmospheric and Ocean Technology', 12, pp 161-170.

Llewellyn S.K and Bent R.B (1973), 'Documentation and Description of the Bent Inospheric Model', AFCRL-TR-73-0657.

Loial C (1996), 'USO and SPTR Correction File', Presented to ERS-2 Radar Altimeter and Microwave Radiometer Commissioning Workgroup, Meeting # 10, ESA - ESRIN, 25 - 26 April 1996.

Luthcke S.B and Marshal J.A (1992), 'Non Conservative Force Model Parameter Estimation Strategy for TOPEX/Poseidon Precision Orbit Determination' NASA Technical Memorandum 104575.

Marsh J.G, Lerch F.J, Putney B.H, Felsentreger T.L, Sanchez B.V, Klosko S.M, Patel G.B, Robbins J.W, Williamson R.G, Engelis T.E, Eddy W.F, Chandler N.L, Chinn D.S, Kapoor S, Rachlin K.E, Braatz L.E, and Pavlis E.C (1989), 'The GEM-T2 Gravitational Model', NASA Technical Memorandum 100746.

Marshal J.A, Luthcke S.B, Andtreasian P.G and Rosborough G.W (1992), 'Modeling Radiation Forces Acting on TOPEX/Poseidon for Precise Orbit Determination', NASA Technical Memorandum 104564.

Marshal J.A, Zelensky N.P, Klosko S.M, Chinn D.S, Luthcke B, Raclin K.E and Williamson R.G (1995), 'The Temporal and Spatial Characteristics of TOPEX/Poseidon Radial Orbit Error', Journal of Geophysical Research, 100 (C12), pp 25,331-25,352.

Moore P (1996(a)) "Personal Communication" , Dept. Civil Engineering, Aston University, Birmingham, UK.

Moore P (1996(b)) "Personal Communication", Dept. Civil Engineering, Aston University, Birmingham, UK.

Moore P and Rothwell D.A (1990), 'A Study of Gravitational and Non-Gravitational Modelling Errors in Crossover Differences', Manuscripta Geodetica, 15, pp 187-206.

Moore P and Ehlers S (1993), 'Orbital Refinement of ERS-1 using Dual Crossover Arc Techniques with TOPEX/Poseidon', Manuscripta Geodetica, 18, pp 249.

Moore P, Ehlers S and Carnochan S (1996(a)), 'Accuracy Assessment and Refinement of the JGM-2 and JGM-3 Gravity Fields for Radial Positioning of ERS-1', Submitted to Journal of Geodesy.

Moore P, Carnochan S and Murphy C.M (1996(b)), 'Absolute and Relative Range Bias Estimation of the ERS-2 Radar Altimeter', Submitted to ESA for publication.

Murphy C.M, Moore P and Woodworth P.L (1996), 'Short-Arc Calibration of the TOPEX/Poseidon and ERS-1 Altimeters Utilizing in Situ Data', Journal of Geophysical Research, 101 (C6), pp 14191-14200.

Nerem R.S, Lerch F.J, Marshal J.A, Pavlis E.C, Putney B.H, Tapley B.D, Eanes R.J, Ries J.C, Schutz B.E, Schum C.K, Watkins M.M, Klosko S.M, Chan J.C, Luthcke S.B, Patel G.B, Pavlis N.K, Williamson R.J, Rapp R.H, Biancale R and Nouel F (1994), 'Gravity Model Development for TOPEX/Poseidon: Joint Gravity Models 1 and 2', Journal of Geophysical Research 99 (C12), pp 24,421-24,447.

Queffeulou P (1994), 'Altimeter Wind and Wave Measurements', CERSAT News, Issue No. 2.

Rapp R.H, Wang Y.M and Nickolaos K (1991), 'The Ohio State 1991 Geopotential and Sea Surface Topography Harmonic Coefficient Models', Report No. 410, Department of Geodetic Science and Surveying, Ohio State University, Columbus, Ohio, U.S.A

Ries J.C, Schum C.K and Tapley B.D (1992), ' Surface Force Modeling for Precision Orbit Determination', Paper presented at IUGG XX General Assembly, Symposium U15.

Roca M and Francis R (1996), 'Identification and Origin of On-Board Bias Jumps', Presented to ERS-2 Radar Altimeter and Microwave Radiometer Commissioning Working Group, Meeting # 9, ESA - ESRIN, 30 - 31 January 1996.

Rosborough G.W (1986), 'Satellite Orbit Perturbations due to the Geopotential', Centre for Space Research Report, CSR-86-1, University of Texas at Austin, U.S.A.

Rosborough G.W and Tapley B.D (1987), 'Radial, Transverse and Normal Satellite Position Perturbations due to the Geopotential', Celestial Mechanics, 40 (1), pp 409-421.

Roy A.E (1988), 'Orbital Motion', Adam Hilger, Bristol, Philadelphia and New York.

Sandwell D.T, Milbert D.G and Douglas B.C (1986), 'Global Non-Dynamic Orbit Improvement for Altimetric Satellites', Journal of Geophysical Research, 91(B9), pp 9447-9451.

Scharroo R (1996), 'ERS-2 Altimeter Range Calibration', Presented to ERS-2 Radar Altimeter and Microwave Radiometer Commissioning Working Group, Meeting #9, ESA - ESRIN, 30 - 31 January 1996.

Scharroo R, Wakker K.F and Mets G.J (1994), 'The Orbit Determination Accuracy of the ERS-1 Mission' In Proceedings of the Second ERS-1 Symposium, Hamburg, Germany, 11-14 October 1993, ESA SP-361, pp 735-740.

Schrama E.J.O (1989),'The Role of Orbit Errors in Processing of Satellite Altimeter Data', Netherlands Geodetic Commission.

Schrama E.J.O (1992), 'Some Remarks on Several Definitions of Geographically Correlated Orbit Errors: Consequences for Satellite Altimetry', Manuscripta Geodetica, 17, pp 282 - 294.

Schum C.K, Yuan D.N, Ries J.C, Smith J.C, Schutz B.E and Tapley B.D (1990), 'Precision Orbit Determination for the Geosat Exact Repeat Mission', Journal of Geophysical Research, 95 (C3), pp 2887-2898.

Schum C.K, Tapley B.D, Kozel B.J, Visser P, Ries J.C and Seago J (1994), 'Precise Orbit Analysis and Global Verification Results from ERS-1 Altimetry', In Proceedings of the Second ERS-1 Symposium, Hamburg, Germany, 11-14 October 1993, ESA SP-361, pp 747-749.

Smart W.M (1953), 'Celestial Mechanics', John Wiley and Sons Inc, New York, U.S.A.

Srokosz M.A (1986), 'On the Joint Distribution of Surface Elevation and Slopes for a Non Linear Sea, with Application to Radar Altimetry', Journal of Geophysical Research, 91, pp 995-1006.

Stanley H.Ray (1979), 'The Geos-3 Project', Jornal of Geophysical Research, 84(B8), pp 3779-3783.

Stum J (1996), 'Status of the OPR-2 Calibration : Existing Differences in OPR Range', Presented to ERS-2 Radar Altimeter and Microwave Radiometer Commissioning Working Group , Meeting # 9, ESA - ESRIN, 30 - 31 Jan 1996.

Tapley B.D and Rosborough G.W (1985), 'Geographically Correlated Orbit Error and its Effect on Satellite Altimetry Missions', Journal of Geophysical Research, 90, pp 11817 - 11831.

Tapley B.D, Born G.H and Parke M.E (1982), 'The Seasat Altimeter Data and it's Accuracy Assessment', Journal of Geophysical Research, 87 (C5), pp 3179-3188.

Tapley B.D, Ries J.C, Davis G.W, Eanes R.J, Schutz B.E, Shum C.K, Watkins M.M, Marshal J.A, Nerem R.S, Putney B.H, Klosko S.M, Luthcke S.B, Pavlis D, Williamson R.G and Zelensky N.P (1994), 'Precise Orbit Determination for TOPEX/Poseidon', Journal of Geophysical Research, 99 (C12), pp 24,383-24,404.

Vonder Haar T.H and Suomi V.E (1971), 'Measurements of the Earth's Radiation Budget from Satellites During a 5 year Period', Journal of Atmospheric Science, 28 (3), pp 305-314.

Wagner C and Melchioni E (1989), 'On Using Precise Laser Ranges to Provide Vertical Control for Satellite Altimetric Surfaces', Manuscripta Geodetica, 14, pp 305-338.

Wagner C. A and Klokocnik (1994), 'Accuracy of the GEM-T2 Geopotential from Geosat and ERS-1 Crossover Altimetry', Journal of Geophysical Research, 99 (B5), pp 9179 - 9201.

Wakker K.F, Zandbergen R.C.A, Naeize M.C and Ambrosius B.A.C (1990), 'Geosat Altimeter Data Analysis for the Oceans around South Africa', Journal of Geophysical Research, 95 (C3), pp 2991-3006.

Walsh E.J , Jackson F.C, Hines D.E, Piazza C, Hevizi L.G, McLaughlin D.J, McIntosh R.E, Swift R.N, Scott J.F, Yungel J.K and Fredrick E.B (1991), 'Frequency Dependence of Electromagnetic Bias in Radar Altimeter Sea Surface Measurements', Journal of Geophysical Research, 96, pp 20571-20583.

Woodworth P.L (1996), 'Final Report for the Project : Objective Analysis Mapping of changes in Large Scale Sea Surface Topography', NERC/MoD Joint Grant Number MS/D/10/15/01 and D/ACSA(R)3/10/4/3/3, Proudman Oceanographic Laboratory , Bidston , U.K.

Yaplee B.S, Shapiro A, Hammond D.L, Au B.B and Uliana E.A (1971), 'Nanosecobd Radar Observation of the Ocean surface from a Stable Platform', IEEE Trans. Geosci. Electron. GE-9, pp 170-174.